UNIVERSITÀ DI PARMA

UNIVERSITÀ DEGLI STUDI DI PARMA

DOTTORATO DI RICERCA IN
NEUROSCIENZE

CICLO XXXVI

Distinctive neural representations of kinematic features of fully visible and point-light displays grasping actions within the action observation network

Coordinatore:
Chiar.mo Prof. Luca Bonini

Tutore:
Chiar.mo Prof. Leonardo Fogassi

Dottorando: Settimio Ziccarelli

Anno Accademico 2022-2023

Publications

Journal Papers

Ziccarelli, S., Errante, A., & Fogassi, L. (2022). Decoding point-light displays and fully visible hand grasping actions within the action observation network. *Human brain mapping*, 43(14), 4293–4309. https://doi.org/10.1002/hbm.25954

Errante, A., Saviola, D., Cantoni, M., Iannuzzelli, K., **Ziccarelli, S.**, Togni, F., Simonini, M., Malchiodi, C., Bertoni, D., Inzaghi, M. G., Bozzetti, F., Menozzi, R., Quarenghi, A., Quarenghi, P., Bosone, D., Fogassi, L., Salvi, G. P., & De Tanti, A. (2022). Effectiveness of action observation therapy based on virtual reality technology in the motor rehabilitation of paretic stroke patients: a randomized clinical trial. *BMC neurology*, 22(1), 109. https://doi.org/10.1186/s12883-022-02640-2

Errante, A., Rossi Sebastiano, A., **Ziccarelli, S.**, Bruno, V., Rozzi, S., Pia, L., Fogassi, L., & Garbarini, F. (2022). Structural connectivity associated with the sense of body ownership: a diffusion tensor imaging and disconnection study in patients with bodily awareness disorder. *Brain communications*, 4(1), fcac032. https://doi.org/10.1093/braincomms/fcac032

Verzelloni, J., Errante, A., Beccani, L., Filippi, M., Bressi, B., Cavuto, S., **Ziccarelli, S.**, Bozzetti, F., Costi, S., Pineschi, E., Fogassi, L., & Ferrari, A. (2021). Can a pathological model improve the abilities of the paretic hand in hemiplegic children? the PAM-AOT study protocol of a randomised controlled trial. *BMJ Open*. http://dx.doi.org/10.1136/bmjopen-2021-053910

Errante, A., **Ziccarelli, S.**, Mingolla, G. P., & Fogassi, L. (2021). Decoding grip type and action goal during the observation of reaching-grasping actions: A multivariate fMRI study. *NeuroImage*, 243, 118511. https://doi.org/10.1016/j.neuroimage.2021.118511

Errante, A., **Ziccarelli, S.**, Mingolla, G., & Fogassi, L. (2021). Grasping and Manipulation: Neural Bases and Anatomical Circuitry in Humans. *Neuroscience*, 458, 203–212. https://doi.org/10.1016/j.neuroscience.2021.01.028

Ziccarelli, S., Errante, A., & Fogassi, L. (under review). Direction and velocity kinematic features of point-light displays grasping actions are differentially coded within the action observation network. *Journal of Neuroscience.*

Errante, A., Saviola, D., Cantoni, M., Iannuzzelli, K., **Ziccarelli, S.**, Togni, F., Simonini, M., Malchiodi, C., Bertoni, D., Inzaghi, M. G., Bozzetti, F., Quarenghi, A., Quarenghi, P., Bosone, D., Fogassi, L., Salvi, G. P., & De Tanti, A. (submitted). Effectiveness of action observation treatment based on pathological model in hemiplegic children: a randomized-controlled trial. *Neurorehabilitation and Neural Repair*.

Ziccarelli, S., Errante, A., & Fogassi, L. (in preparation). Differences in the neural response during the imitation of manipulative actions presented as fully visible and point-light displays.

Posters and Conferences

Ziccarelli, S., Errante, A., & Fogassi, L. (2023). Distinct neural encoding of direction and velocity parameters in parietal and premotor areas during the observation of point light displays grasping actions [Poster Session]. *Society for Neuroscience - SfN,* Washington D.C., United States of America (USA)

Errante, A., **Ziccarelli, S.**, & Fogassi, L. (2023). Effective connectivity between cerebellum and contralateral parietal and prefrontal cortex during observation and imitation of complex bimanual action sequences [Poster Session]. *Society for Neuroscience - SfN,* Washington D.C., United States of America (USA)

Errante, A., Beccani, L., Verzelloni, J., Maggi, I., Filippi, M., Bressi, B., **Ziccarelli, S.**, Bozzetti, F., Costi, F., Fogassi, L., & Ferrari, A. (2022). Effectiveness of action observation therapy based on pathological ameliorative model in the motor rehabilitation of hemiplegic children [Conference Paper]. *Congresso della Società Italiana di Neuropsicologia*, Rovereto, Italy

Ziccarelli, S., Errante, A., Fogassi, L. (2022). Decoding kinematic features of grasping actions presented as point-light displays within the Action Observation Network [Poster Session]. *Amsterdam Brain and Cognition*, Amsterdam, Netherlands (NL)

Ziccarelli, S., Errante, A., Mingolla, GP., Fogassi, L. (2021). Decoding grip type and action goal during the observation of reaching-grasping actions: a multivariate study [Poster Session]. *Organization for Human Brain Mapping*

Abstract (ENG)

Several studies demonstrated that action observation and execution typically recruit inferior parietal and ventral premotor cortex plus the caudal part of inferior frontal gyrus. These areas have been described as the main nodes of the mirror neuron system (MNS). The MNS, by transforming the sensory information of observed motor acts into their corresponding motor representations, enables the immediate understating of others' actions. A wider network that also includes lateral occipito-temporal areas, dorsal premotor and parietal areas, as well as the lateral parts of the cerebellum, has been collectively termed as action observation network (AON). Although the main nodes of AON mostly encode the goal of the observed actions, previous research demonstrated that some areas of this network also process action kinematic features, by elaborating aspects of biological motion. In order to isolate the specific contribution of kinematic information to the decoding of observed actions, previous studies employed the point-light displays (PLDs) technique, in which biological motion is presented without pictorial aspects.

The studies described in the present thesis are aimed at assessing the neural representations of kinematic features of PLDs grasping actions during observation tasks performed by healthy human volunteers. In the first study, by comparing fully visible (FV) and PLDs grasping actions, while controlling for confounding effects due to low-level visual features, motion and context, we aimed at verifying whether: a) the observation of PLDs actions could elicit activations of the AON comparable to that produced by FV stimuli; b) it was possible to disentangle, by means of machine learning algorithms, neural pattern distributions of the activated areas in the two experimental conditions (FV and PLDs). Results showed a comparable bilateral activation of the AON during the observation of both FV and PLDs. Analyses conducted on the BOLD (blood oxygenation level dependent) signal, showed no significant differences in signal intensity between PLDs and FV. These data suggest the recruitment of a similar action coding mechanism. By using multivoxel pattern analysis (MVPA), it was possible to disentangle, with significant accuracy, the neural pattern elicited by observation of

FV from that evoked by observation of PLDs grasping actions in occipital, parietal and premotor areas of the AON.

Taken together, these data reveal that kinematic features conveyed by PLDs stimuli are sufficient to elicit a complete action representation and that action kinematic features can be distinguished within the AON.

While previous neuroimaging studies using PLDs have explored the neural basis of action observation focusing on the distinction between biological and non-biological motion, in particular of whole-body movements, they have not examined the modulation of activity within the AON in response to differences in kinematic parameters of biological actions. In the second study, we investigated the neural substrates activated during the observation of PLDs grasping actions performed with different directions (right, left) and velocities (fast, slow). The main aim of this study was to assess which areas of the AON are mainly involved in encoding differences in direction and velocity of the observed action. By combining univariate and multivariate approaches, we were able to reveal differences in processing specific kinematic information within AON. Univariate results showed that coding differences in stimuli direction activated mainly posterior and lateral occipital areas, as well as occipito-parietal areas. Differences in velocity activated the lateral occipito-temporal cortex and both superior parietal and intraparietal areas. Multivariate results demonstrated that it is possible to decode velocity and direction at the network level, with several areas of the AON contributing to the decoding of either direction or velocity, or both. Taken together, the results of the two types of analyses indicate that posterior parietal nodes of the AON are mainly involved in coding grasping direction and that a wider set of areas, including premotor regions, are crucial for coding grasping velocity.

This evidence could be relevant for future studies aimed at investigating the neural correlates of action imitation based on PLDs stimuli. Futhermore, these insights could be exploited to personalize upper-limb observation-based rehabilitation programs, focusing on action kinematics.

Finally, machine learning-based hand action recognition models could be enhanced by training them on the most informative kinematic features of observed actions.

Abstract (ITA)

Diversi studi hanno dimostrato che l'osservazione e l'esecuzione delle azioni reclutano tipicamente la corteccia parietale inferiore e la corteccia premotoria ventrale, oltre alla parte caudale del giro frontale inferiore. Queste aree sono state descritte come i nodi principali del sistema dei neuroni specchio (mirror neuron system - MNS). Il MNS, trasformando le informazioni sensoriali degli atti motori osservati nelle corrispondenti rappresentazioni motorie, consente di comprendere immediatamente le azioni altrui. Un network più ampio, che comprende anche le aree occipito-temporali laterali, le aree premotorie e parietali dorsali e le parti laterali del cervelletto, è stata definita collettivamente action observation network (AON). Sebbene i nodi principali dell'AON codifichino principalmente il goal delle azioni osservate, ricerche precedenti hanno dimostrato che alcune aree di questa rete codificano anche le caratteristiche cinematiche dell'azione, elaborando aspetti del movimento biologico. Per isolare il contributo specifico delle informazioni cinematiche alla decodifica delle azioni osservate, gli studi precedenti hanno utilizzato la tecnica dei point-light displays (PLDs), in cui il movimento biologico viene presentato senza aspetti pittorici.

Gli studi descritti in questa tesi mirano a valutare le rappresentazioni neurali delle caratteristiche cinematiche di azioni di afferramento con PLDs durante compiti di osservazione eseguiti da volontari umani sani. Nel primo studio, confrontando azioni di afferramento completamente visibili (fully visible - FV) e PLDs, controllando al contempo gli effetti confondenti dovuti alle caratteristiche visive di basso livello, al movimento e al contesto, si è cercato di verificare se: a) l'osservazione di azioni PLDs fosse in grado di elicitare attivazioni dell'AON paragonabili a quelle prodotte da stimoli FV; b) fosse possibile distinguere, mediante algoritmi di machine learning, le distribuzioni dei pattern neurali delle aree attivate nelle due condizioni sperimentali (FV e PLDs). I risultati hanno mostrato un'attivazione bilaterale dell'AON comparabile durante l'osservazione di FV e PLDs. Le analisi condotte sul segnale BOLD (blood oxygenation level dependent) non hanno mostrato differenze significative nell'intensità del segnale tra PLDs e FV. Questi dati suggeriscono il

reclutamento di un meccanismo di codifica dell'azione simile. Utilizzando l'analisi dei pattern multivoxel (multivoxel pattern analysis - MVPA), è stato possibile distinguere, con un'accuratezza significativa, il pattern neurale elicitato dall'osservazione di azioni di afferramento FV da quello evocato dall'osservazione delle azioni di afferramento PLDs nelle aree occipitali, parietali e premotorie dell'AON.

Nel complesso, questi dati rivelano che le caratteristiche cinematiche trasmesse tramite stimoli PLDs sono sufficienti a evocare una rappresentazione completa dell'azione e che le caratteristiche cinematiche dell'azione possono essere distinte all'interno dell'AON.

Precedenti studi di neuroimmagine che hanno utilizzato i PLDs hanno esplorato le basi neurali dell'osservazione dell'azione concentrandosi sulla distinzione tra movimento biologico e non biologico, in particolare dei movimenti del corpo intero, ma non hanno esaminato la modulazione dell'attività all'interno dell'AON in risposta alle differenze nei parametri cinematici delle azioni biologiche. Nel secondo studio, abbiamo indagato i substrati neurali attivati durante l'osservazione di azioni di afferramento presentate tramite PLDs eseguite in diverse direzioni (destra, sinistra) e con diverse velocità (veloce, lenta). L'obiettivo principale di questo studio è stato quello di valutare quali aree dell'AON sono principalmente coinvolte nella codifica delle differenze di direzione e velocità dell'azione osservata. Combinando approcci univariati e multivariati, siamo stati in grado di rivelare differenze nell'elaborazione di informazioni cinematiche specifiche all'interno dell'AON. I risultati univariati hanno mostrato che la codifica delle differenze di direzione degli stimoli attivava principalmente le aree occipitali posteriori e laterali, nonché le aree occipito-parietali. Le differenze di velocità hanno attivato la corteccia occipito-temporale laterale e le aree parietali superiori e intraparietali. I risultati multivariati hanno dimostrato che è possibile decodificare la velocità e la direzione a livello di network, con diverse aree dell'AON che contribuiscono alla decodifica della direzione o della velocità, o di entrambe. Nel complesso, i risultati dei due tipi di analisi indicano che i nodi parietali posteriori dell'AON sono principalmente coinvolti nella codifica della direzione di

afferramento e che un insieme più ampio di aree, comprese le regioni premotorie, sono fondamentali per la codifica della velocità di afferramento.

Questi dati potrebbero essere rilevanti per studi futuri volti a indagare i correlati neurali dell'imitazione di azioni basate su stimoli PLDs. Inoltre, queste informazioni potrebbero essere sfruttate per personalizzare i programmi di riabilitazione dell'arto superiore, basati sull'osservazione, concentrandosi sulla cinematica dell'azione. Infine, i modelli di riconoscimento delle azioni della mano basati sul machine learning, potrebbero essere migliorati addestrandoli sulle caratteristiche cinematiche più informative delle azioni osservate.

1. General Introduction

1.1 Anatomo-functional organization of the primate cortical motor system

In recent decades, several studies have revised our understanding of the organization of the cortical motor areas, revealing a more extensive and intricate parcellation and a more complex functional characterization. In contrast with what was traditionally thought, the motor and premotor cortices have been shown to be subdivided into several areas which were labeled by Matelli and colleagues (1985, 1991) with a letter F and an Arabic number from 1 to 7. The primary motor cortex in the macaque is thus denoted by F1, the areas occupying a more mesial portion of the agranular cortex are F3 and F6, in the dorsal sector are F2 and F7 and finally, on the ventral surface, are F4 and F5 (Figure 1); the latter could be further divided into sectors named F5p, F5a and F5c (Belmalih et al., 2009).

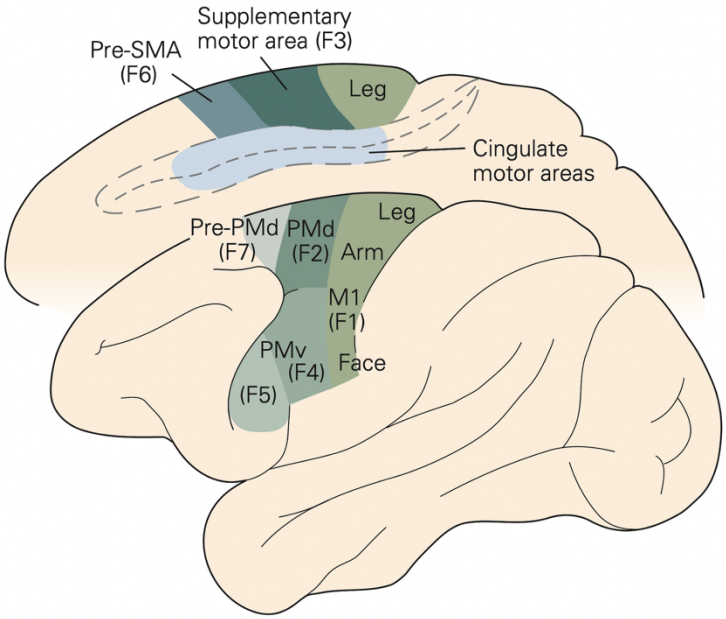

Figure 1. Lateral and mesial representation of macaque brain with functional parcellation of premotor, supplementary-motor and primary motor area. Abbreviations: M1, primary motor cortex; pre-SMA, pre-supplementary motor area; PMd, dorsal premotor cortex; Pre-PMd, pre-dorsal premotor cortex; PMv, ventral premotor cortex (from Kandel et al., 2012, p. 840).

It has been demonstrated that a low-voltage current applied to area F1, elicits fine movements involving even single joints. This area is particularly excitable, meaning that even a mild current can elicit a movement. In contrast, areas like F7 are less excitable, as the current intensity required to induce movement is potentially damaging. Nevertheless, eye movements have been recorded during stimulation of this area (Luppino et al., 1991). Is worth noting that, generally, proximal movements, like torso or shoulder movements, tend to be represented medially on the cortex surface while distal movements, hand and finger movements, more laterally. While more rostral areas in the frontal agranular cortex have extensive connections with other motor areas, they lack direct connections with F1, conversely, areas located more caudally in the cortex are reciprocally connected and maintain also direct connections with F1 (Hickok & Small, 2015).

To better understand the functional role of the primary motor cortex and premotor cortex, is important to consider the connections with other cortical areas. Several parietal and prefrontal areas as well as the cingulate cortex, are reciprocally connected with premotor areas, forming circuits which are implied in various aspects of motor control. Prefrontal connections, primarily with the rostral portion of the premotor cortex, have a role in modulating the aspects of action planning and of motor behavior. This information is then relayed to the caudal premotor sectors, in order to determine which motor acts to execute and their sequence (Borra et al., 2011; Gerbella et al., 2013). Many areas in the premotor cortex, share anatomical connections with parietal areas, which while being involved in coding somatosensory, visual, or both inputs, also play a crucial role in encoding essential information for action programming. Anatomical studies have revealed a parcellation of the superior parietal lobule (SPL), the inferior parietal lobule (IPL) and intraparietal sulcus (IPS) (Arcaro et al., 2011; Colby et al., 1993; Felleman & Van Essen, 1991; Gregoriou et al., 2006; Lewis & Van Essen, 2000; Pandya & Seltzer, 1982; Sakata et al., 1998; Taira et al., 1990), which share specific connections with premotor areas (Figure 2).

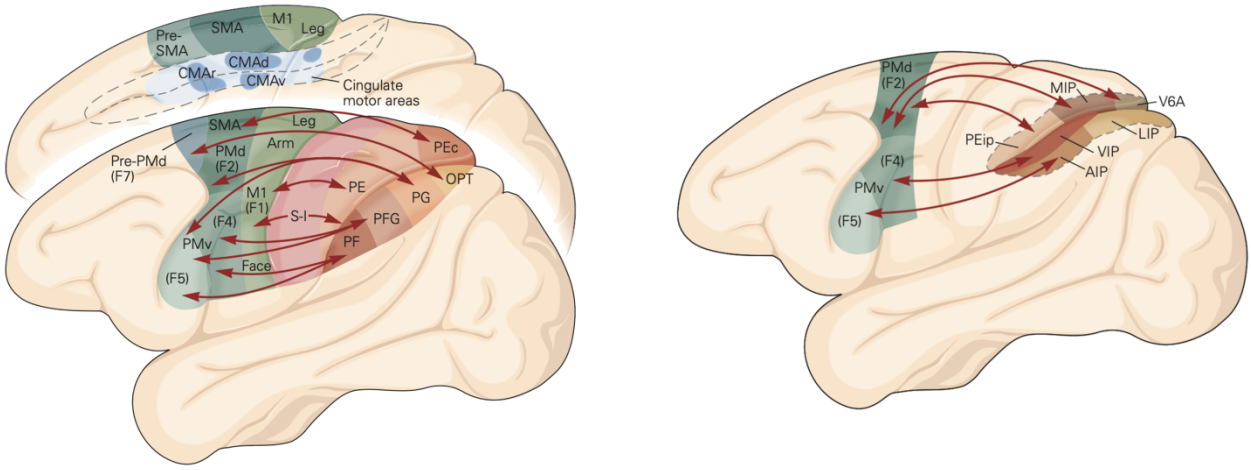

Figure 2. Lateral and mesial view of macaque brain showing the reciprocal connections (arrows) between premotor and parietal areas. In the right panel, connections between premotor areas and those inside the intraparietal sulcus (IPS) are shown. Abbreviations: CMAr, rostral cingulate motor area; CMAv, ventral cingulate motor area; CMd, dorsal cingulate motor area; F, frontal; M1, primary motor cortex; OPT, occipito-parieto-temporal; P, parietal; PE, PF, and PFG are parietal areas according to the nomenclature of von Economo; PMd, dorsal premotor cortex; PMv, ventral premotor cortex; Pre-PMd, predorsal premotor cortex; S-I, primary soma- tosensory cortex; SMA, supplemental motor area; AIP, anterior intraparietal area; LIP, lateral intraparietal area; MIP, medial intraparietal areal; VIP, ventral intraparietal area; PEip, PE intraparietal; V6A, visual area V6A (from Kandel et al., 2021, p. 820).

A key area which is involved in encoding motor acts and not single movements, unlike F1, is the area F5. Rizzolatti and colleagues (1988) demonstrated that neurons in this area respond selectively to certain motor acts, such as grasping or scratching. While both involve comparable finger movements, such as finger flexion and a consequent closure of the hand, there are distinct populations of neurons in F5 which are specifically recruited for each act. This study further showed that F5 neurons respond to the same action goal regardless of the effector used, whether it is the hand or mouth. Neural activity in this cortical area, is related neither to the recruitment of particular muscle groups nor to simple movements, but to motor goal directed motor acts also when performed with different effectors. It has been proposed that in F5 there is a "vocabulary" of motor acts. A study from Jeannerod and colleagues (1995) further demonstrated that some populations of F5 neurons, encode

specific features of such motor acts such as different types of grasps or temporal features of the latter. Further evidence for F5's role in encoding action goal was provided by Umiltà and colleagues (2008) in a study where the monkey was instructed to achieve the same motor goal, taking possession of food, by means of opposite movements by opening or closing the hand using normal or inverted pliers respectively (Figure 3). It has been shown that most of the F5 neurons encoded goal achievement even though the hand movements were opposite.

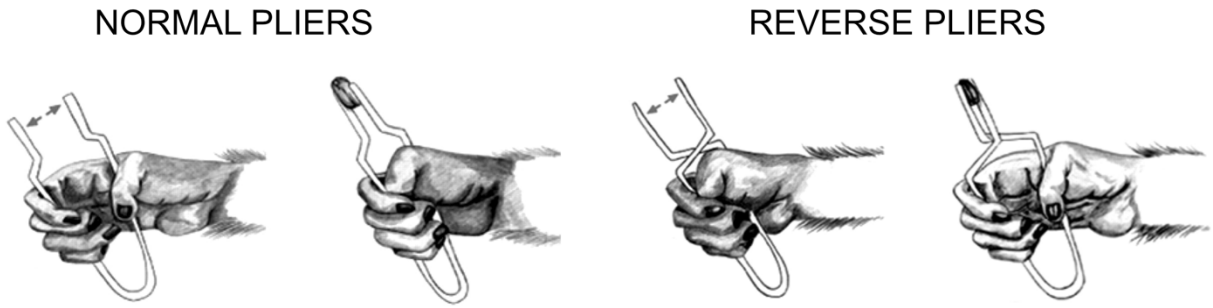

Figure 3. Illustrations of the experimental paradigm. The arrows in the image illustrate the direction of the motion of the pliers' tips (modified from Umiltà et al., 2008).

In addition to having motor properties, some neurons in F5 show selectivity for visual stimuli (Rizzolatti & Gentilucci, 1988) in particular to the presentation of three-dimensional objects (Murata et al., 1997). These are mainly located in the area F5p and are called "canonical neurons". An experimental paradigm consisting in three conditions was used: a) grasping with the visible object; b) grasping in the dark, whereby the monkey could only rely on the previous experience of shape and location of the stimulus; c) looking at the object without grasping it. The results showed that some of the recorded neurons were purely motor responding to grasping in each condition, while others responded significantly to the presentation of the object. This suggests that the discharge of canonical neurons is related to the encoding of the visual stimulus in a motoric manner. This means that when an object is observed, it suggests a potential motor act congruent with the properties of the presented object, independently of whether the act will be executed or not.

The premotor area F5p is strongly connected with the anterior intraparietal (AIP) areas (Borra et al., 2008; Gerbella et al., 2011; Luppino et al., 1999). Neurons in the AIP respond similarly to those in F5p to fixation and manipulation of objects (Sakata et al., 1995). Using a paradigm similar to that used to study the F5p area, three classes of neurons were identified within AIP: motor-dominant, visual-dominant and visuomotor neurons. It has been further demonstrated that two-thirds of AIP neurons show preference for a single or restricted classes of objects (Murata et al., 2000). Studies employing the reversible inactivation of AIP in nonhuman primates, demonstrated that there was a difficulty in hand posture configuration during a grasping task resulting in predisposing the hand more or less correctly only after countless attempts based on tactile exploration of the object to be grasped (Gallese et al., 1994). These results were comparable to those resulting from the inactivation of premotor areas (Fogassi et al., 2001). Collectively, these studies demonstrate that the extensive parieto-premotor circuit are responsible for visuomotor transformations for grasping.

1.2 Mirror neuron system in non-human primates

Within the class of F5 visuomotor neurons two categories of neurons have been identified: canonical neurons and mirror neurons. Canonical neurons, which mainly occupy the F5p area, respond selectively to the presentation of three-dimensional objects which activates a motor representation of a potential motor act congruent with the physical properties of the object to be grasped. Mirror neurons were described for the first time 30 years ago in the monkey area F5c (Di Pellegrino et al., 1992) and PFG (Fogassi et al., 2005; Rozzi et al., 2008). Unlike canonical neurons, mirror neurons do not respond to the simple presentation of three-dimensional object but both when performing a motor act and when observing one performed by another (Figure 4). Therefore, an observed action produces, in the observer's brain, a motor activation, as if the observer was actually executing it.

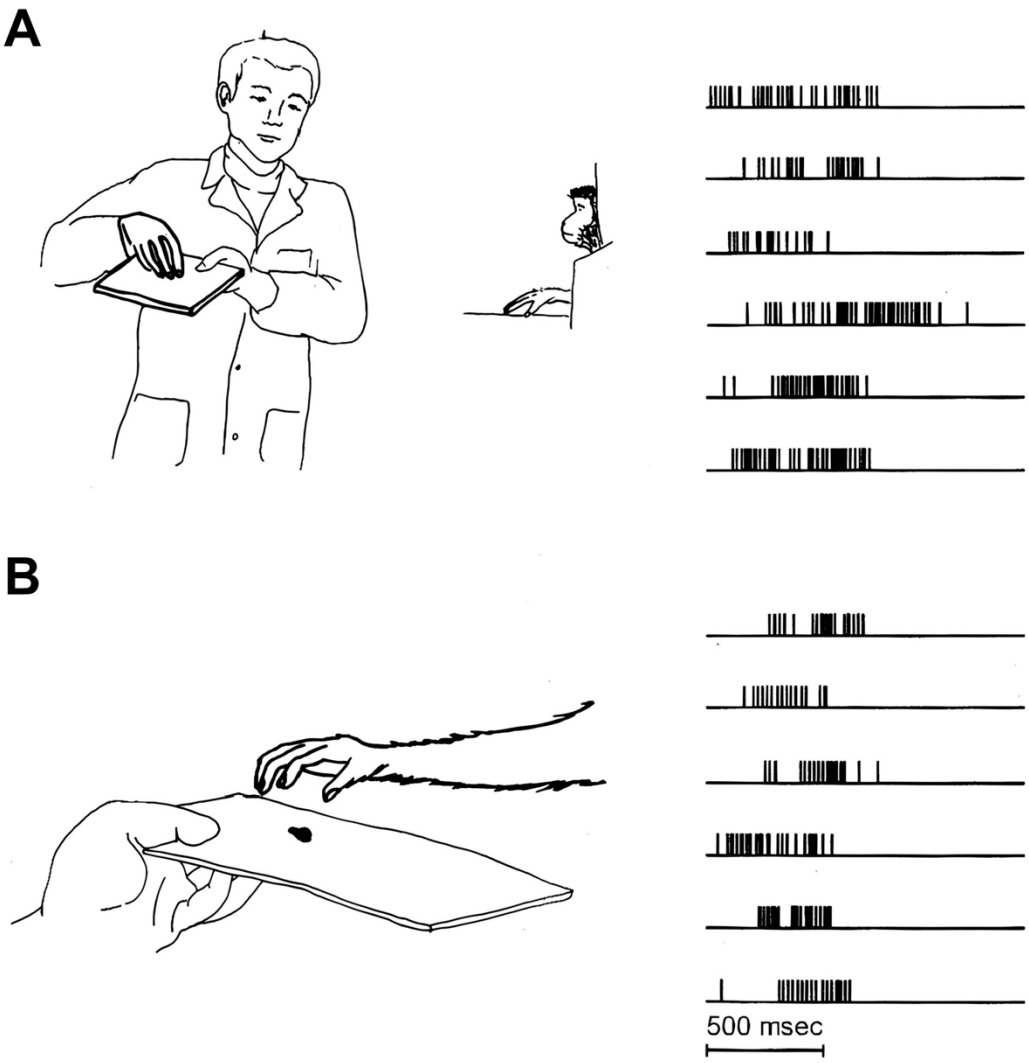

Figure 4.Illustration of tasks (left panels) and neural responses of a mirror neuron (right panels), during grasping observation (A), during grasping execution (B) (from Di Pellegrino et al., 1992).

Based on the similarity between the observed and executed motor actions, mirror neurons can be classified into two main categories: strictly congruent and broadly congruent mirror neurons. The former neurons fire when both the observed and executed actions, in terms of goal and means to achieve it, are the same. In contrast, broadly congruent mirror neurons are activated when the observed and executed actions are similar but not identical (Gallese et al., 1996). The widely accepted coding of motor acts' goals by mirror neurons (Rizzolatti & Luppino, 2001) is further supported by

evidence that this class of neurons does not exclusively respond during the actual observation of the final part of a motor act, instead, they encode what the other is doing even when visual information is incomplete such as when the end of the action is occluded. In an experiment, Umiltà and colleagues (2001) showed that there is a neuronal response when observing an agent moving the hand toward a previously shown target which is subsequently covered thus demonstrating that mirror neurons are able to encode what the agent is performing even if the action itself, that is grasping, is not visible (Figure 5).

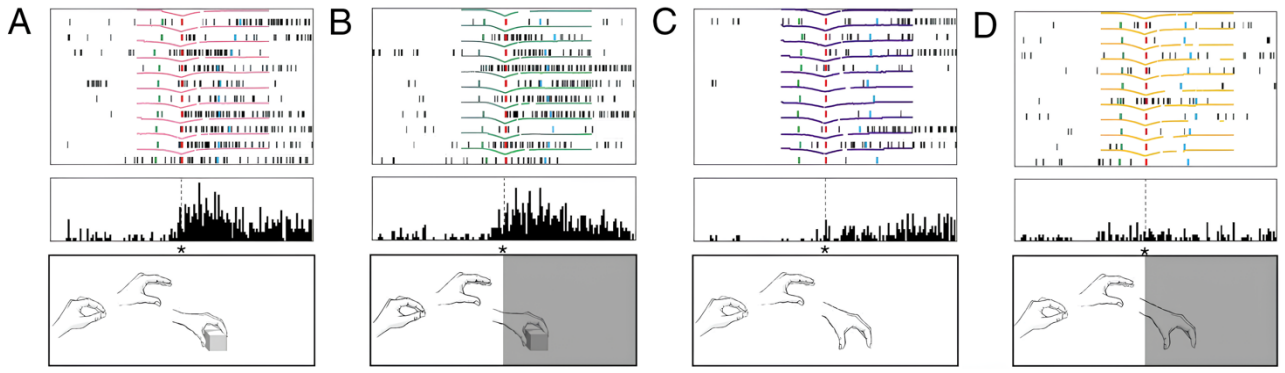

Figure 5. Neural activity of a mirror neuron responding to the observation of grasping and holding in full vision (A) and in hidden condition (B) but not during the fully visible mimed (C) and hidden (D) grasping (modified from Umiltà et al., 2001).

Mirror neurons exhibit responses not only to visual but also auditory stimuli. In this regard, Kohler and colleagues (2002) demonstrated in monkeys that listening to the sound produced by a known action like breaking a peanut without observing it, as compared to different motor acts or unspecified sounds such as white noise, activates a particular set of mirror neurons which respond to specific auditory cues. This suggests that mirror neurons encode actions regardless of the sensory modality through which it is presented.

A fundamental region part of the mirror neuron system (MNS) (Rizzolatti et al., 2014) is the superior region of the temporal lobe sulcus (STS), which despite not discharging during active motor movements, fires during the observation of hand grasping actions (Perrett et al., 1989). Very likely, STS neurons achieve a very high level of stimulus complexity encoding, their response is indeed modulated by the orientation of the gaze of the one performing the action. Specifically, if the gaze is directed toward the object with which one is interacting, STS neurons exhibit a response, while if the gaze is directed elsewhere, there is no significant response (Jellema et al., 2000). The neural activity of this area was further studied by Nelissen and colleagues (2011) using neuroimaging techniques in non-human primates, demonstrating that the secondary somatosensory cortex (SII) and STS are particularly active during action observation (Figure 6).

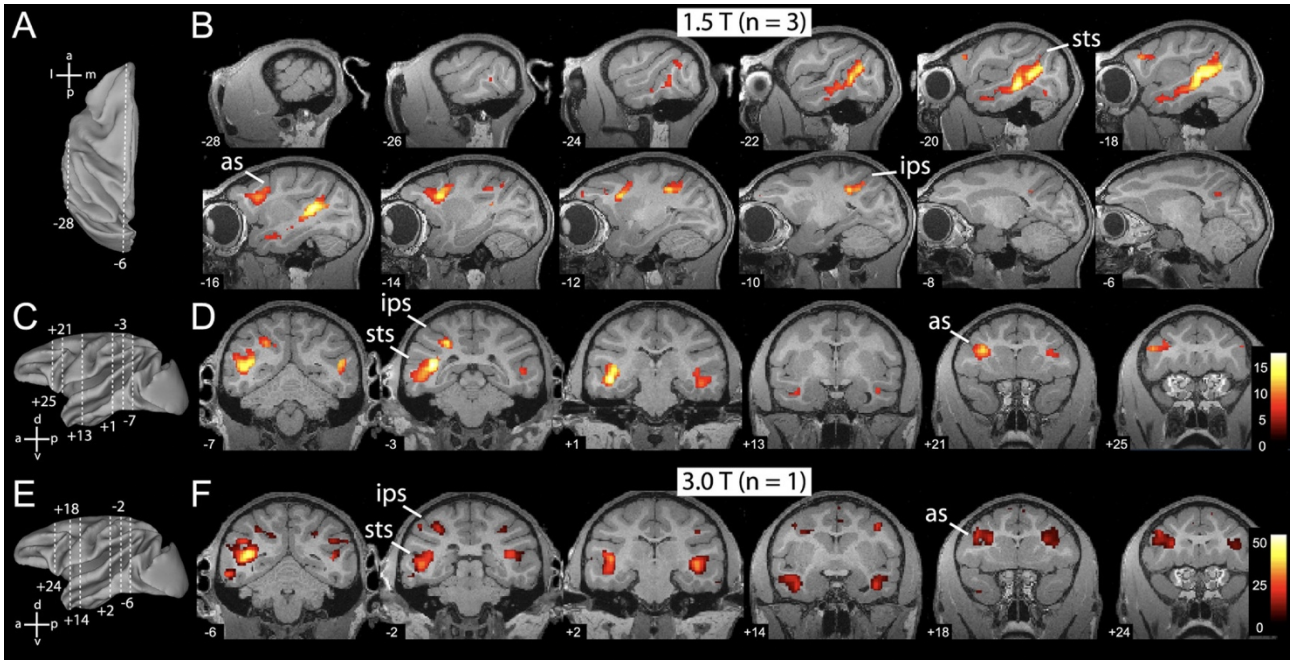

Figure 6. Activation maps of functional magnetic resonance imaging data showing brain activation during the observation of grasping actions in macaque monkeys. Abbreviations: as, arcuate sulcus; ips, intraparietal sulcus; sts, superior temporal sulcus (from Nelissen et al., 2011).

A comparison of brain activations during the observation of grasping actions and static stimuli, revealed action-related increases in neural activity in the parietal lobe, specifically in the PFG and AIP regions. Action-related stimuli as compared to static ones, consistently elicited stronger neural

responses also in STS. This region largely projects to the IPL which is in turn connected with the ventral premotor cortex. Single neuron recordings within the inferior parietal lobule, particularly in the PF and PFG areas, lead to the discovery of neurons with mirror properties, thus demonstrating that such neurons are also present in other brain areas (Fogassi et al., 2005; Rozzi et al., 2008).

Reciprocal anatomo-functional connections between parietal and premotor areas and shared mirror properties, suggest that this circuit is critical for immediate understanding of others' actions. In a study by Fogassi and colleagues (2005), it was shown that neurons within the parietal lobe are differently activated when the same motor act is performed to achieve different goals. The experimental paradigm consisted in a condition in which the monkey had to bring food toward the mouth, and another in which it had to be moved either to a container placed on the shoulder or to another on the table next to the item to be grasped. The results showed that most of the recorded neurons discharged in accordance with the action in which the grasping was embedded; the large majority of them, preferring grasping for eating. The main factor that triggered the neuronal discharge was given by the purpose of the action and not by the kinematic features or by the type of object to be grasped. Several motor acts can be differentially connected depending on the overall purpose of the action. The presence of neurons encoding the ultimate purpose of concatenated series of finalized acts, is crucial for a smooth unfolding of the action.

1.3 Mirror neuron system in humans

Soon after the discovery of mirror neurons in nonhuman primates, the question arose as to whether this class of neurons was also present in humans. There is no doubt that such mechanism is evolutionarily fundamental to social interactions, and therefore it is logical to conclude that this has been preserved during human evolution. Noninvasive techniques such as transcranial magnetic stimulation (TMS), electroencephalograpy (EEG), magnetoencephalography (MEG), positron

emission tomography (PET) and functional magnetic resonance imaging (fMRI), have been used to demonstrate the existence of mirror neuron mechanism in humans (Buccino et al., 2001; Buccino et al., 2004a; Buccino et al., 2004b; Fadiga et al., 1995; Gatti et al., 2017; Gazzola & Keysers, 2009; Gazzola et al., 2007; Grafton et al., 1996; Grezes et al., 1999; Iacoboni et al., 2001; Iacoboni et al., 1999; Koski et al., 2002). Using TMS to send impulses to the motor cortex of healthy participants during the observation of experimenters grasping objects or actions, and simultaneously recording motor evoked potentials (MEP), Fadiga and colleagues (1995) demonstrated participants' hand muscles exhibited a pattern of activity remarkably similar to that observed during actual movement execution. This work already provided compelling evidence for the existence of a neural mirroring system of the observed motor acts, similar to that described in monkeys.

Using functional magnetic resonance imaging (fMRI), researchers were able to localize, with higher spatial accuracy, brain regions that showed higher activity during the observation of others' actions. Buccino and colleagues (2001) revealed, by showing to participants transitive and intransitive actions performed with the mouth, hand, and foot, a somatotopic organization of brain activation patterns in the premotor cortex and parietal areas bilaterally. These findings suggest that a somatotopically organized representation of actions is automatically activated during observation. Further evidence that areas within the human mirror system are activated during both action execution and observation, was provided in a study during which participants were asked to observe, perform, and imagine a reaching action towards an object (Filimon et al., 2007). Activations in both dorsal premotor and parietal areas, were identified in all three tasks. It is worth noting that studies that focused mainly on grasping, with less of the arm transport phase (Rizzolatti et al., 1996), find activations in the inferior frontal gyrus (IFG) and the IPL, compared to tasks involving mainly arm reaching actions (Grafton et al., 1996) that describe activations in more dorsal areas.

Meta analyses of neuroimaging studies in humans (Caspers et al., 2010; Molenberghs et al., 2012) demonstrated that the observation of others performing goal directed actions elicits an increase in BOLD signal in the IPL, ventral premotor cortex, and the caudal sector of the inferior frontal gyrus, regions that are considered homologous to those in monkeys where mirror neurons were first identified (Figure 7). Using single-subject analyses of unsmoothed fMRI data, Gazzola and Keysers (2009), revealed that the overlap of activations during both observation and execution, extends beyond the canonical parieto-premotor circuit, encompassing several cortical areas, such as the dorsal premotor cortex, middle cingulate cortex, somatosensory cortex, superior parietal cortex, and middle temporal cortex. Authors suggested that these areas could play a key role in encoding information about others' actions provided by the mirror mechanism.

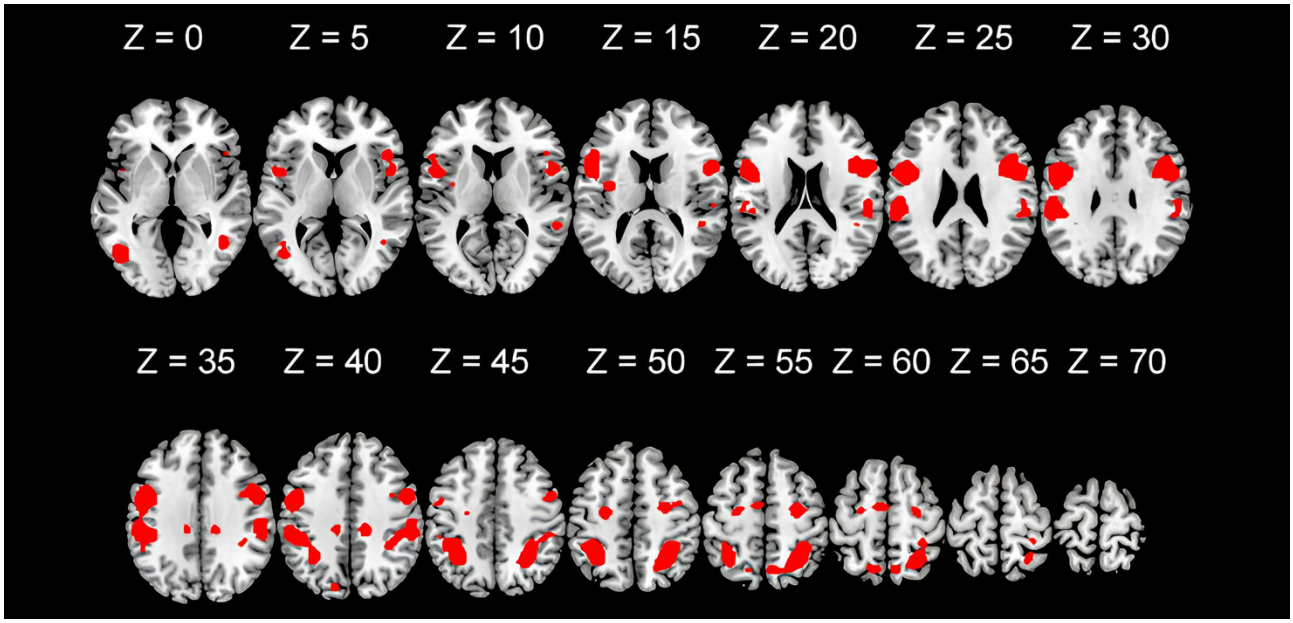

Figure 7. Significant activation clusters, overlayed on axial slices of an MNI human brain template, of 125 human fMRI studies in which authors' results reveal the mirror neuron system activity (Molenberghs et al, 2012).

Evidence of mirror neuron activity in humans was also demonstrated by means of neurophysiological measures such as EEG. The mu rhythm (μ) is a frequency of about 8-13 hz that is recorded in correspondence of the sensorimotor area when at rest. It is completely altered during the observation of motor acts which denotes the underlying cortical activity modulation due to

stimulus processing (Cochin et al., 1999). In an experiment conducted by Muthukumaraswamy and colleagues (2004), researchers explored the connection between mu rhythm and mirror neuron activity. Participants were required to observe videos of a hand approaching an object, either maintaining it flat, shaping into a grasping position or actually grasping the object. In another condition, participants themselves performed grasps similar to those shown in the videos. The results demonstrated a desynchronization of mu rhythm during both observation and actual execution of the grasping action as compared to when the hand was flat or simply shaped for grasping. A study using intracranial recordings of cortical activity with subarachnoid electrodes in a patient, demonstrated similar alpha rhythm desynchronization in the motor cortex representation of the hand and IFG during both observation and execution of index and middle finger movements (Tremblay et al., 2004) further demonstrating that the human mirror neuron system involves a neuronal network comprising sectors of the ventral premotor cortex.

In the past decades, fMRI studies provided compelling evidence supporting the role of goal processing in MNS regardless of agent appearance and/or kinematic features of the performed action. Studies on both humans (Gazzola et al., 2007) and monkeys (Peeters et al., 2009) demonstrated that occipito-temporal and parieto-frontal areas of the MNS were active also when observing a robotic arm performing an action regardless of the effector shape and kinematics differences. Further evidence of the ability to extract goal information regardless of the effector performing the action, was provided by Senna and colleagues (2014) using TMS and MEPs recording in both hand and foot muscles. The results demonstrated that the excitability of both the hand and foot motor area increased when participants observed grasping actions in general, regardless of the effector used to perform them. It's worth noting that the observation of a nonspecific, non-goal directed action, although performed with both effectors, did not modulate the motor areas. This suggests that when a recognizable action goal is performed with an unusual effector, is possible to observe motor facilitation in the muscles typically used to accomplish that goal.

1.3.1 Coding action intention

Similar to monkeys, humans' mirror system plays a crucial role in the coding of the intentions of others. Evidence supporting this notion was demonstrated in a study by Iacoboni and colleagues (2005) during which participants were presented with three different conditions named *context*, *actions* and *intention* respectively. In the first, participants were shown objects placed in a way suggesting that a person was about to have breakfast or just finished a meal. In the second, they observed a hand grasping a mug without any contextual information. The third, presented the same hand holding the mug in both contexts. Data revealed an increased activation of the inferior frontal cortex for the *intention* condition strongly suggesting that this mirror neuron area plays a key role in understanding the intentions of the observed actions (Figure 8). Interestingly, grasping to drink elicits a stronger activation as compared to grasping to put away, indicating that the actions mostly represented in our motor repertoire, recruit the MNS more strongly.

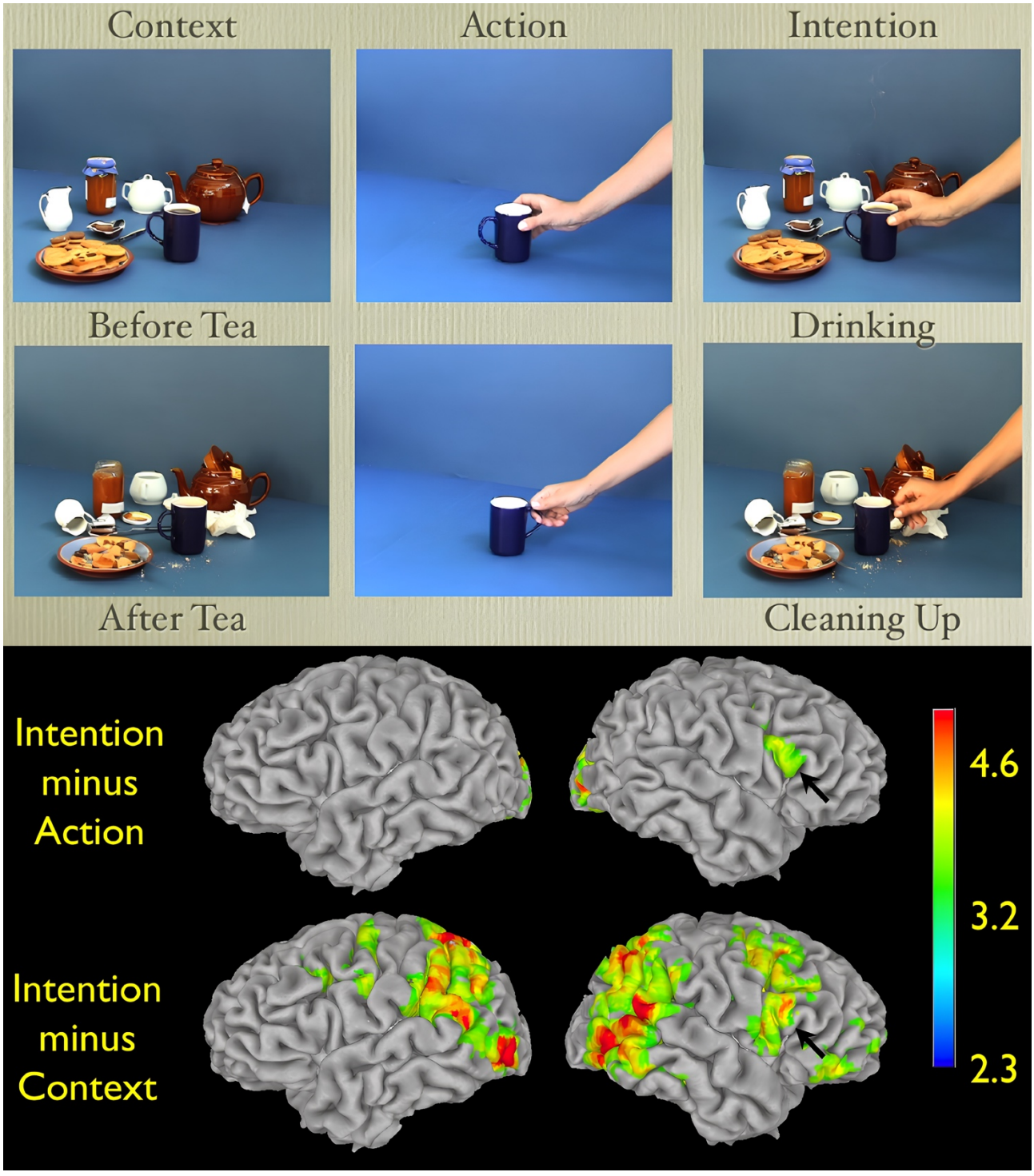

Figure 8. Still frames taken from the *context*, *action* and *intention* experimental conditions (upper panel); in the bottom panel, brain activation maps resulting from the contrast between intention and action (upper row) and intention minus context (bottom row) resulting in an activation of the left inferior frontal gyrus (as pointed by the black arrow) (from Iacoboni et al., 2005).

During the observation of a motor act or a series of them, we intuitively attribute meaning to the movements based on our own motor representations and the activation of our own motor chains. Evidence for the existence of chains of motor acts and the ability of the MNS to code the intention of actions, comes from a study performed on children affected by autism spectrum disorder (ASD) and typically developing children during a task involving both observation and execution of actions (Cattaneo et al., 2007). In this study it was adopted the experimental design used by Fogassi and colleagues (2005) for investigating intention coding in non-human primates. Children were required to observe videos of a person grasping food and either bringing it to their mouth or placing it in a container on the shoulder. Then, they were asked to perform the same actions. During both the observation and action execution tasks, researchers recorded the activity of the mylohyoid muscle, which is recruited during the opening and closing of the jaw. Results showed that typically developing children exhibited an early activation of the mylohyoid muscle when observing grasping-to-eat action, and not when observing grasping-to-place. On the contrary, children affected by ASD displayed no significant muscle activation during the observation of the motor task (Figure 9). Groups differed also in the temporization of the muscular activity response. Typically developing children activated the mylohyoid muscle during the execution of grasping aimed at bringing to the mouth, approximately one second prior to grasping, while children affected by ASD activated this muscle only after grasping. Although indirectly, this suggests that children with ASD lacked the ability to properly select and time a chain of motor acts in order to perform the actions smoothly and effectively. This could suggest that children with ASD may have an incomplete understanding of others' intentions due to a different representation and selection of action chains on their own motor circuits, possibly indicating an impairment in mirroring other's actions.

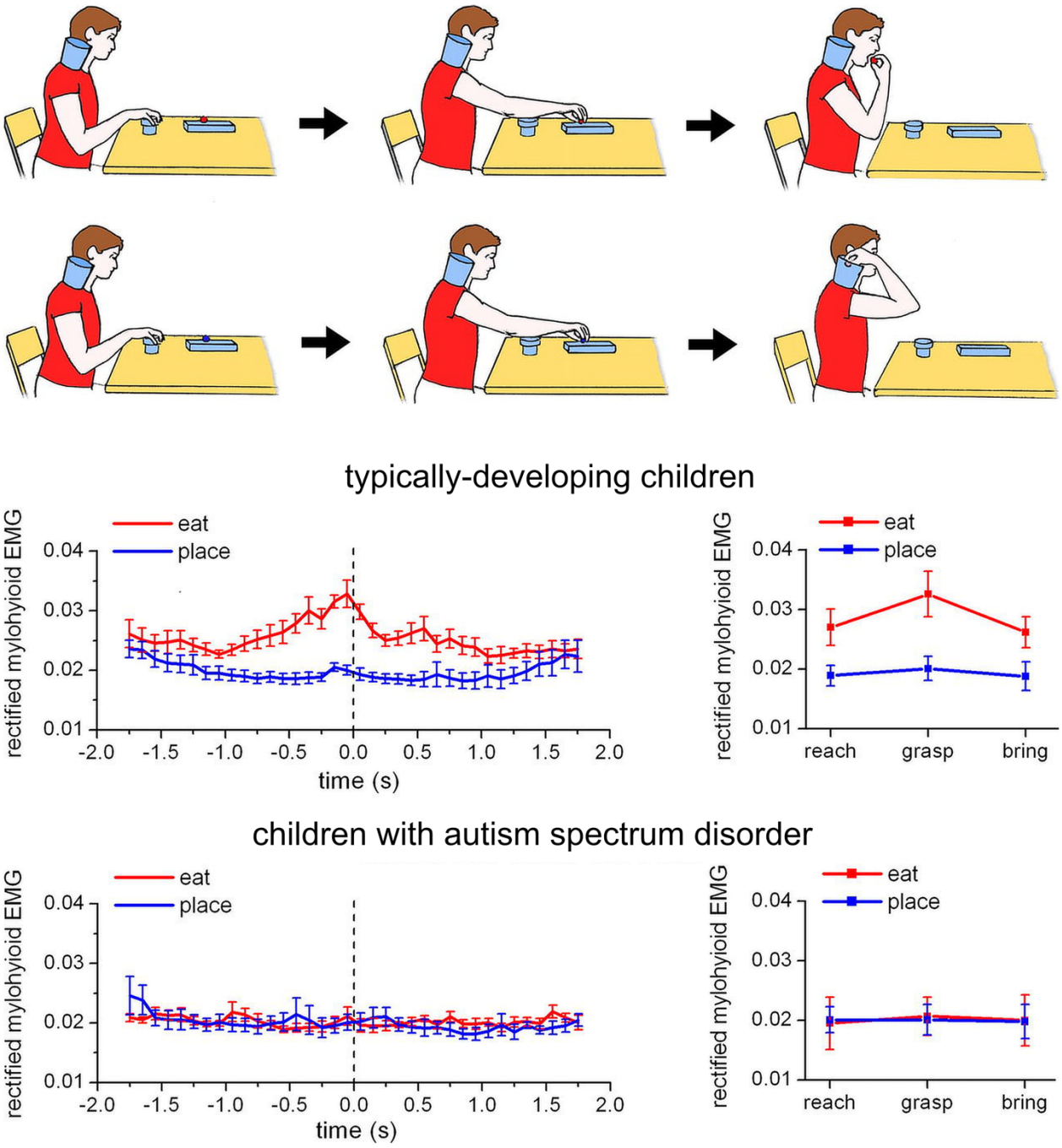

Figure 9. In the upper panel, representation of reach to bring to the mouth (upper row) and grasp to place (bottom row) experimental conditions during both observation and execution tasks. In the bottom panel, time course of the rectified EMG activity of the mylohyoid muscle during the observation task (modified from Cattaneo et al., 2007).

1.3.2 Modulation by motor repertoire

The ability to understand others' intentions is linked to one's own motor repertoire. Previous experience of a particular motor skill influences the brain's response during the observation of actions requiring that ability. By comparing the MNS modulation during the observation of communicative and feeding actions performed by members of different species, namely, humans, dogs and monkeys, Buccino and colleagues (2004a), using fMRI technique, demonstrated that biting activated the premotor cortex and inferior parietal lobule regardless of the observed species, while, observing communicative actions recruited the same areas but only when participants observed a conspecific. This demonstrated that there is a modulation of brain areas involved in matching the visual description of a motor act, onto one's own motor representation of it, when the observed action belongs to the observer's motor repertoire.

The effect of expertise on the modulation of MNS activity, has been demonstrated on expert and naïve dancers. During an fMRI experiment, Calvo-Merino and colleagues (2005) showed specific dance steps to capoeira and classical ballet dancers as well as naïve dancers. The results demonstrated a difference between the two groups of experts that consisted in a stronger MNS modulation during the observation of familiar dance steps as compared to the unfamiliar one. Furthermore, it was subsequently demonstrated that MNS was activated more strongly during the observation of dance steps performed by individuals of the same gender as the observer, demonstrating that motor expertise and not visual experience is crucial in modulating MNS activity (Calvo-Merino et al., 2006).

1.3.3 Neural correlates of action imitation

The ability to match the visual representation of motor action into a motor representation is fundamental for imitative behaviors. Iacoboni and colleagues (1999) conducted an fMRI study during which participants were required to passively observe actions and actively imitate what was

previously observed. During passive observation, participants were presented with a video of a moving finger, a cross on a stationary finger, or a cross on an empty background. In the imitation condition, they were instructed to lift the right finger in response to each stimulus presentation. Results showed a significantly stronger activation of the MNS when comparing trials during which they executed a movement after observing the action and those when the movement was prompted only by the cross. Further research suggested that MNS plays a crucial role not only in imitating observed actions but also in imitation learning. Buccino and colleagues (2004b) conducted an event related fMRI study on participants with no prior guitar playing experience. They were asked to imitate videos representing chord sequences performed by a skilled guitarist. A common activation pattern comprising the IPL, PMv and IFG was found during both the observation of the chords as played by the model and the period right before imitation during which participants were instructed to stay still (Figure 10). Interestingly, during the preparation phase, an increased activation was found in the dorsolateral prefrontal cortex (area 46). Authors proposed a two-step process for imitation learning consisting in a motor representation of the observed actions in the parietal and frontal lobes and a re-elaboration of these latter to adapt them to the specific observed model.

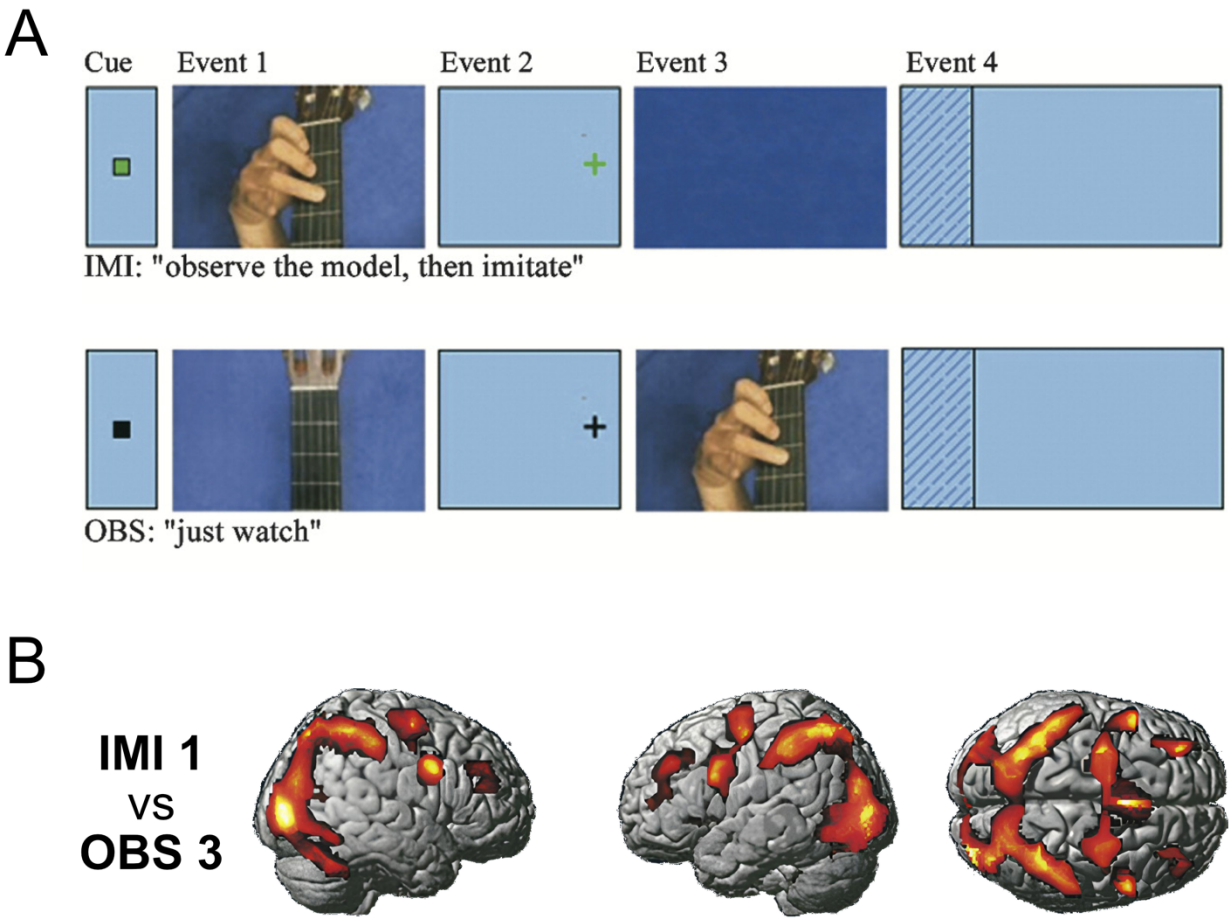

Figure 10. Representation of imitation (IMI) and observation (OBS) conditions of the experimental paradigm and activation patterns. (A) upper row, events during the imitation condition; bottom row, events in the observation conditions. Sentences in quotes represent the task that the participant had to perform. (B) Significant activation resulting from the contrast between the imitation event one and observation event three, both showing the model performing the chord (modified from Buccino et al., 2004b).

Recently, in an fMRI study conducted by Errante and Fogassi (2019a), the authors addressed the issue of how MNS areas are modulated during the observation of novel and complex manipulative actions outside of one's own motor repertoire. The aim was to evaluate whether motor "resonance" in naïve participants is influenced by the degree of similarity with their own motor skills. Participants observed videos of hand-object manipulations performed by an expert, intermediate and naïve model. The fMRI results revealed that observing actions executed by the non-expert model, produced stronger activation in a dorsal-medial parieto-premotor circuit as compared to those elicited by the

observation of the expert models, suggesting a stronger activation of specific MNS areas for actions that better correspond to one's own motor repertoire.

1.3.4 Hierarchical action representation

In a series of fMRI studies aimed at differentiating the neural correlates of action goals representation from those associated with the coding of kinematic aspects of the same actions, researchers employed the repetition suppression (RS) technique which postulates a reduction of a physiologic response to consecutively repeated stimuli. Hamilton and Grafton (2006, 2008) proposed a model suggesting a hierarchical organization of motor representations, with higher levels corresponding to more abstract action features representation. The results showed a RS effect for goal in the anterior portion of the intraparietal sulcus, while, basic trajectory features, in the left superior occipital sulcus and right superior pre-central sulcus (Grafton & Hamilton, 2007; Hamilton & Grafton, 2006). In another experiment from the same authors, by modulating the complexity of the outcome of a motor act, which involved manipulating an object in order to elicit a transformation in the external conditions, they demonstrated a RS effect in IFG, IPS, the supplementary motor area (SMA) and middle frontal gyrus (MFG) thus suggesting the involvement of these areas in coding goals of more complex actions. Recently, Errante and colleagues (2021a) by using multivoxel pattern analysis (MVPA) on fMRI data, investigated the possibility to disentangle grip and goal processing in MNS areas. Participants were asked to perform two tasks: observing and executing actions with two grips and two goals. Results demonstrated that grip type was effectively decoded in several MNS regions, while action goal was accurately decoded in the inferior parietal lobule (Figure 11). These data suggest that a large network of areas could be dedicated to grip encoding, while the inferior parietal cortex plays a crucial role in representing the final action goal.

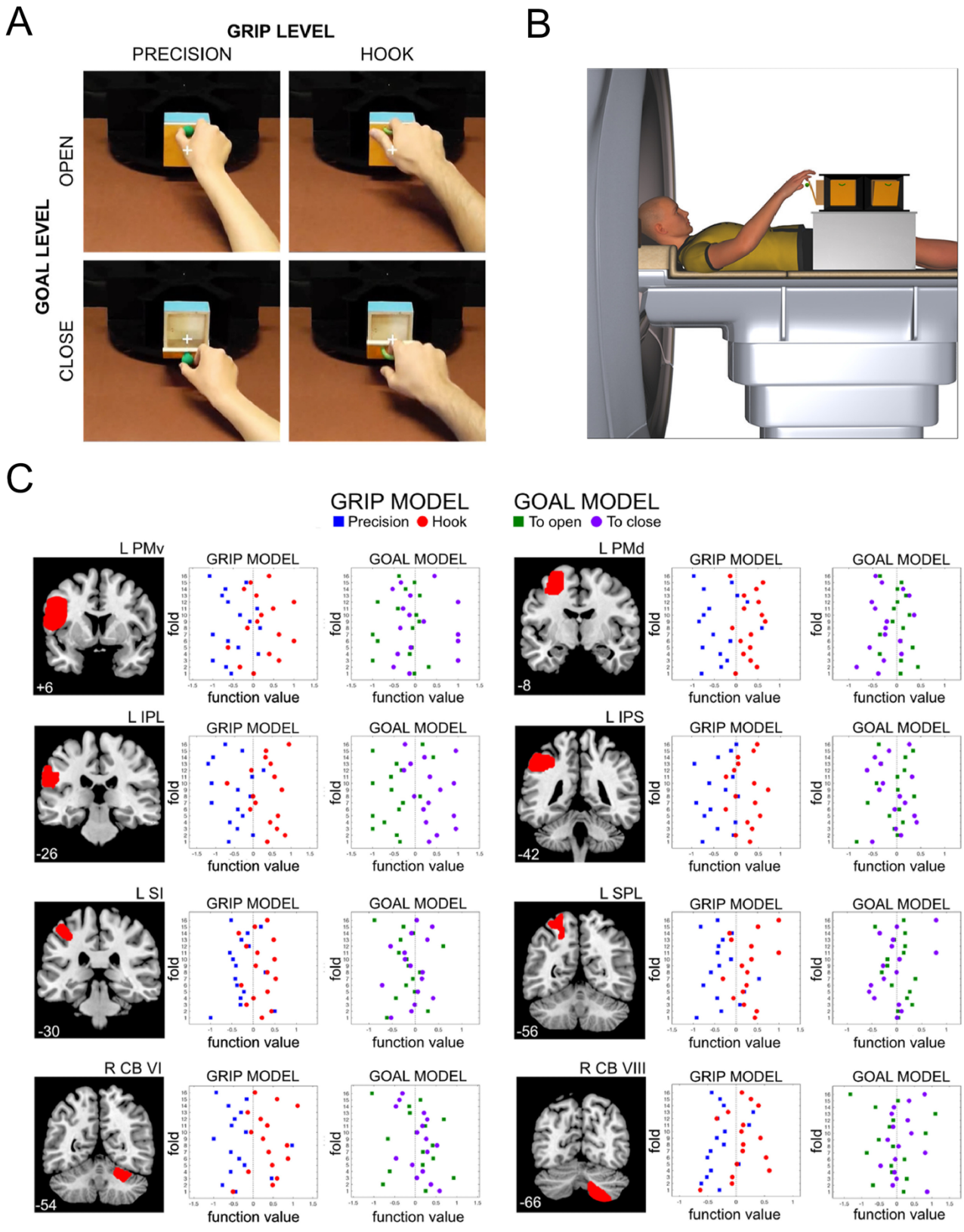

Figure 11. Stimuli, experimental setting inside the MRI scanner and multivoxel pattern analysis results. (A) Static frames of video stimuli representing the combination of different grips (precision, hook) and goals (open, close). (B) Experimental setting during the execution task. (C) Results of multivoxel pattern analysis in different ROIs for both the goal and grip model. A support vector

machine algorithm was trained to find the optimal boundary between classes within each model. Plots show the output value of the machine decision function for each fold (modified from Errante et al., 2021a).

1.4 Neural correlates of biological motion coding

Studies focusing on action observation, described in humans a more extensive network composed by a series of cortical and subcortical brain regions, collectively known as the action observation network (AON), comprising PMv, PMd, IPS, IPL, SPL, the primary somatosensory cortex (SI), occipito-temporal regions (middle temporal gyrus [MT]), the posterior sector of the superior temporal sulcus (pSTS), and the lateral portion of the cerebellum (Abdelgabar et al., 2019; Caspers et al., 2010; Errante & Fogassi, 2020; Filimon et al., 2007; Gazzola & Keysers, 2009; Hardwick et al., 2018; Molenberghs et al., 2012). Some of these areas, mostly overlapping with those of the MNS were not only involved in goal coding, but as previously mentioned, also in elaborating other features of the observed actions such as the context in which these are performed or their kinematic features. The ability to decode the kinematics of observed actions relies on the processing of biological motion (BM) in the temporal cortex, as evidenced by research on both primates and humans (Perrett et al., 1989; Puce & Perrett, 2003) (Figure 12). The ability to perceive and interpret BM is an indispensable tool for successful social interaction and nonverbal communication.

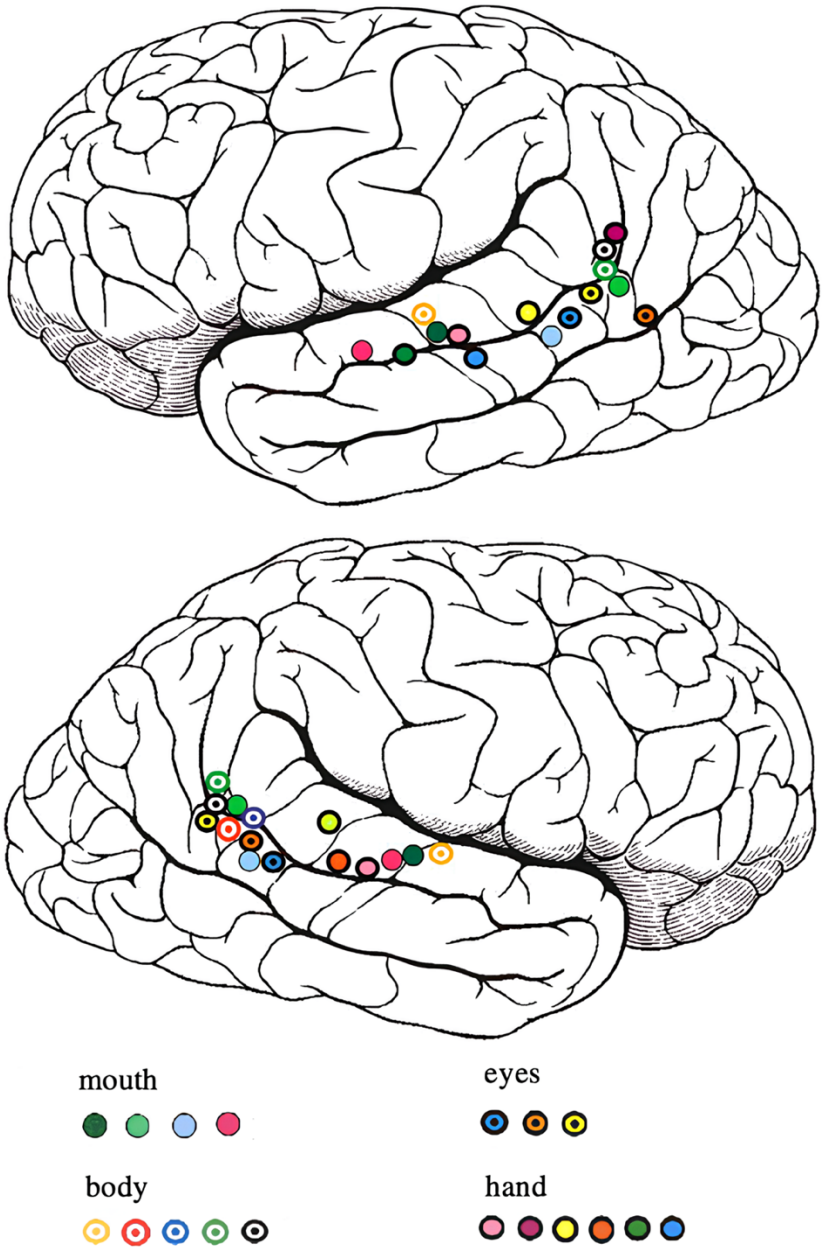

Figure 12. Bilateral activation loci of superior temporal sulcus during the observation of biological motion. Circles of different color correspond to centers of activation identified in different studies (modified from Puce & Perrett, 2003).

1.4.1 Analysis of biological motion in non-human species

Studies on motion sensitivity in monkeys showed the presence of neurons located in the STS that responded to object, faces as well as body motion and rotation. Some neuronal population showed selectivity for translational movements on three orthogonal axes centered on the monkey, others were

selective for rotations on one or more axes, thus, suggesting that this area plays a critical role in processing visual motion information (Perrett et al., 1985). This brain region contains cells with very broad visual receptive fields and derives its input from both dorsal and ventral occipito-temporal areas such as MT (Boussaoud et al., 1990; Felleman & Van Essen, 1991). Subsequent studies on STS cells, highlighted the fact that the integration of form and motion is widespread, and that STS is thus quite heterogeneous with several cells specializing in processing of both limb and whole-body motion (Carey et al., 1997; Jellema et al., 2002; Jellema et al., 2000; Jellema & Perrett, 2002). Most of the biological motion-tuned neurons in STS is highly selective for particular combination of body movements and postures (Jellema et al., 2004; Oram & Perrett, 1996) rendering them, action viewpoint specific. However, numerous STS neurons exhibit consistent responses to a variety of visual changes in the observed scene such as changes in viewing perspective, alterations in stimulus size (corresponding to near versus distant viewing), and position within the visual field (Jellema & Perrett, 2006).

1.4.2 The point-light displays technique

The STS's specialization for processing biological motion suggests that this brain area possess a remarkable ability to extract rich information about actions from visual cues. This is particularly evident during the perception of kinematic properties of biological motion in absence of pictorial contents, as when presented by means of point-light displays (PLDs) technique (Johansson, 1973) (Figure 13).

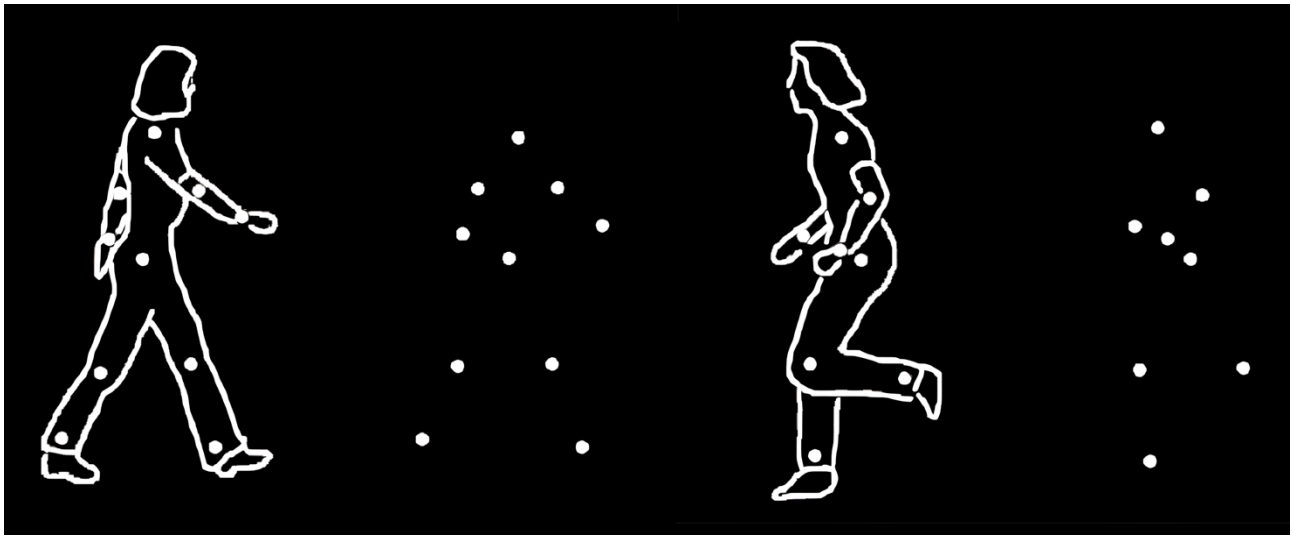

Figure 13. Illustration of point-light displays biological motion stimuli (modified from Puce & Perrett, 2003).

The stimuli represented using this technique, generally consist of small, illuminated dots attached to the joints of a moving body. Despite the absence of any pictorial information, PLDs can still convey motion and kinematic features of biological movement. Behavioral studies employing such technique, have demonstrated that the motion information presented by PLDs is sufficient to discriminate between biological and nonbiological actions (Hiris, 2007; Johansson, 1973; Lapenta et al., 2017) as well as to code specific features of the observed stimuli such as the gender or emotional state of the depicted individual, as well as the amount of effort that is exerted during actions like lifting a weight (Chouchourelou et al., 2006; Kozlowski & Cutting, 1977; Shim et al., 2004). For example, even with minimal visual information, people can accurately infer the emotional content of a ballet from the movement of a dancer's body (Dittrich et al., 1996). This ability is not restricted to the adult human brain. Several studies showed that human infants as young as 3 months old (Fox & McDaniel, 1982) and several other animal species such as rhesus monkeys (Oram & Perrett, 1994), newborn domestic chicks (Regolin et al., 2000; Vallortigara & Regolin, 2006; Vallortigara et al., 2005), as well as bottlenose dolphins (Herman et al., 1990), are able to perceive biological motion through point-light displays.

1.4.3 Neuroimaging evidence of biological motion coding

Both electrophysiological and neuroimaging studies have shown that whole-body PLDs stimuli can convey enough information about human body movements to activate areas belonging to the AON with activation patterns similar to those observed during the presentation of fully visible stimuli. In fact, areas such the lateral occipito temporal cortex (Grossman & Blake, 2002; Jastorff & Orban, 2009; Peelen et al., 2006; Peuskens et al., 2005), and sectors of the parietal (Bonda et al., 1996; Grezes et al., 2001) and frontal cortices (Saygin et al., 2004) responded to PLDs stimuli. In a very comprehensive series of fMRI experiments, Peuskens and colleagues (2005) examined which brain regions exhibited specific activation for biological motion as compared to non-biological one. Stimuli consisted in whole-body biological representation of a walking action and several control conditions such as scrambled, translational and rotational motion, representation of a body silhouette with and without implied motion and action words. The first experiment described in this latter study, mainly focused on the analysis of biological motion while the others were aimed at disentangling features of complex motion and implied action representations. Collectively, the results demonstrate STS activation in processing human biological motion as compared to non-biological motion. Furthermore, also both inferior temporal gyrus and the middle temporal gyrus exhibited stronger activation patterns when comparing biological motion to scrambled motion, suggesting that these areas collectively play a key role in the elaboration of biological motion presented by means of PLDs. Another cortical area involved in the analysis of biological motion is the premotor cortex. An fMRI study by Saygin and colleagues (2004) demonstrated the involvement of frontal areas in coding PLDs biological motion. The experiment consisted in biological, non-biological and static conditions. The whole-body actions presented were, for example, walking, jumping and skipping. The observation of PLDs biological motion compared to scrambled motion, elicited a strong activation response in bilateral sectors of the premotor cortex and inferior frontal gyrus (Figure 14).

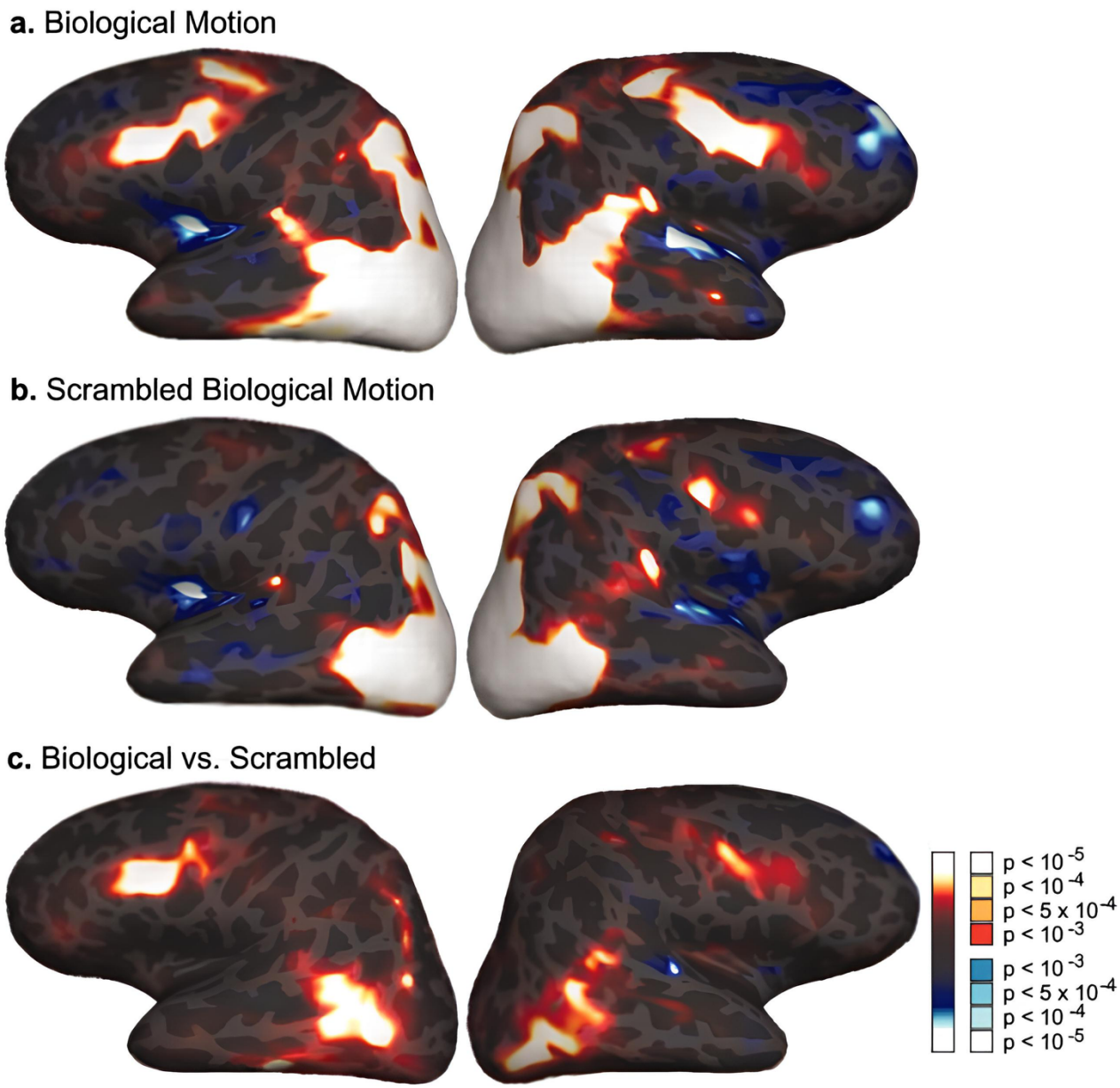

Figure 14. Group activations overlaid on an inflated brain render. (A) Activation maps of biological motion vs baseline; (B) non biological (scrambled) motion vs baseline; (C) contrast between biological motion vs non-biological motion showing the significant bilateral activations of the premotor cortex as well as the lateral occipto-temporal cortex (from Saygin et al., 2004).

These findings support previous results demonstrating that the perception of biological movements represented by means of PLDs, although lacking pictorial information, activate brain regions involved in action perception, demonstrating their sensitivity to specific features of the observed actions.

1.4.4 Correlates of biological motion revealed by electrophysiological measures

Ulloa and Pineda (2007) using EEG, investigated whether a desynchronization of mu rhythm, which is related to MNS activity, underlies sensory-motor processes evoked by the elaboration of PLDs biological motion. Results showed that the observation of PLDs actions produces mu suppression while non biological stimuli (consisting of scrambled versions of the same stimuli) did not, suggesting MNS role in representing human actions from limited kinematic visual cues. The transient and reversible disruption of STS activity by means of repetitive TMS, allowed to investigate sensitivity to biological motion during the observation of PLDs stimuli. Grossman and colleagues (2005) presented volunteers with biological whole-body PLDs movements, and non-biological motion controls stimuli, both embedded in a noise array. Participants were required to discriminate biological motion. Their ability to correctly identify biological motion was significantly impaired following pSTS stimulation. On the other hand, their performance did not change during the discrimination of non-biological motion controls stimuli, and when the TMS stimulation was delivered over visual area MT, thus further demonstrating STS role in biological motion perception. A TMS study from Van Kemenade and colleagues (2012) using continuous theta burst stimulation, investigated the role of STS and of the premotor cortex in biological motion processing. Participants were required to identify a walking action represented as PLDs amid various levels of noise. Results not only confirmed the decrease in sensitivity for biological motion PLDs after STS stimulation but showed the same findings when pulses were delivered to premotor sites. Authors propose that the significant reduction of sensitivity during biological motion perception after the stimulation of the premotor cortex, suggests its role in modulating the response to biological motion processing.

1.4.5 Biological motion analysis impairments in patients

Lesion studies on patients, although often limited by small samples, are generally in agreement with the previously described electrophysiological and neuroimaging literature. Case

studies on patients with bilateral lesions of the occipito-temporal and occipito-parietal cortices, indicate patients' impaired ability in identifying human actions presented as PLDs (McLeod et al., 1996; Vaina et al., 1990). Furthermore, unilateral damage to the inferior parietal cortex, right temporal lobe (Vaina & Gross, 2004), multiple lesions of superior parietal, lateral temporal, and medial frontal areas (Battelli et al., 2003), have been linked to impairments in biological motion perception. One study on 60 stroke patients with unilateral lesions, found that premotor and parietal, as well as temporal regions, such as STS, are linked to BM perception deficits (Saygin, 2007).

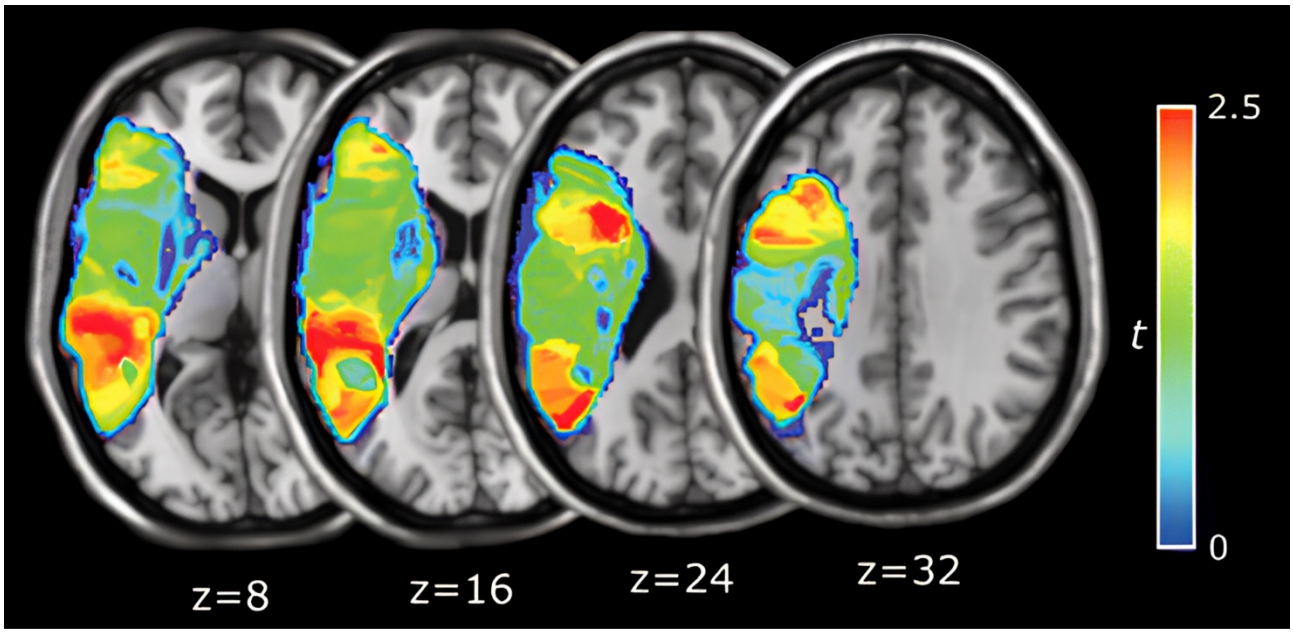

Figure 15. Axial slices showing the *t*-statistic values of the voxel-based lesion-symptom mapping analysis computed between the accuracy scores during the biological motion detection task of lesioned and intact patients. At high *t*-scores, corresponds a significant effect of lesion on biological motion perception (from Saygin, 2007).

Aims and hypothesis

The main aim of this thesis is to investigate the role of the AON in decoding differences in kinematic features of observed PLDs actions. One of the main hypotheses is that the observation of PLDs grasping actions stimuli would elicit activations in the AON similar to those observed in response to fully visible (FV) videos. Thus, the kinematic information conveyed by the observation of such visually impoverished stimuli, is sufficient to elicit a complete action representation. Another hypothesis is that is possible to decode, within the AON, differences in specific kinematic features of the observed PLDs grasping action, namely direction and velocity, and that specific areas of the AON would contribute differentially to the elaboration of variations in such kinematic characteristics.

It is well established that the observation of another's FV action, activates a series of brain regions of the AON. Some of these areas play a key role in generating in the observer an internal motor resonance with the observed action (Rizzolatti et al., 2014) while others take part in the elaboration of additional features of the observed actions such as kinematics (Errante et al., 2021a; Filimon et al., 2007; Koul et al., 2018) which could be studied using point-light displays (Johansson, 1973) that allow to convey only kinematic information about the observed action. Previous neuroimaging studies demonstrated that some AON areas are recruited by the elaboration of kinematic information conveyed by whole-body PLDs (Peelen et al., 2006; Peuskens et al., 2005; Saygin et al., 2004). It is worth noting that these focused mainly on the investigation of the differences between whole-body biological and non-biological motion perception.

The first study in this thesis investigates the possible differential recruitment of the AON areas during the observation of PLDs versus FV hand grasping actions (Ziccarelli et al., 2022). We focused on transitive actions performed with the upper limb and not on whole-body intransitive actions, which

were often used as experimental stimuli in previous literature. Furthermore, our comparison is not between biological and non-biological stimuli but between biological PLDs and FV stimuli, thus allowing to demonstrate the importance of kinematic feature decoding for understanding and representing another's action. We presented participants with PLDs and FV grasping stimuli and several control conditions for each set of stimuli, allowing us to control for multiple confounding effects such the amount of visual information, direction of motion and context.

The first hypothesis was that information conveyed by PLDs videos is sufficient to elicit an activation of the AON comparable to that of FV stimuli suggesting that also PLDs stimuli evoke a full action representation. Thus, the BOLD signal intensity would be comparable between the main experimental conditions in AON regions.

The second hypothesis was that the neural patterns distribution evoked by the main experimental conditions could be disentangled, within the AON, by means of machine learning approaches. This finding would provide compelling evidence that in specific AON regions there is sufficient information to effectively disentangle between PLDs and FV stimuli features.

Although some studies sought to investigate differences between action kinematics during the observation of fully visible stimuli (Errante et al., 2021a; Grafton & Hamilton, 2007), to our knowledge, there are currently no studies investigating the modulation of AON activation during the observation of PLDs biological grasping actions performed with changes in kinematic parameters, such as direction (right and left) and velocity (fast and slow). The overarching aim of the second study of this thesis was to investigate the role of the AON in kinematic features encoding, by combining both univariate and multivariate analyses.

Specifically, the first hypothesis was that differences in direction and velocity kinematic parameters would activate different sectors of the AON. This would demonstrate that there are regions mainly recruited in coding differences in directions and others in coding differences in velocities.

The second hypothesis was that both direction and velocity, as well as their combinations, are significantly decoded at the network level. A further, subsequent hypothesis was that specific regions of the AON would contribute differently to the decoding of kinematic differences between directions and velocities.

The results of this thesis could be relevant in providing compelling evidence for the involvement of specific regions in encoding and interpreting kinematic information during action observation laying the groundwork for investigating the neural mechanisms underlying action imitation and motor learning, based on the observation of stimuli conveying only kinematic information, such as PLDs.

2. Study 1: Decoding point-light displays and fully visible hand grasping actions within the action observation network

2.1 Abstract

Action observation typically recruits visual areas and dorsal and ventral sectors of the parietal and premotor cortex. This network has been collectively termed as action observation network (AON). Within this network, the elaboration of kinematic aspects of biological motion is crucial. Previous studies investigated these aspects by presenting subjects with PLDs videos of whole-body movements, showing the recruitment of some of the AON areas. However, studies focused on cortical activation during observation of PLDs grasping actions are lacking. In the present fMRI study, we assessed the activation of AON in healthy participants during the observation of both PLDs and fully visible hand grasping actions, excluding confounding effects due to low-level visual features, motion and context. Results showed that the observation of PLDs grasping stimuli elicited a bilateral activation of the AON. ROI analyses performed on visual and sensorimotor areas showed no significant differences in signal intensity between PLDs and fully visible experimental conditions, indicating that both conditions evoked a similar motor resonance mechanism. Multivoxel pattern analysis (MVPA), revealed significant decoding of PLDs and fully visible grasping observation conditions in occipital, parietal and premotor areas belonging to AON. Data show that kinematic features conveyed by PLDs stimuli are sufficient to elicit a complete action representation, suggesting that these features can be disentangled within the AON from the features usually characterizing fully visible actions. PLDs stimuli could be useful in assessing which areas are recruited, when only kinematic cues are available, for action recognition, imitation and motor learning.

2.2 Introduction

During the observation of an action performed by another individual, a mechanism provided by the MNS allows the observer to automatically understand another's action by matching its visual description onto one's own motor representation of the same action (Rizzolatti et al., 2014). Mirror neurons have been originally found in monkey ventral premotor cortex (F5) and then in the inferior parietal lobule (PFG) (Di Pellegrino et al., 1992; Fogassi et al., 2005); subsequently, neurons with mirror properties have been found in other cortical areas, such as, for example, the anterior intraparietal area (AIP) (Lanzilotto et al., 2019; Maeda et al., 2015), dorsal premotor cortex (PMd) (Papadourakis & Raos, 2019; Tkach et al., 2007) and pre-supplementary motor cortex (pre-SMA) (Lanzilotto et al., 2016; Yoshida et al., 2011).

By using electrophysiological and neuroimaging techniques, a comparable parieto-premotor MNS has been described also in humans, homologous to that of monkeys, that includes the ventral premotor cortex (PMv) plus the inferior frontal gyrus (IFG) and the inferior parietal lobule (IPL) (Molenberghs et al., 2012). Further studies demonstrated that mere action observation recruits an extended network of cortical and subcortical areas, collectively called AON, including PMd, a sector of intraparietal sulcus (IPS), superior parietal lobule (SPL), primary somatosensory cortex (SI), occipitotemporal areas (middle temporal area (MT)), posterior superior temporal sulcus (pSTS), and the lateral part of cerebellum (Abdelgabar et al., 2019; Errante & Fogassi, 2020; Filimon et al., 2007; Gazzola & Keysers, 2009); see also (Caspers et al., 2010; Hardwick et al., 2018; Molenberghs et al., 2012).

Within the AON, there are parietal and frontal areas crucial for generating in the observer an internal motor resonance with the observed action (Rizzolatti et al., 2014). Some of these areas have also been proposed to take part in the elaboration of additional features of the observed actions (Kemmerer, 2021), including kinematics (Filimon et al., 2007; Koul et al., 2018), type of grip used to achieve the final action goal (Errante et al., 2021a; Grafton & Hamilton, 2007) and contextual information (Amoruso et al., 2016; Iacoboni et al., 2005).

The decoding of the kinematic aspects of observed actions relies on the elaboration of biological motion by high order visual areas located in the inferotemporal cortex, as it has been clearly demonstrated in both monkeys and humans (Caspers et al., 2010; Perrett et al., 1989). The outcome of this elaboration is then provided to the AON. Interestingly, within this latter network, the PMd sector has been shown to play a role in decoding observed actions complying with the "two-thirds power law" (Casile et al., 2010), which describes the relation between the speed and the trajectory of biological movements (Lacquaniti et al., 1983). According to this law, the movement velocity depends on the trajectory curvature, namely velocity is lower in more curved parts than in less curved parts of the trajectory. One method that allows to study the kinematic properties of biological motion, in absence of pictorial content, is that of PLDs (Blake & Shiffrar, 2007; Johansson, 1973; Pavlova, 2012; Thornton, 2006). Using this technique, consisting in small lights attached to the main joints of one's body on a dark background, so that only the lights are visible, it is possible to present visually impoverished stimuli of several human behaviors. Behavioral data showed that motion information conveyed by PLDs is enough to distinguish biological from non-biological actions (Hiris, 2007; Johansson, 1973; Lapenta et al., 2017) and also to recognize features such as, for example, the gender or the emotional state of the observed agent, or the effort exerted when lifting a weight (Chouchourelou et al., 2006; Kozlowski & Cutting, 1977; Shim et al., 2004). Furthermore, the results of previous electrophysiological and neuroimaging studies employing whole-body PLDs stimuli suggested that these latter can convey sufficient information about movements of the human body to activate sensory-motor processes within some of the areas of the AON, similar to those typically involved during fully visible action observation (Bonda et al., 1996; Grossman & Blake, 2002; Peelen et al., 2006; Peuskens et al., 2005; Saygin et al., 2004; Ulloa & Pineda, 2007; van Kemenade et al., 2012). Interestingly, not only human adults are able to perceive ad extract information by PLDs, but also human infants (Pavlova et al., 2001; Simion et al., 2008) and even monkeys (Jastorff et al., 2012).

This technique has also found important applications in the clinical field. For example, recent evidence on people with autism spectrum disorder shows that deficits are particularly evident when

biological motion is needed to infer intention, action goal or emotion from an observed action (Federici et al., 2020). The authors also propose that an analysis of the distinct levels of biological motion by means of PLDs technique, aimed at assessing brain processing of specific spatio-temporal components of the action, may be useful for deepening the understanding of this syndrome, laying the foundation for future clinical investigations in early infancy.

Most of neuroimaging evidence obtained during observation of PLDs concerns only whole-body movements, while very few studies focused on upper limb actions. One of them, by Lestou and colleagues (2008) investigated with fMRI the brain activation obtained during observation of upper limb PLDs actions (such as knocking, lifting, waving, throwing) combined with their mental simulation. The study showed the activation of several areas including IPL, SPL, PMv, as compared to mere observation. However, the results of pure observation are not explicitly reported. Another study, performed by Quadrelli and colleagues (2019) with electroencephalographic technique, showed that in nine-months infants it is possible to elicit an attenuation of alpha band activity during the observation of the reaching phase of a silhouette of a grasping action, suggesting that this type of stimulus is able to elicit a motor resonance mechanism. Altogether, these studies suggest that the motor system can be activated by observation of impoverished version of upper limb actions.

The present fMRI study aimed at investigating the activation of the AON in healthy human participants during mere observation of hand grasping actions presented in PLDs version *vs* fully visible version, in order to reveal, at the level of cortical activation, the importance of the decoding of kinematic features for understanding others' actions. The use of several control conditions allowed us to assess more precisely the role of AON areas in encoding grasping action features in both PLDs and fully visible stimuli, excluding confounding effects due to low level visual features, motion and contextual information. To address the specific contribution of different AON areas in the encoding of PLDs and fully visible actions, we used a combined approach based on univariate analysis and multivariate pattern analysis (MVPA), this latter allowing to extract finer grain information. Using this latter approach, we were able to investigate whether information encoded in AON areas during

the observation of PLDs and fully visible stimuli could be disentangled with machine learning approaches.

2.3 Materials and Methods

2.3.1 Participants

Twenty-three healthy human volunteers (12 female; mean age 25.5 years; range 21-32 years) with no history of neurological or orthopedic disorders, and of drug or alcohol abuse, participated in the study. All participants were right-handed according to the Edinburgh Handedness Inventory (Oldfield, 1971). Informed consent was obtained in accordance with Helsinki declaration. The study was approved by the local ethics committee (Comitato Etico Area Vasta Emilia Nord – AVEN; code NEUROIMAGE_UNIPR).

2.3.2 Stimuli

Experimental stimuli consisted of video events showing grasping actions either fully visible (Fully visible set) or as point-light displays (Point-light displays set). All videos lasted 2s.

Fully visible set

In this set, videoclips showed a FV human right hand grasping an object (*FV_Grasp*) (Figure 16A). Videos were recorded from a lateral perspective (90° angle) in a well-lit environment on a neutral background by means of a digital HD camera (© GoPro, Inc., USA) with a frame rate of 25/s and a resolution of 1920x1080p. In order to use a wide set of stimuli, we recorded 4 grasping actions each performed with a different grip (whole hand, five-fingers grip, three-fingers grip and precision grip) congruent with the size of the object to be grasped, for a total number of 16 grasping videos. The first static frame of each grasp stimulus was used as a control condition (*FV_Static*).

To control for possible effects due to velocity and direction of motion of the observed stimuli, a box-like stimulus moving in the same direction at linear velocity, with colors and size/shape similar

to those of a human arm, was created using an image editing software (© Affinity Photo v 1.6.7, Serif Europe Ltd) and animated in Final Cut Pro X (v 10.5.1, Apple Inc.) (*FV_Box*). In order to create *FV_Box* videos, first we carried out 2D kinematic analysis (© Tracker v 5.1.5, 2020, Douglas Brown) to calculate the velocity profile of the wrist in each grasping video (Figure 16C). Then we used these velocity data to animate the box, maintaining the same direction and mean velocity of each *FV_Grasp* video. Thus, the experimental grasping videos and the box control condition were matched for movement direction and mean velocity.

A further control condition was the scrambled version of *FV_Grasp* videos (*FV_Scrambled*). This was realized using an ad hoc script capable of dividing each frame of the experimental stimuli in squares of 10x10 pixels and randomize the position of each square in each frame, so that the basic visual features (e.g. contrast, luminance, color, etc.) were the same of the original video, but the contents of the latter were no longer recognizable (Figure 16A).

Point light displays set

In this set, videoclips showed PLDs stimuli created starting from FV stimuli in order to reduce at minimum the pictorial aspects of the stimulus, keeping the same kinematic features (Figure 16B). In order to accurately match joints trajectory, grasping stimuli were realized by tracking the movement of the hand joints for each frame, using the tracker feature included in Motion software (v 5.5.1, Apple Inc.) and by placing, on each joint, a white point of 9 px diameter (*PLD_Grasp*). The first static frame of each PLD grasp stimulus was used as a control condition (*PLD_Static*) (Figure 16B). The PLDs box-like stimuli were created by overlapping a series of white points (ø 9 px) to the edges of the FV box, forming a silhouette of the box shape (*PLD_Box*).

The same ad hoc script used for FV stimuli was used to randomize the position of each square in each frame of the PLDs grasping stimuli so that the point configuration was not recognizable in spite of the same amount of visual basic information (*PLD_Scrambled*).

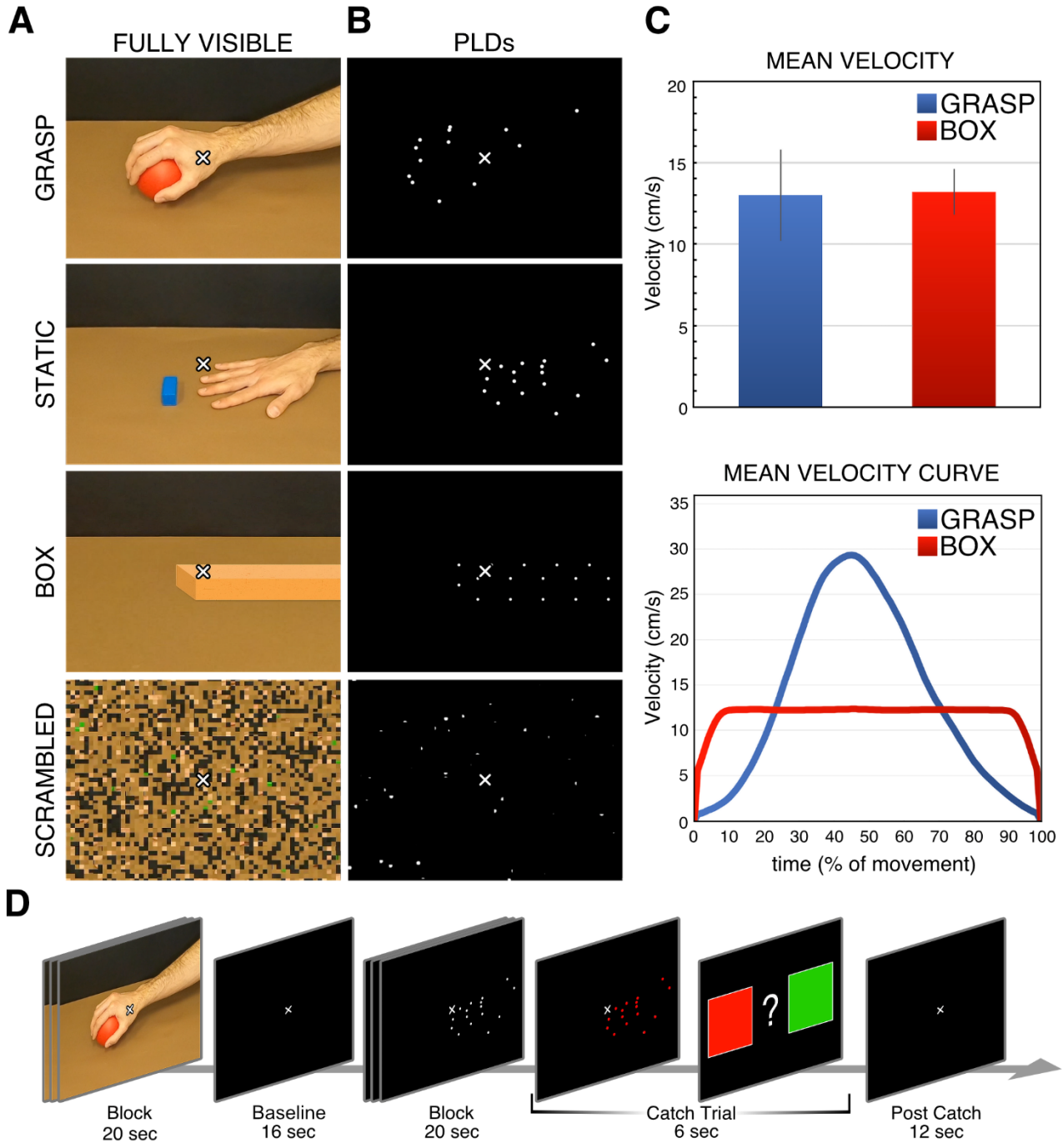

Figure 16. Stimuli and paradigm. Illustrations of fully visible (A) and point light displays (B) sets including experimental and control stimuli. (C) Top. Mean wrist velocity of all grasping actions and matched mean box velocity. Bottom. Velocity profiles of the wrist and the box, the latter moving linearly. (D) Action observation paradigm, presented in six functional runs, formed by independent blocks of 20 s, each consisting of ten randomly presented videos of the same condition, alternated with a baseline period of 16 s.

2.3.3 fMRI task

Before fMRI scanning, participants were briefly informed about the scanning procedure in order to help them to familiarize with the experimental environment and setting. During MR scanning, they laid supine in the bore of the scanner in a dimly lit environment.

The experiment was performed in a single imaging acquisition session divided in six functional runs each lasting 4 minutes and 56 seconds (148 volumes) during which participants had to observe the video stimuli presented by means of a digital goggles system (Resonance Technology, Northridge, CA) (60 Hz refresh rate) with a resolution of 800 horizontal pixels x 600 vertical pixels and horizontal eye field of 30°. To dampen scanner noise, sound-attenuating (30 dB) headphones were employed. During the whole imaging session, a white cross was presented in the center of the screen, and participants were instructed to fixate it. Each run was acquired using a block paradigm. Each block lasted 20 s and comprised 10 videos of the same experimental or control condition. During a single run, a total of 8 blocks were presented, one for each condition. A total of 48 blocks were presented during the whole imaging session, for a total of 480 trials (60 trial per condition). Blocks were interleaved by a fixation no-videoclip event lasting 16 s used as baseline during which only the fixation cross at the center of a black background was visible.

In order to monitor participants' attention to the visual stimuli, catch trials were presented, in 25% of the blocks, equally distributed among all conditions. During the catch trial, participants observed a video stimulus (2 s duration) whose color was altered by applying a color correction filter (blue, red, green) (Final Cut Pro X 10.5.1, Apple Inc.), after which they had to indicate the main color of the stimulus, using a response pad, by selecting one of the two options presented on the screen (4 s time window). On all valid given answers, participants were accurate 99% of the times. In order to remove potential signal artifacts due to the hand movement, a 12 second signal denoising period (post-catch), in which participant had to remain still, followed the attention task (Figure 16D).

2.3.4 fMRI data acquisition

Both Anatomical T1-weighted and functional T2*-weighted MR images were acquired with a 3T General Electric scanner (MR750 Discovery) equipped with an 8-channel receiver head-coil. Functional volumes were acquired with the following parameters: 40 axial slices of functional images covering the whole brain acquired in an interleaved bottom-up order using a gradient-echo echo-planar imaging (EPI) pulse sequence, slice thickness = 3.0 mm, interslice gap = 0.5 mm, 64 ×64 ×37 matrix with a spatial resolution of 3.5 ×3.5 ×3.5 mm, TR = 2000 ms, TE = 30 ms, FOV = 205 ×205 mm^2, flip angle = 90°, in plane resolution = 3.2 ×3.2 mm^2. A morphological 3D T1-weighted (Bravo_Mik) volume was acquired as anatomical reference. Its acquisition parameters were: 192 slices, 512 x 512 matrix, spatial resolution 0.9 x 0.5 x 0.5mm, TR = 9700 ms, TE 4 ms, FOV = 252 x252 mm, flip angle 90°.

2.3.5 fMRI data analysis

Data Preprocessing and Analysis

Processing was carried out using SPM12 (Wellcome Department of Imaging Neuroscience, University College, London, UK; http://www.fil.ion.ucl.ac.uk/spm) on MATLAB R2017a (The Mathworks, Inc.). The first four volumes of each run were discarded to allow T1 equilibration so that magnetization could reach a steady state. For each participant, all volumes were preprocessed using the same standard pipeline. Images were spatially realigned to the first volume of the first functional run and un-warped to correct for between scan motion, and slice timing corrected considering slice acquisition order. Spatial transformation parameters derived from the segmentation and spatial normalization of the anatomical T1-weighted images to the Montreal Neurological Institute (MNI) space were then applied to the realigned EPIs and re-sampled in 2 ×2 ×2 mm^3 voxels using a 4^{th} degree B-spline interpolation in space. Lastly, all functional T2*-weighted volumes were spatially smoothed with an 8-mm full-width half-maximum isotropic Gaussian kernel (FWHM).

Data were analysed using a random-effects model (Friston et al., 1999), implemented in a two-level procedure. In the first level analysis, single-subject fMRI time series were modelled using the general linear model. The design-matrix included the onsets and the durations of all experimental and control condition as well as the response of catch trial conditions for each of the six functional runs. Each predictor (*FV_Grasp, FV_Static, FV_Box, FV_Scrambled, PLD_Grasp, PLD_Static, PLD_Box, PLD_Scrambled*), including ten consecutive videos in a block, was modelled as a single epoch lasting 20 s. The catch trials were modelled as consecutive blocks lasting 18 s (*Catch_Trial;* 2 s color altered stimulus, 4 s explicit response, plus 12 s post-catch signal denoise period). Rest periods between blocks were considered as implicit baseline. Contrasts between each experimental/control condition *vs* implicit baseline were calculated. Specific effects were tested using *t* statistical parametric maps, with degrees of freedom corrected for non-sphericity at each voxel. In the second level group-analysis, corresponding *t*-contrast images of the first-level conditions, except for *Catch-Trial*, were entered into a flexible ANOVA with sphericity-correction for repeated measures (Friston et al., 2002). In particular, since we did not want to test for all possible main effects and interactions, we modelled two factors specifying our scans and conditions, corresponding to: a) subjects, modelling participants variability; b) conditions, modelling task effects.

Within this model, in order to exclude the confounding effects due to the context, direction, mean velocity of the movement and low-level visual processing, the activation maps resulting from the contrast between experimental condition *FV_Grasp* and its corresponding control conditions (*FV_Static, FV_Box, FV_Scrambled; collectively termed as FV_Ctrls*) were calculated. In addition, *PLD_Grasp* condition was contrasted with its corresponding PLDs controls (*PLD_Static, PLD_Box, PLD_Scrambled; collectively termed as PLD_Ctrls*). The rationale for this type of analysis is that experimental stimuli were embedded with information about (a) the context in which the action was performed, (b) kinematic aspects, for example, velocity and movement direction and (c) low level visual characteristics. All these features are concurrent and collectively contribute to the encoding of the grasping action. Thus, the subtraction of these characteristics altogether allowed us to better assess

which areas mostly contribute to the encoding of grasping actions, after excluding confounding effects.

Significant brain activations shared between FV and PLD contrasts, were assessed by means of a conjunction analysis (*FV_Grasp vs FV_Ctrls ∧ PLD_Grasp vs PLD_Ctrls*) revealing cortical areas involved in both experimental conditions. In order to highlight general significant cortical activation for FV or PLDs contrasts, a global analysis was conducted (*FV_Grasp vs FV_Ctrls & PLD_Grasp vs PLD_Ctrls*) (see ROI analysis below). Statistical inference was drawn at a voxel level, corrected with Family-Wise Error (FWE) with a threshold of $P < 0.01$.

Lateralization index analysis

In order to assess activation pattern distribution between the two hemispheres, we performed a lateralization analysis using LI-toolbox (Wilke & Lidzba, 2007). This index is computed, firstly, by calculating the number of voxels surviving a statistical threshold in each hemisphere and then applying the formula $(\Sigma_{left} - \Sigma_{right})/ (\Sigma_{left} + \Sigma_{right})$, yielding a lateralization index value ranging from -1 to 1. Positive values correspond to left lateralization, whilst negative values correspond to right lateralization.

Contrast images of PLDs and FV grasping conditions from each subject were entered as input in the toolbox and one default value threshold ($t = 3$) was applied to all images. An inter-hemispheric exclusive mask of +/-5mm was applied, masking out the midline. Finally, the lateralization index was computed following the previously described formula.

ROI selection and analysis

To examine potential differences between BOLD activations in FV and PLDs conditions, a region of interest (ROI) analysis was performed. ROIs were selected using an anatomical approach starting from the group level results of the global analysis. Brain areas revealed by global analysis were determined by means of cytoarchitectonic probabilistic maps of the human brain using SPM-

Anatomy toolbox v. 2.1 (Eickhoff et al., 2005). In order to determine which anatomical areas were included in the activation map, global analysis pattern was overlayed onto cytoarchitectonic probabilistic maps and the cytoarchitectonic area corresponding to the maxima of each cortical cluster, plus adjacent areas with a high assigned probability, were selected. This allowed the selection of 19 cortical ROIs, located in left hemisphere (see Fig. 4, 5, 6, for a visualization of ROI positions).

ROIs masks were created using Anatomy toolbox v. 3.0 (Eickhoff et al., 2005), Automated Anatomical Labelling atlas (AAL) included in the WFU-PickAtlas Toolbox (https://www.nitrc.org/projects/wfu_pickatlas; (Maldjian et al., 2003)), the Human Motor Area Template (HMAT; http://lrnlab.org; (Mayka et al., 2006)) and Brainnetome Atlas (https://www.nitrc.org/projects/bn_atlas; (Fan et al., 2016)). To preserve only the voxels within the activation pattern, we used a masking procedure provided by MRIcron software (https://www.nitrc.org/projects/mricron). In addition, a spherical ROI built in the white matter (CTRL_WM; r = 4.5 mm, x = -20, y = 42, z = 2) was used as control and created by means of MarsBaR software for SPM (http://masbar.sourceforge.net/).

The average BOLD signal change across all significant voxels was extracted separately in each ROI using the SPM Rex Toolbox (http://web.mit.edu/swg/rex). BOLD signal change was compared between all conditions by means of repeated measures ANOVAs. Significant differences were assessed with post-hoc comparisons computation by using paired-sample *t*-test with *Bonferroni* correction for multiple comparisons.

Multivoxel pattern analysis

To detect all fine information included in the fMRI data patterns, MVPA was conducted on the un-smoothed normalized T2* functional brain images using Pattern Recognition for Neuroimaging Toolbox (PRoNTo v.2.1; (Schrouff et al., 2013)), a MATLAB (The MathWorks Inc.) based toolbox.

The intensity value of each voxel (*feature*) is represented as a series of points in a multidimensional space (*feature space*). Then a classifier algorithm is trained and employed to find the optimal separating boundary between the *features*, associated to a categorical label corresponding to the experimental conditions, in the feature space. After training and testing the classification model, which consists of applying a trained model to the tested set of data, the classifier returns a predicted label for different brain patterns. The performance of the classifier in discriminating between different conditions is assessed on new data not previously used to train it.

In order to perform MVPA analyses, the experimental design elements, i.e. *labels*, *onsets*, *duration* and *number* of each block and *interscan interval* were specified. The un-smoothed normalized T2* functional brain images belonging to the experimental conditions (*FV_Grasp* and *PLD_Grasp*) for each subject were selected (1380 volumes total) and then a first level mask, including only voxels containing relevant features and discarding those with non-relevant information, i.e., voxels outside the brain, was applied to the data. Successively, a linear kernel included in PRoNTo toolbox, was used to compute a similarity matrix. The kernel function, by calculating the dot product of each *feature* in pairs, returns a value characterizing the similarity between each pair, creating a kernel matrix of the feature space. A first degree polynomial detrending was applied to the data since fMRI data represent continuous temporal series. As a second level masks, the same ROIs used in the univariate analysis (See paragraph "ROI Selection and Analysis" and Table 1) were entered, in order to focus on specific sets of *features*.

A binary classification model was computed using a Support Vector Machine algorithm (SVM) which, using the similarity matrix previously determined, computes a hyperplane that splits the feature space, maximizing the margin that separates values belonging to the two experimental conditions, finally extracting the weight vectors running perpendicularly to the hyperplane. For each binary classification model, *FV_Grasp* functional images were assigned to class 1 and *PLD_Grasp* to class 2.

The performance of the classifier and its ability to generalize the results of its computations on an independent non trained dataset, was assessed by means of a leave one subject out cross validation scheme. Specifically, the entire dataset was separated into two sets: one used for training and the other for test. The number of folds in which data were partitioned was equal to the number of subjects. The set of data used for training was equal to the number of subjects minus one. The learned function was then used to predict the labels on the remaining unused subject's data. Further operations were applied to the data, including sample averaging within subjects, mean centring the features using training data and dividing the data vectors by their Euclidean norm. In order to estimate the model *P*-value, 1000 permutations were run so that the model was retrained by the specified number of times. Model accuracy and the area under curve were computed to assess model performance.

2.4 Results

2.4.1 Univariate analysis

Figure 2 shows cortical activation maps, FWE corrected at a voxel level with a significance threshold of $P < 0.01$, overlaid on an MNI template. Contrast between *FV_Grasp vs* baseline shows a large activation pattern in the left cerebral hemisphere, including occipito-temporal (pMTG, pFG) and occipito-parietal (SPOC) clusters, superior and inferior parietal areas (SPL, IPS, IPL), both dorsal and ventral sector of premotor cortex (PMd, PMv), pars triangularis of the IFG, SMA. In the right cerebral hemisphere, clusters were roughly symmetrical but less extended than in the left hemisphere. No significant activation of IPL and SMA was found in the right hemisphere. Subcortical clusters were localized in the thalamus at the level of the Pulvinar (bilaterally), and in cerebellum, including bilateral lobules VI, Crus I, VIIb and VIIIb (Figure 17A).

The contrast between *PLD_Grasp vs* baseline shows a pattern rather similar to that of *FV_Grasp* condition, although the activation in the former condition was more bilateral than in the latter one. Further differences consist in the absence of activation of left IFG, pars triangularis, the presence of a small cluster in the posterior sector of the left middle cingulate cortex (pMCC) and the

bilateral activation of inferior parietal cortex. Subcortical activations were comparable to those of *FV_Grasp* (Figure 17B).

The activation map corresponding to the contrast between *FV_Grasp vs* all fully visible control conditions (*FV_Static, FV_Box, FV_Scrambled*) revealed activated clusters in areas pMTG, pFG, SPOC, SPL, PMd, bilaterally, although more extended in the left hemisphere. Some clusters were fully lateralized to the left hemisphere, such as those in PMv, IPL, pMCC. Subcortical clusters were localized in left pulvinar, cerebellar lobules VI and Crus I bilaterally, and right lobule VIIb (Figure 17C).

Cortical activation map derived from the contrast between *PLD_Grasp vs* all point-light displays control conditions (*PLD_Static, PLD_Box, PLD_Scrambled*) revealed bilateral clusters in areas pMTG, pFG, SPOC, SPL, IPS, IPL, PMd and PMv. A significant cluster was also present in the left pMCC. Additional subcortical structures included the lateral sectors of cerebellar lobules VI, Crus I and VIIb bilaterally (Figure 17D).

Figure 17E shows the conjunction analysis between *FV_Grasp* and *PLD_Grasp*, *vs* their corresponding controls. This analysis revealed shared bilateral clusters in pMTG, pFG, and SPL, and left-lateralized clusters in SPOC, IPL, IPS, PMd and PMv. Subcortical clusters were localized in cerebellar lobules VI and VIIb, bilaterally, while the cluster in Crus I was more evident on the right. The cortical activation map emerging from global analysis reveals clusters significantly active in either *FV_Grasp*, *PLD_Grasp*, or in both conditions, each *vs* its respective controls (Figure 17F) (Supplementary table 1). The pattern obtained with this analysis was used to define the areas in which to perform a subsequent ROI analysis.

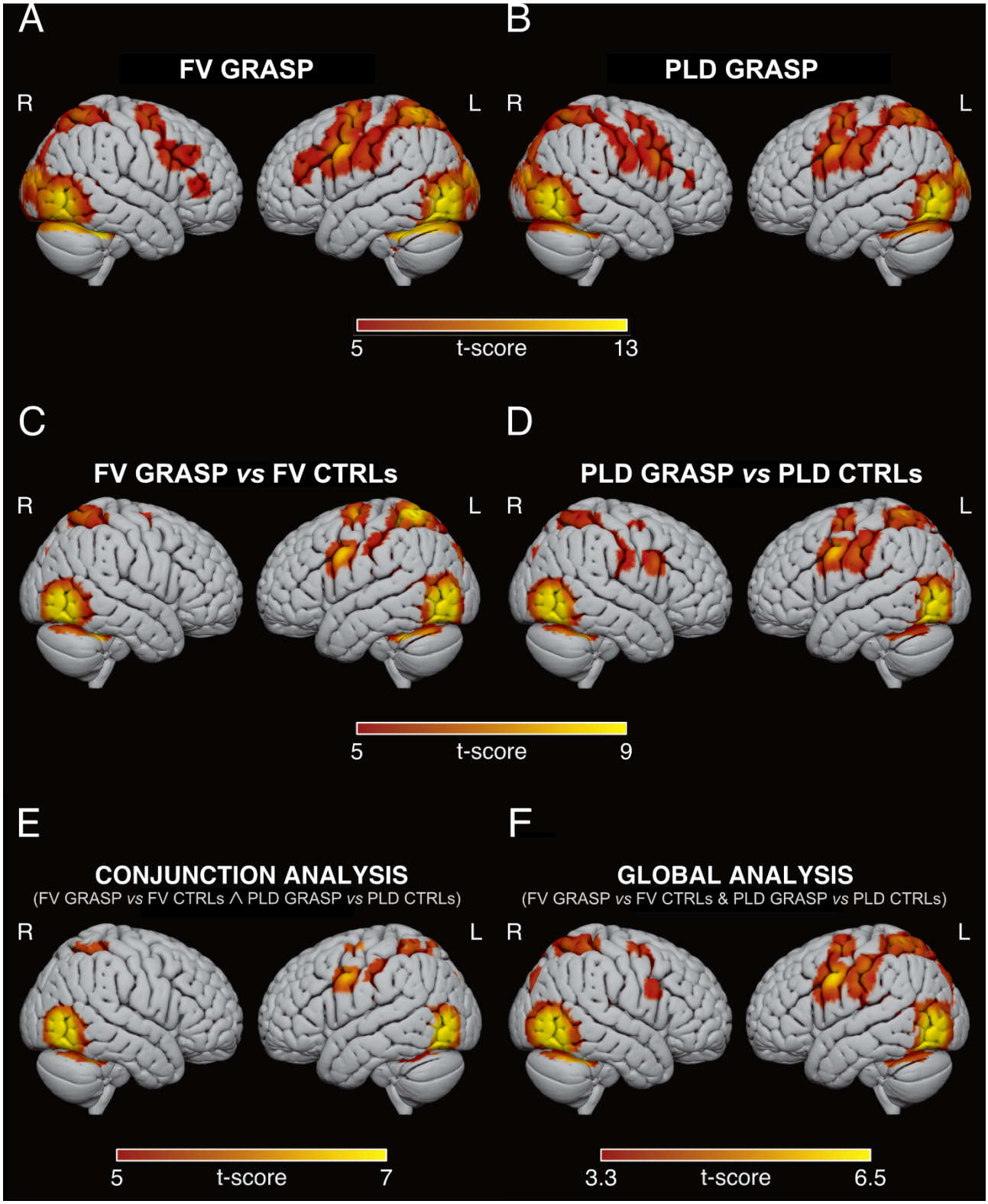

Figure 17. Cortical activations projected onto a 3D MNI152 Brain template (Surfice; https://www.nitrc.org/projects/surfice/). (A) Contrast between the observation of FV_Grasp and baseline. (B) Contrast between the observation of PLD_Grasp and baseline. (C) Contrast between FV_Grasp and all corresponding controls. (D) Contrast between PLD_Grasp and its respective

control conditions. Conjunction (E) and global (F) analysis between FV_Grasp and PLD_Grasp vs their corresponding controls.

2.4.2 Lateralization analysis

Lateralization index computation showed a significant difference ($P < 0.001$) between PLDs (mean = 0.04, s.d. = 0.15) and FV (mean = 0.21, s.d. = 0.16) grasping conditions, indicating a more bilateral pattern for observation of PLDs grasping (Figure 18).

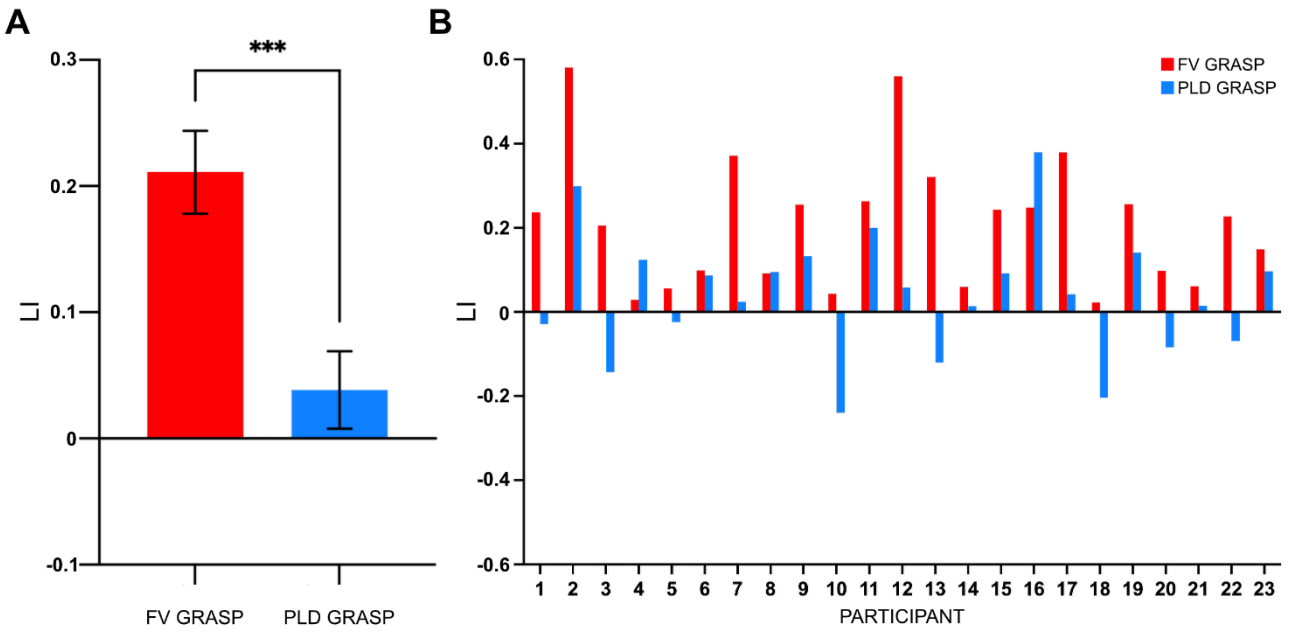

Figure 18. Lateralization index (LI) analysis results at group (A) and single subject (B) level. Positive values correspond to left lateralization, whilst negative values correspond to right lateralization. In (A), the data show a significant difference (P < 0.001) in LI between PLDs (mean = 0.04, s.d. = 0.15) and FV (mean = 0.21, s.d. = 0.16) grasping conditions. Error bars indicate the standard error of the mean.

2.4.3 ROI analysis

Comparisons between BOLD signal change in the different conditions were also carried out by means of a ROI analysis, in cortical areas chosen following an anatomical approach (see "ROI

Selection and Analysis"). For each ROI, BOLD signal change was compared between conditions by means of repeated measure ANOVA and significant differences were assessed with post-hoc comparisons by using paired-sample *t*-test with Bonferroni correction.

The analysis carried out revealed a significant effect for all considered ROIs except for the CTRL_WM ROI [$F_{(1,7)} = 0.75$, $P < 0.63$, $\eta 2 = 0.03$]. We clustered the remaining cortical ROIs using a functional criterion. Significant effects between conditions were found in:

(a) *Visual* ROIs: V4_hOc4la [$F_{(1,7)} = 82.72$, $P < 0.001$, $\eta 2 = 0.79$], V5_hOc5 [$F_{(1,7)} = 82.12$, $P < 0.001$, $\eta 2 = 0.79$], pMTG [$F_{(1,7)} = 32.90$, $P < 0.001$, $\eta 2 = 0.60$], FG2 [$F_{(1,7)} = 41.64$, $P < 0.001$, $\eta 2 = 0.65$], FG4 [$F_{(1,7)} = 35.16$, $P < 0.001$, $\eta 2 = 0.62$], SPOC [$F_{(1,7)} = 23.45$, $P < 0.001$, $\eta 2 = 0.52$] (Figure 19);

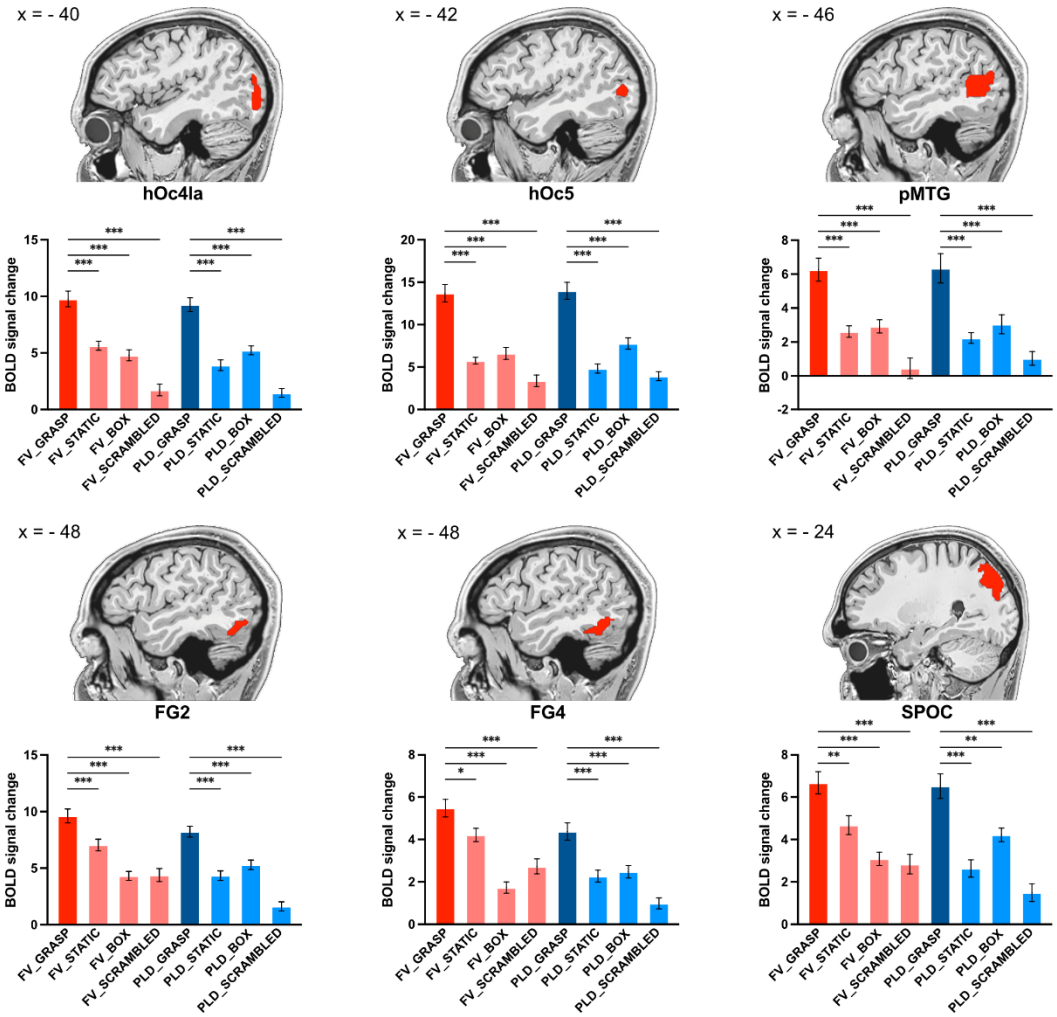

Figure 19. Results of the ROI analyses on visual areas. Histograms show the BOLD signal change in each ROI. The red colored bars refer to FV conditions, blue to PLDs ones. Vertical lines in the

histograms indicate standard error of the mean. Above each histogram, the corresponding ROI is represented on a sagittal slice of a human left hemisphere. Asterisks indicate significant effects corrected for multiple comparisons (P<0.05*, P<0.01**, P<0.001***; Bonferroni corr.).

(b) *Parieto-premotor* ROIs: SPL_5L [$F_{(1,7)} = 32.41$, $P < 0.001$, $\eta 2 = 0.60$], SPL_7A [$F_{(1,7)} = 42.51$, $P < 0.001$, $\eta 2 = 0.66$], SPL_7PC [$F_{(1,7)} = 38.82$, $P < 0.001$, $\eta 2 = 0.64$],], aIPS_IP1 [$F_{(1,7)} = 16.65$, $P < 0.001$, $\eta 2 = 0.43$], aIPS_IP3 [$F_{(1,7)} = 25{,}60$, $P < 0.001$, $\eta 2 = 0.54$], IPL_PFt [$F_{(1,7)} = 16.93$, $P < 0.001$, $\eta 2 = 0.43$], SMG [$F_{(1,7)} = 22.68$, $P < 0.001$, $\eta 2 = 0.51$], PMd [$F_{(1,7)} = 23.58$, $P < 0.001$, $\eta 2 = 0.52$], PMv [$F_{(1,7)} = 19.97$, $P < 0.001$, $\eta 2 = 0.48$] (Figure 20);

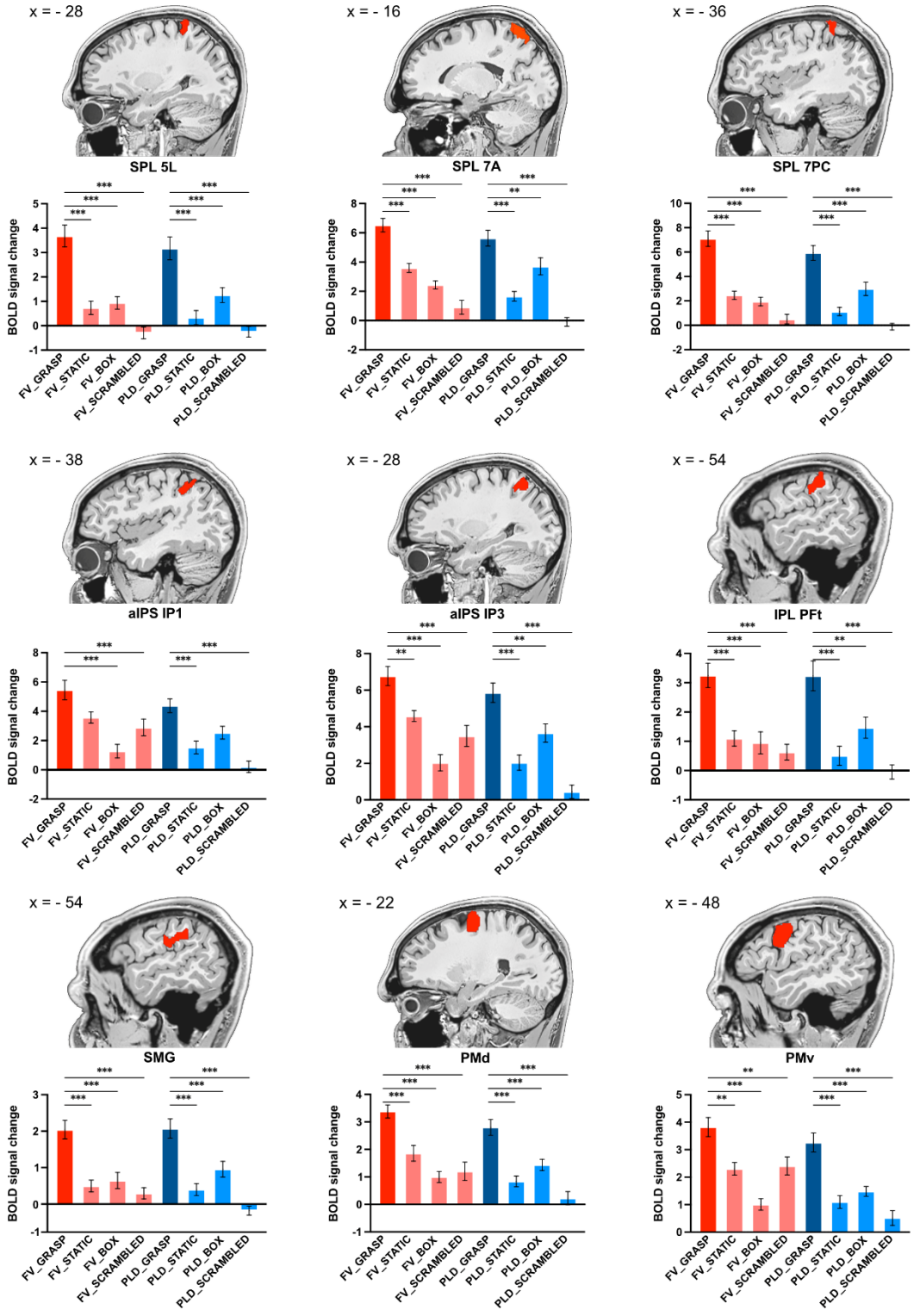

Figure 20. Results of the ROI analyses on parieto-premotor areas. Histograms show the BOLD signal change in each ROI. The red colored bars refer to FV conditions, blue to PLDs ones. Vertical lines in the histograms indicate standard error of the mean. Above each histogram, the corresponding ROI is represented on a sagittal slice of a human left hemisphere. Asterisks indicate significant effects corrected for multiple comparisons (P<0.05*, P<0.01**, P<0.001***; Bonferroni corr.).

(c) *Somatomotor* ROIs: PSC_2 [$F_{(1,7)} = 21.85$, $P < 0.001$, $\eta 2 = 0.50$], PSC_3b [$F_{(1,7)} = 13.60$, $P < 0.001$, $\eta 2 = 0$], pMCC [$F_{(1,7)} = 17.48$, $P < 0.001$, $\eta 2 = 0.44$] (Figure 21).

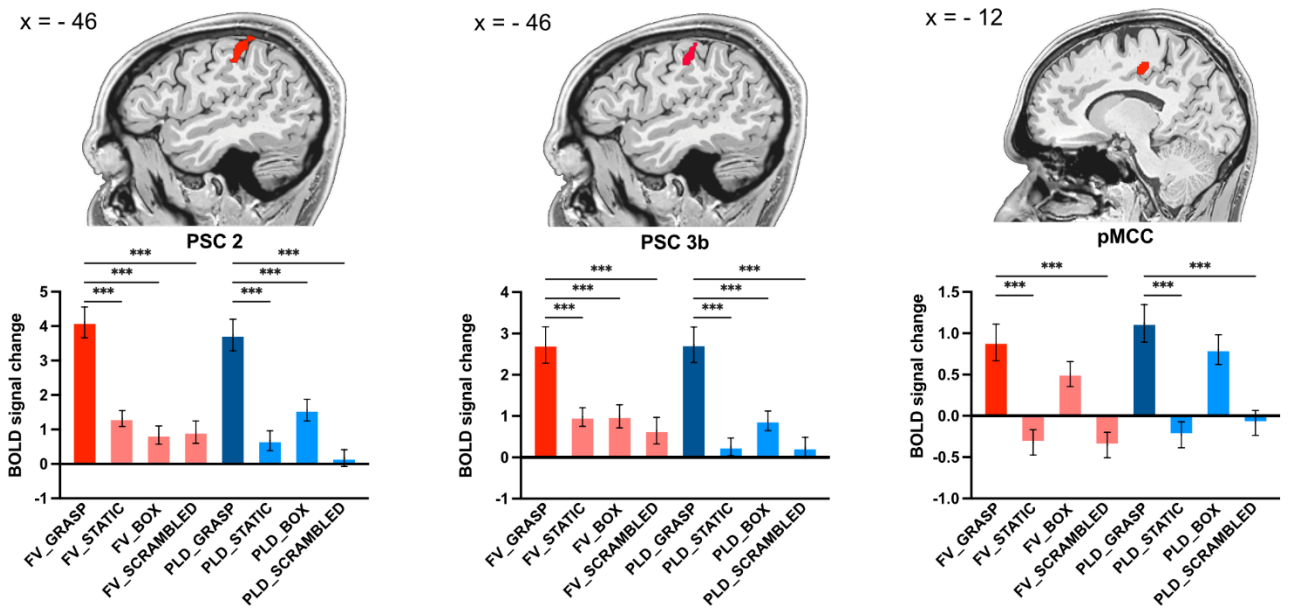

Figure 21. Results of the ROI analyses on somatomotor areas. Histograms show the BOLD signal change in each ROI. The red colored bars refer to FV conditions, blue to PLDs ones. Vertical lines in the histograms indicate standard error of the mean. Above each histogram the corresponding ROI is represented on a sagittal slice of a human left hemisphere. Asterisks indicate significant effects corrected for multiple comparisons (P<0.05*, P<0.01**, P<0.001***; Bonferroni corr.).

Post-hoc tests showed no significant difference between experimental conditions (*FV_Grasp* and *PLD_Grasp*) in all considered ROIs. Instead, a significant difference between FV experimental condition and all its corresponding control conditions (*FV_Grasp vs FV_Static*, *FV_Box*, *FV_Scrambled*) was observed in: V4_hOc4la ($P < 0.001$), V5_hOc5 ($P < 0.001$), pMTG ($P < 0.001$), SPOC ($P < 0.001$), FG2 ($P < 0.001$), FG4 ($P < 0.05$), SPL_5L ($P < 0.001$), SPL_7A ($P < 0.001$), SPL_7PC ($P < 0.001$), aIPS_IP3 ($P < 0.01$), IPL_PFt ($P < 0.01$), SMG ($P < 0.001$), PSC_2 ($P < 0.001$), PSC_3a ($P < 0.001$), PSC_3b ($P < 0.001$), PMv ($P < 0.01$), PMd ($P < 0.001$).

Considering PLDs conditions, the analysis revealed a significant difference between *PLD_Grasp vs* its corresponding controls (*PLD_Static*, *PLD_Box* and *PLD_Scrambled*) in the

following ROIs: V4_hOc4la ($P < 0.001$), V5_hOc5 ($P < 0.001$), pMTG ($P < 0.001$), SPOC ($P < 0.01$), FG2 ($P < 0.001$), FG4 ($P < 0.001$), SPL_5L ($P < 0.001$), SPL_7A ($P < 0.01$), SPL_7PC ($P < 0.001$), aIPS_IP3 ($P < 0.01$), IPL_PFt ($P < 0.01$), SMG ($P < 0.001$), PSC_2 ($P < 0.001$), PSC_3a ($P < 0.01$), PSC_3b ($P < 0.001$), PMv ($P < 0.001$), PMd ($P < 0.001$).

In pMCC, no significant difference was found between both *FV_Grasp vs FV_Box* ($P = 1$; n.s.) and *PLD_Grasp vs PLD_Box* ($P = 0.09$; n.s.), in aIPS_IP1 between *FV_Grasp vs FV_Static* ($P = 0.06$; n.s.) and *PLD_Grasp vs PLD_Box* ($P = 0.07$; n.s.). Note that in this latter ROIs *P*-values were close to significance threshold, although not reaching it.

2.4.4 Multivariate analysis

The analysis, performed by computing a binary classification model using an SVM algorithm and performing the permutation testing for 1000 times on the un-smoothed normalized T2* functional brain images belonging to *FV_Grasp* and *PLD_Grasp* experimental conditions for each subject, revealed significant decoding accuracy in the following ROIs: FG4 (model accuracy = 69.57%, $P < 0.05$), SPOC (model accuracy = 69.57%, $P < 0.05$), SPL_7A (model accuracy = 78.26%, $P = 0.001$), SPL_7PC (model accuracy = 78,26%, $P < 0.01$), PMd (model accuracy = 67.39%, $P < 0.05$) and PMv (model accuracy = 73.91%, $P = 0.01$) (Figure 22).

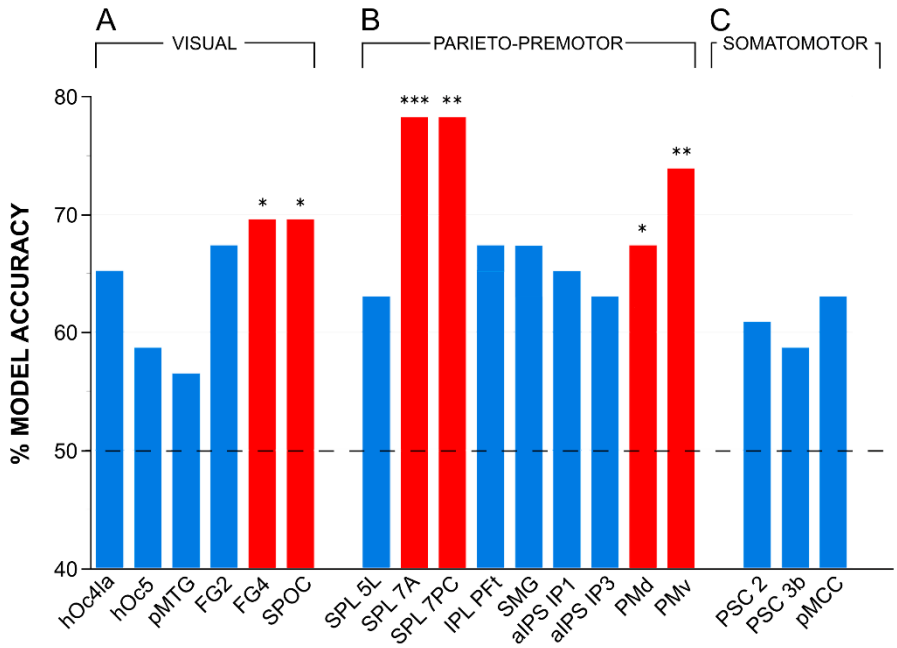

Figure 22. Results of the MVPA analyses. Histograms show the percentage of model accuracy in each ROI clustered in visual, parieto-premotor and somatomotor areas. The dotted line represents the chance level. Red colored bars show the ROIs with a significant (P<0.05*, P<0.01**, P<0.001***) model accuracy assessed by means of a permutation testing (n° permutation = 1000).

No significant above threshold model accuracy was found in the remaining ROIs (Table 1).

	ROI	ACCURACY %	P-VALUE	AUC	CLASS 1 %	CLASS 2 %
VISUAL	hOc4la	65.22	0.06	0.70	73.91	56.52
	hOc5	58.70	0.17	0.63	65.22	52.17
	pMTG	56.52	0.28	0.63	69.57	43.48
	FG2	67.39	0.08	0.72	69.57	65.22
	FG4	**69.57**	**0.04**	**0.81**	**69.57**	**69.57**
	SPOC	**69.57**	**0.03**	**0.75**	**73.91**	**65.22**
PARIETO-PREMOTOR	SPL 5A	63.04	0.12	0.66	60.87	65.22
	SPL 7A	**78.26**	**0.001**	**0.78**	**78.26**	**78.26**
	SPL 7PC	**78.26**	**0.003**	**0.78**	**69.57**	**86.96**
	IPL PFt	67.39	0.06	0.75	73.91	60.87
	SMG	67.39	0.08	0.72	78.26	56.52
	aIPS IP1	65.22	0.08	0.70	65.22	65.22
	aIPS IP3	63.04	0.12	0.70	73.91	52.17
	PMd	**67.39**	**0.04**	**0.80**	**78.26**	**56.52**
	PMv	**73.91**	**0.01**	**0.75**	**86.96**	**60.87**
SOMATOMOTOR	PSC 2	60.87	0.18	0.69	65.22	56.52
	PSC 3b	58.70	0.24	0.67	65.22	52.17
	pMCC	63.04	0.14	0.60	78.26	47.83
	CTRL WM	54.35	0.44	0.64	60.87	47.83

Table 1. MVPA detailed results of the binary support vector machine classification models. Model accuracy and the Area Under Curve (AUC) were computed to assess model performance. Significant values are indicated in boldface.

In order to evaluate the contribution of the voxels to the decision function in each ROI, we computed the weight maps of the classification models for both *FV_Grasp* and *PLD_Grasp* conditions (Figure 23). A voxel's weight parameter reflects the contribution of that voxel to the

discrimination process. Since all voxels with a value different from zero contribute to the function value, we represented the intensity of each weight with a colour grading: colder colours for the weights with an intensity < 0; warmer ones for intensities > 0. Weights with a positive value tend to move the classification boundaries towards class 1 (*FV_Grasp*), on the contrary those with a negative one, towards class 2 (*PLD_Grasp*).

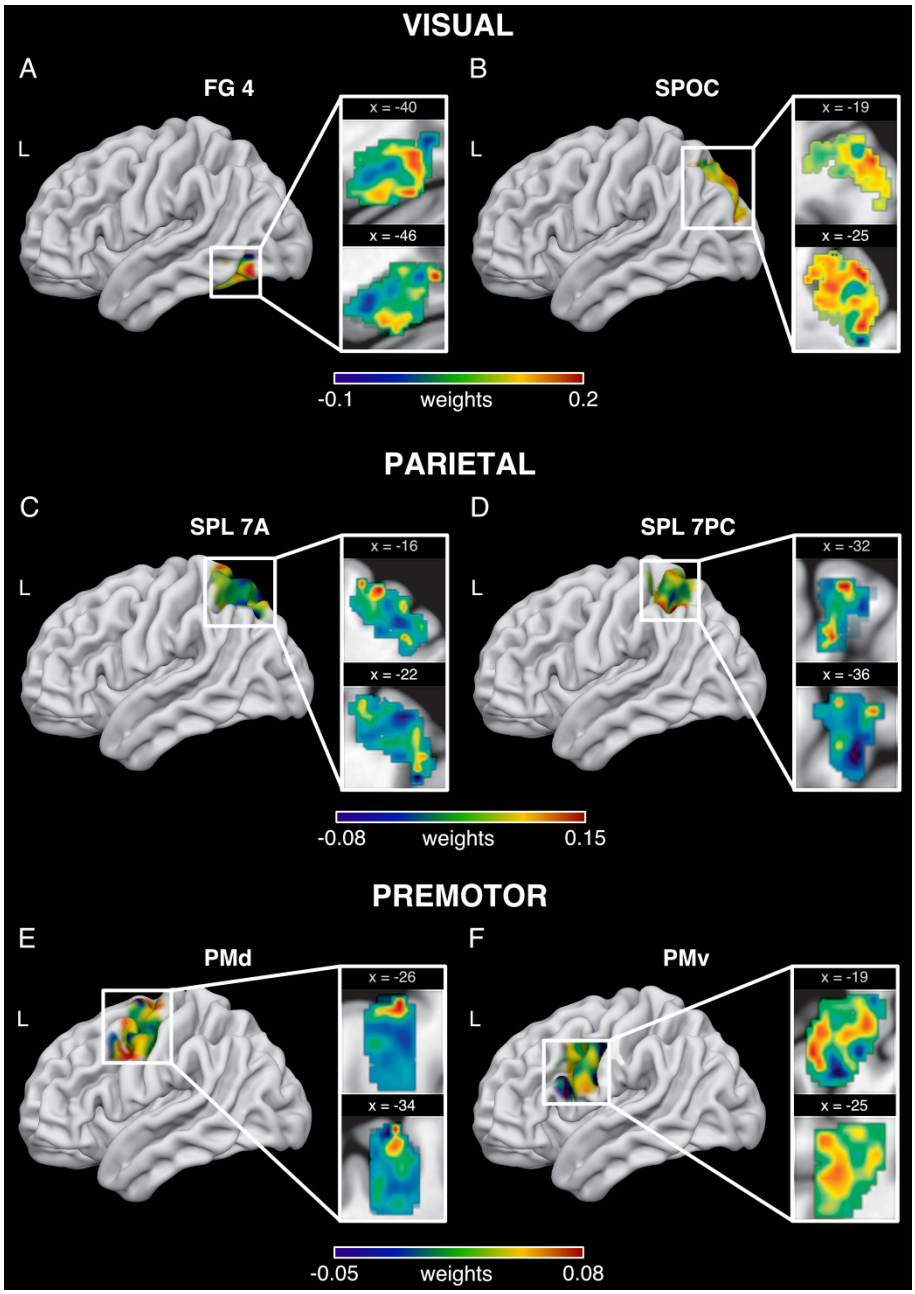

Figure 23. Weights maps of the ROIs in which the classification model reached statistical significance. Results are projected on an ICBM152 brain template (Surfice; https://www.nitrc.org/projects/surfice/) and on a magnified portion taken from two sagittal slices. Color bars indicate the relative importance of the voxel in the decision function with warmer colors

indicating the most discriminative voxels for class 1 (FV_Grasp) and colder colors for class 2 (PLD_Grasp). Weights maps are represented separately for visual (A-B), parietal (C-D) and premotor (E-F) areas.

2.5 Discussion

In the present fMRI study, healthy participants observed hand grasping actions performed by a fully visible human hand or PLDs representation of it. The results show that: (a) kinematic information conveyed by observation of PLDs hand grasping action elicits activation of the AON; (b) the activation pattern is more bilateral during observation of PLDs stimuli than during observation of fully visible grasping, that is lateralized to the left hemisphere; (c) activation, assessed within multiple ROIs, is comparable between the experimental conditions; (d) visual, parietal and premotor cortex discriminate between the two versions of grasping actions with significant decoding accuracy

A large body of studies demonstrated that observation of hand grasping actions recruits a bilateral cortical network of occipito-temporal, parietal and premotor areas belonging to the AON (Caspers et al., 2010; Hardwick et al., 2018). It is well established that areas of this network code the goal of an observed action. However, activation within AON could also involve the processing of low-level visual characteristics, motion aspects (e.g., linear velocity and motion direction), as well as the elaboration of the target object and the context in which the action is performed. To exclude all these effects, leaving only those features that still allow to decode action goal, we introduced control conditions, thus subtracting potential confounds from both PLDs and fully visible experimental conditions. The contrast between PLDs grasping condition and all its controls revealed a bilateral activation pattern including occipito-temporal, posterior parietal and premotor areas known to be involved in the processing of observed actions, corresponding to the AON. This demonstrates that the information conveyed by PLDs hand grasping stimuli is enough to elicit activation in AON, suggesting the involvement of a motor resonance mechanism similar to that elicited by fully visible

actions. Thus, the observation of a visually impoverished grasping performed with a specific effector, in our case a right hand, is sufficient to activate areas coding action goal even when low-level visual characteristics (contrast, luminance), motion direction and velocity, as well as static hand-shape pattern, are excluded. Therefore, the remaining biological kinematic information is still able to elicit this mechanism. Neuroimaging studies using observation of PLDs versions of whole-body complex movements revealed an activation of some areas within the AON (Beauchamp et al., 2003; Grossman & Blake, 2002; Peelen et al., 2006; Peuskens et al., 2005; Saygin et al., 2004; Vaina et al., 2001). Beauchamp and colleagues (Beauchamp et al., 2003), comparing observation of fully visible whole-body human actions with PLDs ones, showed that inferior temporal cortex and fusiform gyrus were more strongly activated by fully visible videos than by PLDs. Studies focused on the perception of whole-body PLDs, comparing biological with non-biological motion, consistently showed activations in temporal and occipital areas (Grossman & Blake, 2002; Peelen et al., 2006; Peuskens et al., 2005). On the other hand, there are studies showing the recruitment of parietal areas during observation of whole-body biological PLDs stimuli, in particular of IPS and SPL (Grèzes et al., 2003; Vaina et al., 2001). The present study, that is focussed on the observation of PLDs hand grasping actions, is in line with the above findings, while adding new information, since it also shows premotor cortex activations and a more extended parietal activation pattern, which includes IPL, part of human parieto-premotor MNS, usually recruited in both observation and execution of hand grasping actions (Caspers et al., 2010; Hardwick et al., 2018).

The activation of occipito-temporal areas, that in the present study includes V4, MT/V5, pMTG and pFG, very likely reflects the elaboration of biological motion, also in line with previous studies (Chang et al., 2018; Grossman et al., 2000; Grossman & Blake, 2002; Peelen et al., 2006; Pelphrey et al., 2005; Servos et al., 2002). Indeed, the random motion of PLDs in the scrambled control condition and the motion of the PLDs box control stimuli, although sharing several low-level visual characteristics and motion features with the experimental stimuli, elicited a weaker activation

in these areas. This suggests their tuning to biological features of motion rather than to motion in general. The activation of IPL and PMv is in line with the results of a large body of studies on action observation of fully visible stimuli (Caspers et al., 2010; Hardwick et al., 2018), thus suggesting the involvement of a common motor resonance mechanism in both PLDs and fully visible grasping stimuli. These regions can be involved in coding action goal as well as specific aspects of performed acts, for example grip type and action outcome (Binkofski et al., 1999; Errante et al., 2021a; Grafton & Hamilton, 2007). The activation also involves areas within the so-called "dorsal circuit" such as PMd, SPL and SPOC (Cavina-Pratesi et al., 2010; Filimon et al., 2007; Gallivan et al., 2009; Gazzola & Keysers, 2009), usually considered as involved in the observation, as well as in the execution of reaching motor acts. However, more recent human and monkey studies reported that the dorsal parieto-premotor circuit plays an important role in processing grasping/manipulation components (Errante & Fogassi, 2019a; Nelissen et al., 2017). Noteworthy, in the present study, also the ROI analysis reveals that activation of areas within the dorsal circuit was higher during observation of grasping actions as compared to the box control condition, although in this case the stimulus was moving with the same direction and mean velocity, thus reaching the same portion of space of the PLDs hand. Therefore, the involvement of dorsal areas could reflect the processing of other features of observed grasping acts, such as hand/finger posture for grip configuration and the desired end state of an action, very likely as during the observation of fully visible grasping (Errante et al., 2021a; Majdandzic et al., 2009). A similar activation pattern, even though more left-lateralized, was observed when contrasting fully visible grasping experimental condition and its controls. The AON activation elicited by the observation of fully visible grasping stimuli is in line with previous literature on action observation (Caspers et al., 2010; Hardwick et al., 2018).

Interestingly, conjunction analysis between the two experimental conditions after subtraction of the respective control conditions, indicates that a specific set of shared areas including left SPL and IPL as well as PMd and PMv are similarly activated. This suggests that although the processing

of PLDs actions relies only on the available biological kinematic features, nonetheless this latter information is sufficient to elicit in the observer a full action representation.

The more left-lateralized activation obtained during observation of fully visible grasping actions can be explained by a motor resonance mechanism that allows the observer to understand the action goal, likely grounded on a *praxic* knowledge that, in right-handed individuals, is usually left-lateralized (Biagi et al., 2010; Binkofski et al., 1999; De Renzi, 1982). The activation of a more bilateral pattern during observation of PLDs grasping actions suggests that very likely this type of processing is based on the elaboration of movement kinematic features, by the recruitment of the parieto-premotor grasping network of both hemispheres, in order to extract information about the final action goal.

Although ROI analysis reveals that in both PLDs and fully visible actions signal intensity was comparable in all considered areas, it is reasonable to suppose that spatial distribution of the activation pattern may differ between the two conditions. This was tested by means of MVPA, the results of which show different features patterns in FG, SPOC, SPL, PMd and PMv. The classification model accuracy was statistically significant, showing that spatially distributed information can correctly disentangle, in the considered ROIs, the two classes of experimental conditions.

Differences in FG pattern may be attributable to a dissimilarity in the appearance and visual complexity of the two types of hand grasping stimuli, as well as to the presence of the object in fully visible grasping condition (Weiner & Zilles, 2016). In fact, this is a high order extrastriate visual area, that is known to be also recruited during observation of actions performed with a visible upper limb (Hardwick et al., 2018), as well as by object-directed hand movements (Grosbras et al., 2012). Thus, visual appearance of the fully visible grasping stimuli as well as its complex visual characteristics, such as shape, colour, and texture may be key factors in discriminating the two activation patterns.

Visual dorsal stream area SPOC has been reported to be recruited during both execution (Cavina-Pratesi et al., 2010; Gallivan et al., 2009) and observation (Filimon et al., 2007) of arm reaching actions, as well as of objects within reach (Gallivan et al., 2009). This region includes human V6 and V6A, the latter being involved in the visual analysis of the transport phase of reaching-grasping actions (Pitzalis et al., 2015). Although in our study SPOC is recruited in a comparable manner in terms of BOLD intensity during observation of both PLDs and fully visible grasping actions, a possible interpretation is that differences in pattern distribution are mainly due to the prevalence, in fully visible condition, of information about arm movement and the presence of the object within reach.

The MVPA results also indicate a high-level accuracy (~80%) in decoding between PLDs and fully visible actions in SPL and in PMd. This is not surprising because, as previously described, both the dorsal and ventral parietal and premotor areas are involved in the processing of reaching but also of some features of the observed grasping, such as specific grip configuration (Errante & Fogassi, 2019a; Errante et al., 2021a). Here, however, the decoding accuracy in SPL and PMd could not be explained only by differences in reaching movement features or grip configuration because both PLDs and fully visible actions were matched for these characteristics. Thus, a further possible interpretation is that dorsal areas differentially encode proprioceptive information associated to fully visible hand-object interaction (Casile et al., 2010; Errante & Fogassi, 2019a). In addition, it is also plausible that the more complete vision of the arm in fully visible actions elicits a more specific representation of this effector in the dorsal areas, according with their somatotopic organization.

Finally, pattern differences in PMv could be in principle attributed to the processing of the action goal and/or kinematic features of the movement. However, these variables were matched between the two main conditions. Therefore, the possible role of PMv in decoding between PLDs and

fully visible grasping actions could be related to object presence only in fully visible stimuli (Grèzes et al., 2003).

2.6 Conclusions

Activation of AON evoked by PLDs stimuli, in particular, in parietal and-premotor areas, demonstrates that motion features are sufficient to determine goal encoding without any confounding effect relative to the observation of contextual information. In addition, the use of machine learning methods allowed us to assess which areas of the AON play a key role in disentangling between PLDs and fully visible stimuli and, together with data from literature, whether they encode specific features of the observed grasping action. Based on the present data, in the future it could be interesting to investigate whether kinematic information provided by PLDs stimuli is exploited during motor learning tasks to improve some aspects of action execution such as precise hand/finger configurations.

From a clinical perspective, the present results could be useful to improve the observation-based methods for rehabilitation in patients with motor disorders (Buccino, 2014; Franceschini et al., 2012; Pelosin et al., 2010; Sgandurra et al., 2013). The implementation of PLDs stimuli in the clinical rehabilitation setting could bring improvements for a personalized therapy focused not only on the imitation of the action performed by another individual in terms of goal achievement, but also in the imitation of the kinematics of the observed action, achieving a finer use of the hand.

The application of deep learning models and neural networks to identify features of biological motion has seen a rapid growth, leading to the creation of specific tools for such purposes (Insafutdinov et al., 2017; Nath et al., 2019; Toshev & Szegedy, 2014). Such machine learning approaches have been used with whole body PLDs stimuli of several human actions which were entered as input in complex pattern classification algorithms (Tanisaro et al., 2017) and in convolutional neural networks (Peng et al., 2021). The use of deep learning-based classification

models to improve hand actions recognition, by extracting the kinematic features from PLDs actions of both healthy people and patients, could be useful in the field of human-robot interaction.

3. Study 2: Direction and velocity kinematic features of point-light displays grasping actions are differentially coded within the action observation network

3.1 Abstract

The processing of kinematic information embedded in observed actions is an essential ability for understanding others' behavior. Previous research showed that the AON may encode some action kinematic features. However, our understanding of how direction and velocity are encoded within the AON is still limited. In this study, we employed event-related fMRI to investigate the neural substrates specifically activated during observation of hand grasping actions presented as point light displays, performed with different directions (right, left) and velocities (fast, slow). Twenty-three healthy adult participants of either sex took part in the study. To identify brain regions differentially recruited by grasping direction and velocity, univariate and multivariate pattern analysis were performed. The results of univariate analysis demonstrate that direction is encoded in occipito-temporal and posterior visual areas, while velocity recruits lateral occipito-temporal, superior parietal and intraparietal areas. Results of MVPA further show: a) significant decoding accuracy of both velocity and direction at the network level; b) a critical role of both lateral occipito-temporal and parietal areas in decoding both direction and velocity; c) a contribution of bilateral premotor areas to velocity decoding. These results indicate that posterior parietal nodes of the AON are mainly involved in coding grasping direction and that premotor regions are crucial for coding grasping velocity, while lateral occipito-temporal cortices play a key role in encoding both parameters. The current findings could have implications for observational-based rehabilitation treatments of patients with motor disorders and artificial intelligence-based hand action recognition models.

3.2 Introduction

The human ability to process kinematic information conveyed during action observation can be crucial for understanding others' behavior. Indeed, kinematic parameters, such as duration, velocity, direction, provide crucial information about the features of the observed action. The encoding of such kinematic parameters starts with the analysis of biological motion in high-order visual areas (Caspers et al., 2010), which then provide key information to further cortical areas involved in action processing. In order to study biological motion kinematic properties of the observed action, in absence of pictorial contents, a useful technique is that of point light displays (PLDs) (Blake & Shiffrar, 2007; Johansson, 1973; Pavlova, 2012; Thornton, 2006). It has been shown that this information, although impoverished, is sufficient to allow the encoding of the action goal of another individual (Ziccarelli et al., 2022), as well as of one's emotional state (Chouchourelou et al., 2006), or the effort exerted when an observed agent lifts a weight (Shim et al., 2004).

It is well known that observation of actions performed by others in full vision activates several cortical areas, belonging to the AON. The main nodes of this system in humans include the ventral premotor cortex (PMv), inferior frontal gyrus (IFG) and the inferior parietal lobule (IPL), that are endowed with mirror properties (Molenberghs et al., 2012), and a more extended set of areas including lateral occipito-temporal cortex (LOTC; hMT/V5), posterior superior temporal sulcus (pSTS), superior parietal (SPL) and intraparietal (IPS) areas, primary somatosensory cortex (SI), and dorsal premotor cortex (PMd) (Filimon et al., 2007; Gazzola & Keysers, 2009; Hardwick et al., 2018). Recently also the lateral part of cerebellum (VI) has been included in this network (Abdelgabar et al., 2019; Errante & Fogassi, 2020; Filimon et al., 2007; Gazzola & Keysers, 2009; Hardwick et al., 2018). It has been proposed that the areas of the AON can specifically encode several characteristics of the observed actions (Kemmerer, 2021), including kinematic features (Errante et al., 2021a; Grafton & Hamilton, 2007). Regarding these latter, AON areas are recruited by the elaboration of kinematic information conveyed by both whole body and effector specific PLDs, as demonstrated by

neuroimaging and electrophysiological studies (Peelen et al., 2006; Saygin et al., 2004; Ulloa & Pineda, 2007; van Kemenade et al., 2012; Ziccarelli et al., 2022). Previous neuroimaging studies, using PLDs stimuli, focused mainly on the investigation of the differences between whole-body biological and non-biological motion perception (Peuskens et al., 2005; Saygin et al., 2004). Nevertheless, there are no studies investigating the modulation of AON activation by the observation of biological actions performed with different velocities and directions, devoid of any pictorial information. In this study, we combined both univariate and multivariate analyses to reveal differences in processing specific kinematic information within AON areas specifically aiming at evaluating whether: a) differences in direction and velocity kinematic parameters activate different areas of the AON; b) it is possible to decode action kinematic features within the AON using multivariate approaches, estimating the specific contribution of AON regions in this process.

3.3 Materials and Methods

3.3.1 Participants

Twenty-three healthy human volunteers (11 female; mean age 23 years; range 20 - 30 years) with no history of neurological or psychiatric disorders, and of drug or alcohol abuse, participated in the study. All participants were right-handed according to the Edinburgh Handedness Inventory (Oldfield, 1971). Informed consent was obtained in accordance with Helsinki declaration. The study was approved by the local ethics committee (Comitato Etico Area Vasta Emilia Nord – AVEN; code NEUROIMAGE_UNIPR).

3.3.2 Stimuli

Experimental stimuli consisted in 2 seconds videos of PLDs grasping actions performed by an actor with the right hand with two different velocities (fast and slow) in right and left directions (Figure 24A). In order to use a diverse set of stimuli, grasping actions were performed with four different grips (whole hand, five-finger, three-finger, and precision). Videos were recorded from a frontal perspective (180° angle) in a well-lit environment on a black background by means of an HD camera with a frame rate of 240 fps and a resolution of 1080 × 720p. PLDs were realized using 20 small green spheres (1 cm diameter) attached to the hand, wrist and arm joints. Videos were post-processed in Final Cut Pro X (v10.6.1, Apple Inc.) using the chroma key technique performing inverse keying, so that the spheres appeared as white dots on a black background.

In order to assess velocity differences between the fast and slow grasping stimuli, a 2D kinematic analysis was performed (Tracker v6.0.3, 2021, Douglas Brown) by calculating, in each video, the velocity profile of the wrist (Figure 24B). Values were smoothed using a gaussian-weighted moving average filter provided in MATLAB R2021a (The Mathworks, Inc.) in order to account for the noise in the recorded data. Plotting the velocity data over the movement time percentage, allowed for comparisons between trials that differed in durations. The percentage of acceleration and deceleration of each action was further calculated (Figure 24C).

The percentage of the action acceleration phase was computed starting from the beginning of the movement until the maximum velocity peak, while the percentage of deceleration from the velocity peak to the end of the grasping action. Furthermore, averaged velocity curves were generated for each specific combination of direction and velocity allowing for a more straightforward comparison of the differences between stimuli velocities, as indicated by the descriptive statistics in Table 2.

	Mean velocity cm/s (SD)	*Range*	*Velocity Peak cm/s (SD)*	*Range*
RIGHT FAST	71.76 (44.66)	41.6 – 84.56	140.48 (32.65)	92.24 – 164.50
RIGHT SLOW	8.09 (7.47)	5.97 – 9.49	23.09 (5.58)	17.08 – 27.09
LEFT FAST	62.32 (48.03)	52.39 – 67.85	142.84 (17.05)	118.87 – 156.83
LEFT SLOW	10.59 (8.07)	9.36 – 12.89	24.45 (4.21)	18.95 – 29.21

Table 2. Descriptive statistics of averaged velocity curves for each specific combination of direction and velocity

3.3.3 fMRI task

Participants were informed about the fMRI scanning process in order to familiarize them with the experimental setting. During MR scanning, they laid supine in the bore of the scanner in a dimly lit environment.

The experiment was conducted in a single imaging session. It was divided into five functional runs, each lasting 6 minutes (with 180 volumes). During each run, participants were required to observe video stimuli presented on digital goggles (Resonance Technology, Northridge, CA) with a 60 Hz refresh rate, a resolution of 800 horizontal pixels × 600 vertical pixels, and a horizontal eye field of 30°. Sound-attenuating (30 dB) headphones were employed in order to dampen scanner noise. Participants were instructed to fixate a white cross presented in the center of the screen on a black background for the entire duration of the imaging session. Each run was acquired with an event-related design in which stimuli were presented using a randomized sequence. A total of 208 video stimuli (52 for each combination of direction and velocity) were presented during the whole experiment. Grasping videos were randomly interleaved by null events (Friston et al., 1999), consisting in a white cross in the center of a black background. These events ranged in duration from a minimum of 2 seconds to a maximum of 14 seconds, in steps of 2 seconds.

In order to monitor participants' attention to the visual stimuli, catch trials were randomly presented during each run. During the catch trial, participants observed a 2 second color filtered video stimulus (red, blue, green, yellow, magenta) after which they had to indicate, by pressing a button on a response pad, the main color of the stimulus by selecting one of the two options presented on the screen (4 seconds time window). The average performance of correct responses was 94%. In order to remove potential signal artifacts due to the hand movement, after this attention task, a 12 second signal denoising period (post-catch) was introduced, during which participant had to remain still while fixating the white cross on the center of the black screen (Figure 24D).

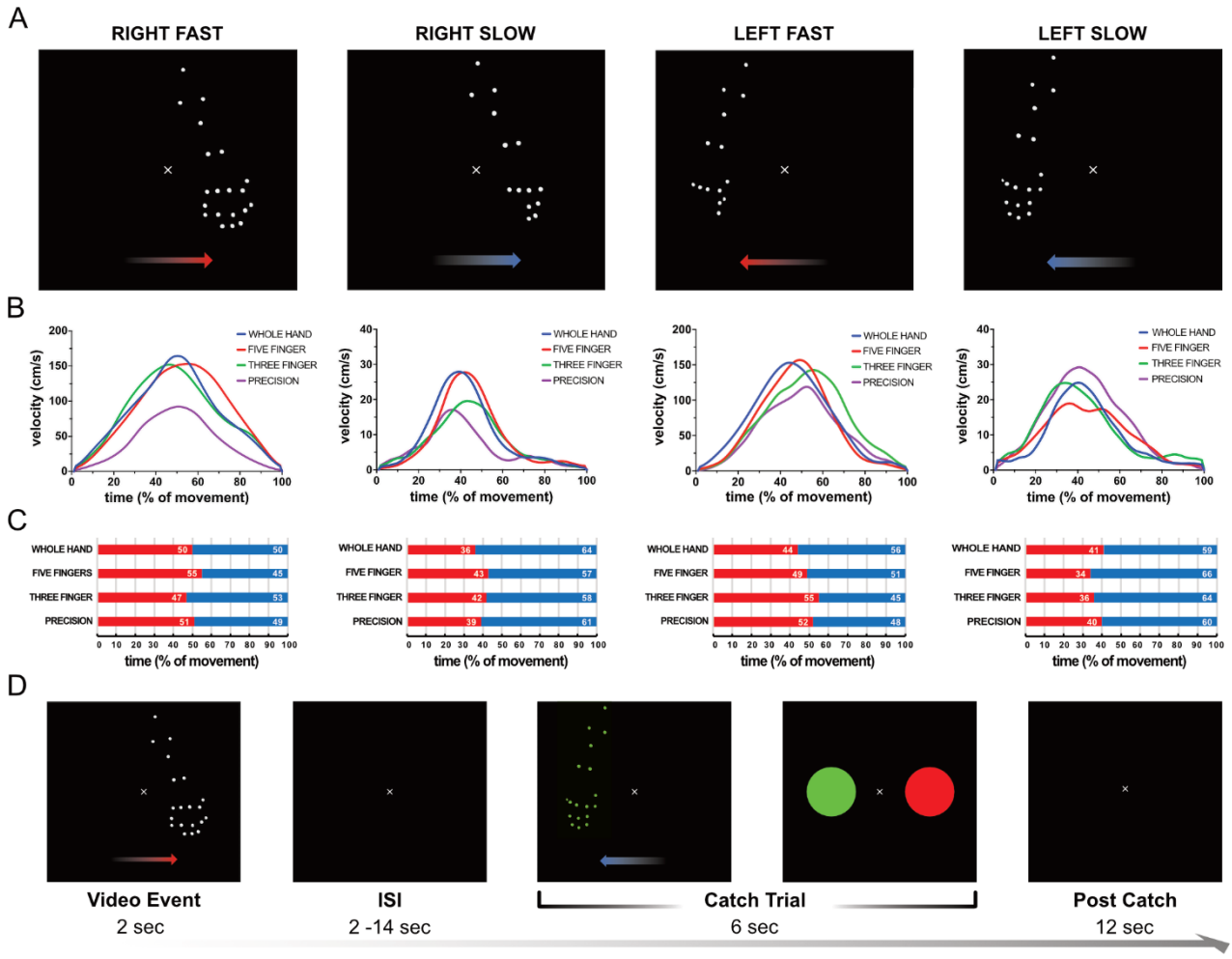

Figure 24. Stimuli and experimental paradigm. From (A) to (C), in left-to-right order each graph represents data from each specific combination of direction and velocity as follows: i) RIGHT FAST; ii) RIGHT SLOW; iii) LEFT FAST; iv) LEFT SLOW. (A) Examples of static frames of PLDs grasping stimuli. In left-to-right order the presented grips are as follows: i) whole hand; ii) three finger; iii)

precision; iv) five finger. (B) Velocity curves of the four types of grips presented in the videos. Note that the scale of the ordinate (stimulus velocity) for the fast stimuli is different from that for the slow stimuli. (C) Horizontal bar graphs showing the acceleration (red) and deceleration (blue) phases, expressed as percentages of movement time of each type of grip. (D) Event related experimental paradigm consisting in video events interleaved by an interstimulus interval (ISI). Catch trials were followed by a post-catch denoising period to allow BOLD signal to reach baseline.

3.3.4 fMRI data acquisition

Anatomical T1-weighted and functional T2*-weighted MR images were acquired with a 3T General Electric scanner (MR750 Discovery) equipped with an 8-channel receiver head-coil. Functional volumes acquisition parameters were the following: 40 axial slices of functional images covering the whole brain acquired in an interleaved bottom-up order using a gradient-echo echo-planar imaging (EPI) pulse sequence, slice thickness = 3.0 mm, interslice gap = 0.5 mm, 64 × 64 × 37 matrix with a spatial resolution of 3.5 × 3.5 × 3.5 mm, TR = 2000 ms, TE = 30 ms, FOV = 205 × 205 mm^2, flip angle = 90°, in plane resolution = 3.2 × 3.2 mm^2. A morphological 3D T1-weighted (Bravo_Mik) volume was acquired as anatomical reference. Its acquisition parameters were: 192 slices, 512 × 512 matrix, spatial resolution 0.9 × 0.5 × 0.5 mm, TR = 9700 ms, TE = 4 ms, FOV = 252 × 252 mm, flip angle 90°.

3.3.5 fMRI data analysis

Data Preprocessing and Analysis

SPM12 (Wellcome Department of Imaging Neuroscience, University College, London, UK; http://www.fil.ion.ucl.ac.uk/spm) on MATLAB R2021a (The Mathworks, Inc.) was used to process the acquired MRI data. To allow T1 equilibration so that the magnetic field could reach a steady state, the first four volumes of each run were discarded. The participant's volumes were preprocessed using the same pipeline. Images were spatially realigned to the first volume of the first functional run, un-

warped to correct for between scan motion and slice timing corrected considering slice acquisition order. Spatial transformation parameters derived from the segmentation and spatial normalization of the anatomical T1-weighted images to the Montreal Neurological Institute (MNI) space were then applied to the realigned EPIs and re-sampled in 2 × 2 × 2 mm^3 voxels using a 4^{th} degree B-spline interpolation in space. A 4-mm full-width half-maximum isotropic Gaussian kernel (FWHM) smoothing was applied to all functional T2*-weighted volumes.

Data were analysed using a random-effects model (Friston et al., 1999), implemented in a two-level procedure. Single-subject fMRI time series were modelled using the general linear model in the first level analysis and the design-matrix included the onsets and the durations of all conditions modelled as events as well as the response of catch trial conditions modelled as an event comprising the video observation (2 seconds), response selection (4 seconds) and post-catch denoise period (12 seconds) for each of the five functional runs. Null events were considered as implicit baseline. Conditions resulting from the combination of 2 velocities × 2 directions × 4 grips, were computed for each subject and contrasted with the implicit baseline. Differences in duration of the movement in fast and slow videos, were taken into account by explicitly modelling them as a regressor. Head motion parameters were also entered as multiple regressors. Specific effects were tested using *t* statistical parametric maps, with degrees of freedom corrected for non-sphericity at each voxel.

In the group-analysis, corresponding *t*-contrast images of the first-level conditions for each participant, except for *Catch-Trial*, were entered into a one way ANOVA with sphericity-correction for repeated measures (Friston et al., 2002). In order to highlight the areas mainly involved in coding each combination of the experimental conditions, namely direction and velocity, *t*-contrasts were generated (RIGHT FAST, RIGHT SLOW, LEFT FAST, LEFT SLOW). Furthermore, *F*-contrasts were performed in order to examine brain regions that exhibited significant activity related to differences in direction, or velocity.

3.3.6 Regions of interest definition

Bilateral anatomically defined regions of interest (ROIs) were selected from Anatomy toolbox v3.0 (Eickhoff et al., 2005) (Table 3). ROIs used in this study were selected based on both anatomical and functional criteria since they have also been described as part of the AON (Hardwick et al., 2018). The selected ROIs were subsequently combined into an ad-hoc atlas created using ImCalc SPM12 toolbox (Wellcome Department of Imaging Neuroscience, University College, London, UK; http://www.fil.ion.ucl.ac.uk/spm).

Left hMT/V5 (Left LOTC)	Right hMT/V5 (Right LOTC)
Left PO1 PIP (Left SPOC)	Right PO1 PIP (Right SPOC)
Left SPL 7PC	Right SPL 7PC
Left SPL 7A	Right SPL 7A
Left hIP3 MIP (Left mIPS)	Right hIP3 MIP (Right mIPS)
Left hIP2 AIP (Left aIPS)	Right hIP2 AIP (Right aIPS)
Left hIP1 VIP (Left vIPS)	Right hIP1 VIP (Right vIPS)
Left IPL PF	Right IPL PF
Left IPL PFt	Right IPL PFt
Left 6d1 (PMd1)	Right 6d1 (PMd1)
Left 6d2 (PMd2)	Right 6d2 (PMd2)
Left Area 44 (PMv)	Right Area 44 (PMv)

Table 3. Anatomically defined ROIs from Anatomy toolbox v3.0 toolbox (Eickhoff et al., 2005).

3.3.7 Multivoxel pattern analysis

In order to make a fine-grained analysis of fMRI data patterns, we performed a multivoxel pattern analysis (MVPA) on linear combination of first-level beta estimates, using Pattern Recognition for Neuroimaging Toolbox (PRoNTo) (Schrouff et al., 2016), running on MATLAB (The MathWorks Inc.)

For each participant the experimental design elements, that is the fMRI data, onsets and condition labels were specified. To exclude voxels outside the brain that carry non-relevant information, a first level whole brain binary mask was employed. The ad-hoc atlas was used for the computation of the feature set as a second level mask and employed in this analysis in order to jointly analyse the neural pattern of relevant brain areas.

A multi-kernel learning (MKL) classifier with L1 regularization was used to classify between neural patterns in the AON ROIs simultaneously. The idea behind MKL was to combine each ROI feature set by assigning different weights to each kernel function. Each kernel corresponded to a different subset of features, that is the ROIs neural pattern distribution. The L1 regularization, also known as LASSO (Least Absolute Shrinkage and Selection Operator), was incorporated into the MKL framework to promote sparsity in the model which allowed the selection of relevant features both at the feature and kernel level. By imposing a penalty on the sum of the absolute values of the model's coefficients, L1 regularization allowed for smaller weights for less important features, effectively driving some coefficients to zero. This resulted in feature selection, where only a subset of the most relevant features was used in the model, that is a subset of regions and voxels that carried predictive information. Thanks to this approach, it was possible to rank the ROIs according to their contribution to each classification model, excluding those with zero contribution. Furthermore, an L1 multiclass SVM algorithm (L1 MCL) was employed, allowing to find the optimal hyperplanes that separate more than two different classes in a high-dimensional feature space. A total of two L1 MKL

(*Direction* and *Velocity*) models and one L1 MCL (each specific combination of direction and velocity) model were created. For the *Direction* model, class one and two correspond to RIGHT and LEFT respectively, while for the *Velocity* model, to FAST and SLOW. Regarding the L1 MCL model, the different classes were RIGHT FAST (class one), RIGHT SLOW (class two), LEFT FAST (class three), LEFT SLOW (class four).

To increase the predictive model performance, we optimized the hyperparameter using a k fold on subject out nested cross-validation (k = 5) which was used only to estimate the value of the hyperparameter leading to the highest performance. A leave one condition out cross validation scheme was used to assess the performance of the classifier and its ability to generalize the results of its computations on a part of the dataset on which it was not trained. The entire dataset was separated into a set used for training and the other for test. The number of folds in which data were partitioned was equal to the number of conditions so that the training set was equal to the number of conditions minus one. Further computations consisted in mean centring the features using training data and dividing the data vectors by their Euclidean norm. The latter is particularly important in order to take into account the different ROIs size for a more accurate comparison. One thousand permutations were run to estimate the model *p*-value, retraining it for the specified number of times with permuted labels and targets. Another measure of the model performance is the area under curve (Beauchamp et al., 2003) which was computed for each L1 MKL model. Weight contribution was calculated both at a region level to investigate the contribution of each ROI to the decision function, and at a voxel level providing insights on the discriminative patterns within the areas. Furthermore, the computation of the reproducibility of the regions ranking was performed in order to examine the consistency of the ranking across the cross-validation folds (Schrouff et al., 2018).

3.4 Results

3.4.1 Univariate analysis

Figure 25 shows brain activation maps on an MNI brain template with a significance threshold of p = 0.01 FWE corrected at a voxel level. Figure 25A shows bilateral significant activation clusters resulting from the *t*-contrast between RIGHT FAST conditions against baseline in posterior occipital (pOC), lateral occipito-temporal (LOTC), superior parieto-occipital cortex (SPOC) and posterior fusiform gyrus (pFG), posterior sector of the superior temporal sulcus (pSTS), superior parietal (SPL) and intraparietal (IPS) areas as well as dorsal and ventral premotor areas (PMd, PMv). Other significantly activated clusters are present in the pre-supplementary motor area (preSMA), posterior sector of the middle cingulate cortex (pMCC), posterior sector of the somatosensory cortex (Area 2) and anterior insula (aI). Subcortical clusters are located in the anterior sector of the putamen, pulvinar and in the cerebellar lobules VI and left VIIb. Activation patterns in both cortex and cerebellum, similar to those previously described, result from the contrast between RIGHT SLOW conditions against baseline (Figure 25B), although less extended and with no clusters in the putamen and anterior insula. In both conditions, left LOTC cluster is more activated as compared to the contralateral sector. The LEFT FAST and LEFT SLOW conditions, when contrasted against baseline (Figure 25C, D), activate the same cortical and cerebellar areas as the RIGHT FAST and RIGHT SLOW conditions. However, the activation in the LOTC area is stronger on the right side for both LEFT conditions. Furthermore, in LEFT FAST brain activations, as compared to the LEFT SLOW condition, there is a small significant cluster in the anterior left putamen.

To investigate the main effects of direction and velocity, *F*-contrasts were employed. Activation maps are overlaid on an MNI brain template and with a significance threshold of p = 0.01 FWE corrected at a cluster level. *F*-contrast for direction (Figure 25E) shows bilateral activation in pOC, pFG and in the SPOC as well as in the cerebellar lobule VI. The *F*-contrast for velocity shows

bilateral activations in LOTC areas bilaterally and SPL as well as the medial IPS (mIPS). In the right hemisphere, the parietal activation cluster was more extended rostrally including also a small posterior portion of Area 2 (Figure 25F) (Supplementary table 2).

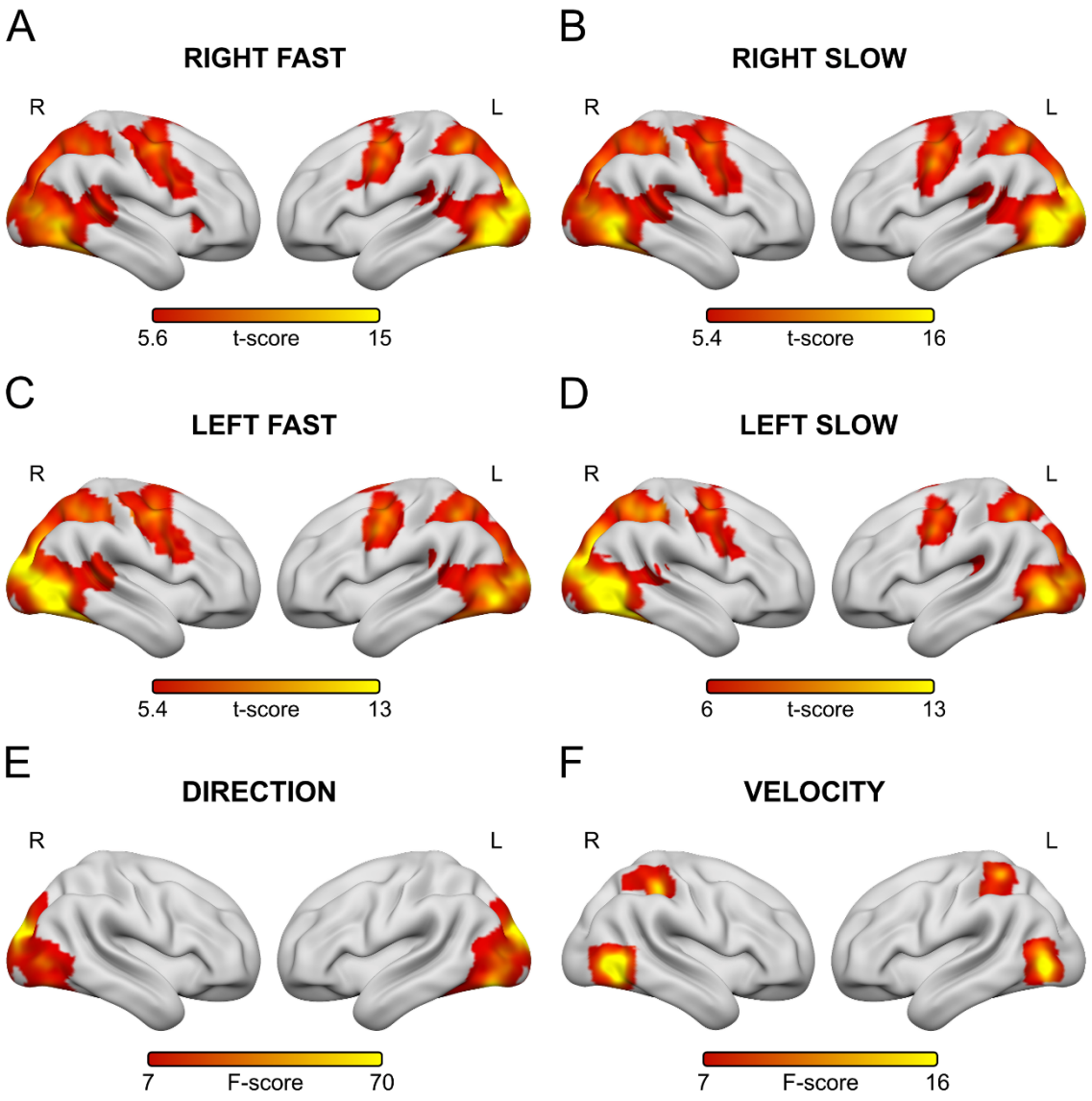

Figure 25. Cortical activations projected onto a 3D Brain template (Surfice; https://www.nitrc.org/projects/surfice/). (A) Contrast between RIGHT FAST and baseline. (B) Contrast between RIGHT SLOW and baseline. (C) Contrast between LEFT FAST and baseline. (D) Contrast between LEFT SLOW and baseline. (E) F-Contrast of DIRECTION effect. (F) F-Contrast of VELOCITY effect.

3.4.2 Multivoxel pattern analysis

The analysis revealed that both L1 MKL models were significantly accurate in discriminating between *Direction* and *Velocity* as well as L1 MCL in discriminating between each specific combination of these two kinematic parameters. Details about each model performance is listed in Table 4. The L1 MKL *Direction* model revealed significant model decoding accuracy (84.01%, p = 0.001, AUC = 0.92, p = 0.001) in classifying between linear combination of beta images belonging to RIGHT and LEFT conditions for each subject. ROIs contributing to the L1 MKL *Direction* classification model are listed in the supplementary table 3. The L1 MKL *Velocity* model computed on the linear combination of beta images of FAST and SLOW conditions for each subject, was significantly accurate in discriminating the neural patterns belonging to these conditions (model accuracy = 74.31%, p = 0.001, AUC = 0.79, p = 0.001). L1 MKL *Velocity* ROIs contribution to the classification model are listed in supplementary table 4.

Model name	**Accuracy (%)**	**Accuracy (p)**	**AUC**	**AUC (p)**	**Class 1 acc (%)**	**Class 2 acc (%)**	**Class 3 acc (%)**	**Class 4 acc (%)**
L1 MKL Direction	84.01	< 0.001	0.92	< 0.001	83.59	84.38	-	-
L1 MKL Velocity	74.31	< 0.001	0.79	< 0.001	72.74	75.78	-	-
L1 MCL Dir * Vel	55.61	< 0.001	-	-	58.88	59.38	46.88	59.38

Table 4. MVPA classification models performance summary. For the L1 MKL Direction model class 1 corresponds to RIGHT and class 2 to LEFT. For the L1 MKL Velocity model class 1 corresponds to FAST and class 2 to SLOW. For the L1 MCL model classes from 1 to 4 correspond to RIGHT FAST, RIGHT SLOW, LEFT FAST and LEFT SLOW respectively. AUC = Area under curve; Acc = Accuracy.

To investigate the stability of the selection of regions across folds of the L1 MKL models, we computed also the reproducibility measure for both *Direction* (model reproducibility = 0.97) and *Velocity* model (model reproducibility = 0.98). Contribution to the *Direction* and *Velocity* models, both at a ROI and voxel level, is represented in Figures 26 and 27 respectively.

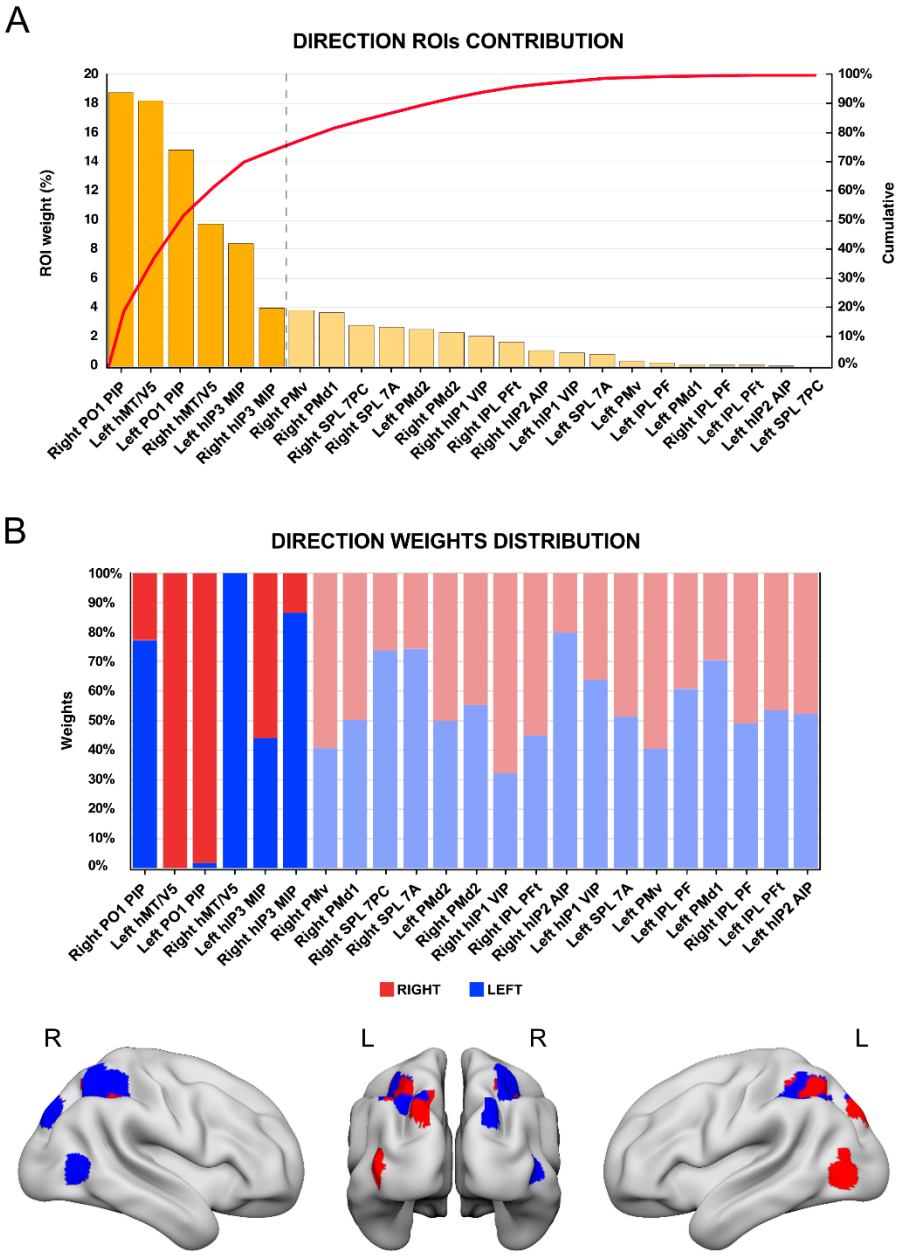

Figure 26. Direction model weights distribution at a Region of Interest and voxel level of direction multi-kernel model. (A) L1 MKL Direction weight distribution at a ROI level. Weight computation at a ROI level is represented as a bar graph with dark yellow ones, leftward of the vertical dotted line, showing the ROIs that collectively contributed to explain 75% of the model. The red line shows the cumulative percentage of the total weight contribution to the classification. (B) Upper panel is showing the weight distribution at a voxel level within AON areas as a bar graph, with red bars indicating the percentage of weights most discriminative for RIGHT class and blue ones for LEFT class. Bottom panel shows the results of the weight computation at a voxel level projected on an inflated brain template (Surfice; https://www.nitrc.org/projects/surfice/) with the same color coding previously described.

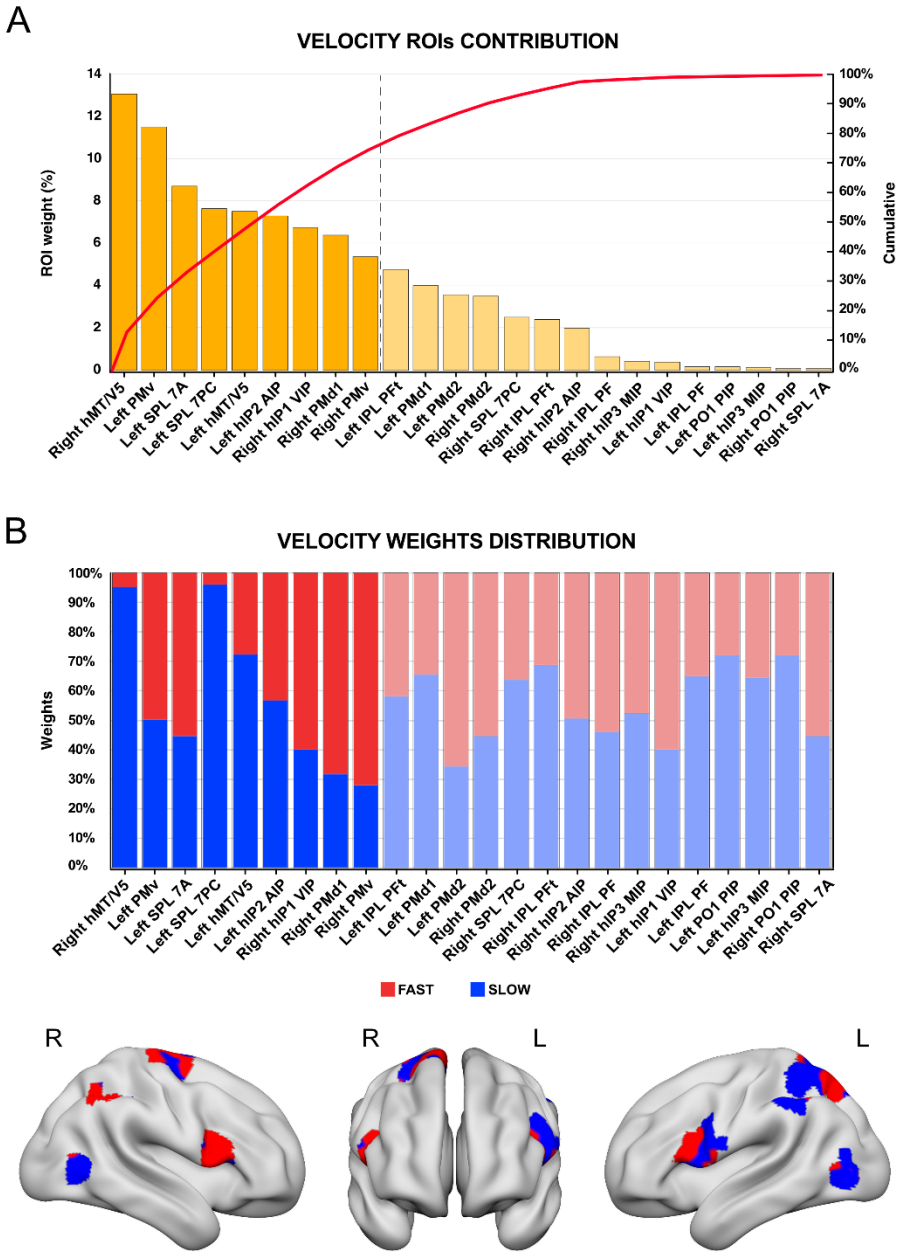

Figure 27. Velocity model weights distribution at a Region of Interest and voxel level of velocity multi-kernel model. (A) L1 MKL Velocity weight distribution at a ROI level. Weight computation at a ROI level is represented as a bar graph with dark yellow ones, leftward of the vertical dotted line, showing the ROIs that collectively contributed to explain 75% of the model. The red line shows the cumulative percentage of the total weight contribution to the classification. (B) Upper panel is showing the weight distribution at a voxel level within AON areas as a bar graph, with red bars indicating the percentage of weights most discriminative for FAST class and blue ones for SLOW class. Bottom panel shows the results of the weight computation at a voxel level projected on an ICBM152 inflated brain template (Surfice; https://www.nitrc.org/projects/surfice/) with the same color coding previously described.

L1 MCL model which classified between RIGHT FAST, RIGHT SLOW, LEFT FAST and LEFT SLOW conditions altogether, where chance level is 25%, showed significant decoding accuracy (55.61%, p = 0.001). Furthermore, each class achieved an above threshold significant decoding accuracy (RIGHT FAST model accuracy = 56.88%, p = 0.001; RIGHT SLOW model accuracy = 59.38%, p = 0.002; LEFT FAST model accuracy = 46.88%, p = 0.004; LEFT FAST model accuracy = 59.38%, p = 0.001).

3.5 Discussion

In the present fMRI study, healthy participants observed grasping actions presented as PLDs, performed with two velocities, fast and slow, in two different directions, right and left. The results confirm that the kinematic information conveyed by the observation of PLDs grasping actions elicits activation of the AON. Univariate analyses reveal that bilateral posterior occipital and posterior parietal areas of this network are mainly recruited in coding differences in stimulus direction, while velocity is mainly coded in occipito-temporal and parietal areas, bilaterally. By means of multivariate analyses we further demonstrate that both direction and velocity, as well as their combinations, are significantly decoded at the network level. More specifically, AON regions decode kinematic features and contribute differently to the classification models. Weights estimation at a voxel level, as compared with univariate analysis, reveals a wider set of regions decoding differences in direction such as lateral occipito-temporal, posterior parietal and intraparietal areas, as well as differences in velocity, that is lateral occipito-temporal, superior parietal and premotor areas.

A distributed network of areas within the AON, including bilateral LOTC and SPOC codes differences in direction of the observed PLDs grasping action. In particular, multivariate analysis expands these findings by showing that the areas that mostly contribute to the decoding of differences of stimuli direction are not limited to these regions but include also sectors of the mIPS bilaterally.

The analysis of voxel weights distribution further suggested that areas of the left hemisphere mostly contribute to the decoding of actions performed towards the contralateral, right portion of space, while those of the right hemisphere to those performed leftwards. These results are in line with previous neuroimaging studies in humans, which showed that the LOTC plays a key role in coding motion direction (Kamitani & Tong, 2006; Zeki et al., 1991). This has also been confirmed by TMS studies showing that stimulation of this area produces impaired motion perception (Beckers & Zeki, 1995; Sack et al., 2006). It is worth noting that studies on the role of this area mainly used gratings or clockwise and counterclockwise dots rotary motion as visual stimuli. In contrast, our stimuli, although conveying exclusively kinematic information, provide more behaviorally relevant representation of the hand. Using a similar paradigm, in a previous study (Ziccarelli et al., 2022) we demonstrated that LOTC exhibits a stronger response to PLDs grasping actions as compared to the overall motion sharing the same kinematic features. In addition, the present study demonstrates that this area can already decode more complex information about action kinematics, such as differences in the observed grasping direction.

Concerning SPOC, neuroimaging studies in humans showed that this area is involved in visual motion perception (Cardin et al., 2012; Pitzalis et al., 2010) and in both observation (Filimon et al., 2007) and execution (Cavina-Pratesi et al., 2010; Gallivan et al., 2009) of arm reaching actions. Our findings add additional pieces of evidence, by demonstrating that SPOC significantly contributes to the decoding of differences in direction of observed grasping actions when only kinematic information is available.

To our knowledge there are no studies describing the role of mIPS in decoding differences in stimulus direction during action observation, while it has been demonstrated its involvement in action execution (Davare et al., 2012). Our results show that it is possible to decode differences in grasping direction within the mIPS during action observation, a novel finding that adds a crucial dimension to our understanding of its involvement in encoding specific features of the observed action.

Taken together, univariate and multivariate analyses revealed that velocity information is represented in a distributed network of AON areas such as bilateral LOTC, IPS, and both PMd and PMv cortex, as well as in the left SPL. Weights distribution within these regions showed that most of them contributed similarly to the decoding of the two velocities except for LOTC, which greatly contributed to the classification of actions performed with a slow velocity. This could be due to the fact that slow grasping actions might provide, regardless of stimulus duration, more distinct and clear motion cues which can be elaborated and classified with greater accuracy. Neuroimaging studies on humans focusing on the role of LOTC in coding stimulus velocity, demonstrated that this is not only a motion direction sensitive area but also plays a crucial role in the perception of the speed of gratings or dartboard patterns (Gaglianese et al., 2023; Lingnau et al., 2009). This is also confirmed by studies using both repetitive and single-pulse TMS, showing that after the stimulation of these areas, deficits in speed perception emerge (Matthews et al., 2001; McKeefry et al., 2008). Taken together, our findings reveal that LOTC is recruited during processing of hand-related stimuli such as grasping actions and contains enough information to disentangle different velocities suggesting a broader role of this area in elaborating complex visual information related to action kinematics.

In addition to visual areas, parietal and premotor areas also contain enough information to decode stimulus velocity. This result is in line with previous literature showing that both superior parietal and premotor dorsal areas modulated their activity during the observation of a visible arm reaching a target with different velocities (Di Dio et al., 2013). The present study extends these latter findings by showing that parietal and premotor areas are also modulated by differences in the velocity of grasping actions, suggesting that the capacity of disentangling different velocities of observed actions can subserve finer decoding of others' actions. Interestingly, our data demonstrate that not only dorsal but also ventral bilateral sectors of the premotor cortex decode differences in velocity, suggesting that the whole premotor cortex is involved in coding specific features of the observed

action, such as grip configuration (Errante et al., 2021a; Grafton & Hamilton, 2007) and in the decoding of velocity kinematic parameters.

Furthermore, our data show that also the anterior and ventral sectors of the IPS, which are connected with PMv both anatomically (Borra et al., 2008; Luppino et al., 1999; Thiebaut de Schotten et al., 2012) and functionally (Davare et al., 2011), play a role in decoding differences in action velocity. The functional coupling with PMv may suggest an interplay between these two areas, not only in coding aspects of grasping and visuomotor transformations (Errante et al., 2021b), but also in extracting velocity kinematic features during action observation.

3.6 Conclusions

Kinematic information conveyed by PLDs grasping actions, activates a wide set of occipito-temporal, parietal and premotor areas within the action observation network. Using multivariate approaches based on multi-kernel classification algorithms, it was possible to identify multiple sets of areas, within the AON, contributing differently to the decoding of direction and velocity. Based on these data, future studies will address how this information is used when individuals are required to imitate actions based only on the kinematic parameters of the observed action. This could also shed light on the mechanisms underlying action planning and the subsequent execution of complex motor tasks. The design of rehabilitation programs based on action observation (Buccino, 2014; Franceschini et al., 2012; Pelosin et al., 2010; Sgandurra et al., 2013; Verzelloni et al., 2021) might be shaped by these current findings as well. Finally, the present results could also be exploited for improving hand actions recognition and classification models based on machine learning (Zhang et al., 2020), by extracting the most relevant kinematic features from the analysis of the observed actions. These features could then be used to develop artificial intelligence systems capable of understanding and generating actions in a realistic and natural way.

4. General discussion

Human sensitivity to biological motion plays a key role for the understanding of others' behavior, also when it is characterized solely by biological kinematic information as presented by means of point-light displays (PLDs). As a matter of fact, crucial information about the features of the observed action is provided by kinematic parameters of biological motion, such as duration, velocity, direction. The present thesis is aimed at investigating the involvement of specific AON areas in decoding differences in fully visible (FV) and point-light displays (PLDs), as well as in kinematic features of the observed PLDs actions performed with different velocities and directions. Taken together, these results show that: a) kinematic features, conveyed by PLDs grasping action, elicit an activation of the AON comparable to that of FV stimuli, suggesting that this information is sufficient for action understanding; b) differences between FV and PLDs stimuli can be decoded in parieto-premotor areas of the AON highlighting their potential role in disentangling the features of the two sets of stimuli; c) differences in direction and velocity kinematic parameters can be decoded at the network level; d) AON regions contribute differently to the decoding process, with both lateral occipito-temporal and parietal areas decoding both direction and velocity features, and premotor areas being mainly involved in velocity decoding.

The results presented in this thesis add new fundamental information on the neural correlates of the observation of PLDs hand grasping actions. Here, are described activations of the human parieto-premotor areas of the AON, which are usually reported being activated during the observation of FV actions, where information about the effector, context and object, is available (Caspers et al., 2010; Hardwick et al., 2018). By using PLDs we controlled for such information, thus keeping only those features that still allow to decode action goal, showing that the AON can elaborate kinematic information from visually impoverished stimuli in order to produce a complete action representation through a motor resonance mechanism similar to that elicited by FV actions. These specific results

were further confirmed in the second study of this thesis, which showed a similar activation of AON areas during the observation of grasping actions similar to those presented in the first study. Furthermore, by modulating direction and velocity kinematic parameters, we were able to identify specific sectors of the AON mainly recruited in decoding differences between such action features.

The lateral occipito-temporal cortex (LOTC) is an area which plays a key role in coding biological motion during the observation of PLDs (Chang et al., 2018; Grossman et al., 2000; Grossman & Blake, 2002; Peelen et al., 2006; Pelphrey et al., 2005; Servos et al., 2002). LOTC activations were also described in our first study. It is worth noting that, although both random and coherent motion of PLDs presented in the scrambled control condition and box control condition, respectively, share low-level visual and motion features with the experimental stimuli, they elicited a significantly weaker activation in these areas. This strongly suggests that LOTC is mainly tuned to biological features of motion as compared to motion in general. In support of that, data from the second study showed that LOTC is significantly activated by differences in both stimuli direction and velocity. Although LOTC involvement in motion perception was demonstrated by neuroimaging (Kamitani & Tong, 2006; Zeki et al., 1991) and transcranial magnetic stimulation (TMS) studies (Beckers & Zeki, 1995; Sack et al., 2006) using stimuli such as gratings, we further demonstrated that LOTC can already decode more complex information about biological action kinematics. This is important, because it means that differences in kinematic action features can be already decoded in high order visual areas. Future experiments could investigate the timing of LOTC activation during observation of PLDs action and the change in its functional connectivity with other AON regions.

Previous data focusing on arm reaching actions suggested that the dorsal sectors of AON are modulated by velocity (Di Dio et al., 2013). We further demonstrated that, in these areas, is possible to decode differences not only in reaching velocity but also in grasping velocity and direction. Furthermore, we added new information about the functional role of the ventral premotor cortex

(PMv) showing that, although it has been classically described as involved in goal coding, it can also distinguish between observed action velocities. This finding is in line with recent research suggesting that the premotor cortex codes several kinematic aspects of the action, such as grip configuration (Errante et al., 2021a). PMv role in coding different aspects of observed action may be used to guide the selection and execution of appropriate motor plans in response to the visual stimuli. Future investigations could assess how this area is modulated in situations in which it is necessary to correctly respond to stimuli varying in speed and/or trajectory in order to achieve the desired outcome.

These findings could be relevant for the design of more tailored rehabilitation programs based on action observation for patients affected by disorders impacting the upper limb functions. Prior to that, it would be fundamental to assess how the kinematics of observed actions are encoded by pathological populations, such as in children affected by cerebral palsy (CP), which are characterized by movement disorders due to congenital non-progressive brain lesions occurring during fetal or infant development. Recent therapeutic approaches based on action observation (action observation therapy – AOT), were employed in children with unilateral cerebral palsy (UCP), showing improvements in upper limb functions. Noteworthy, a stronger recruitment of the MNS during the observation of a pathological model as compared to a healthy model was demonstrated (Errante et al., 2019b). These findings further indicate that the MNS plays a key role in decoding the kinematics of the observed actions, suggesting that a training program, based on action kinematic information presented by means of PLDs, could effectively enhance fine motor skills by leveraging these kinematic features.

Recently, artificial intelligence (AI) and deep learning (DL) models have found multiple applications into everyday life. Some AI and DL algorithms have been developed in order to track animal body and limb movements (Insafutdinov et al., 2017; Nath et al., 2019; Zhang et al., 2020). Thanks to this technology, it would be possible to create a series of grasping-classifiyng models in

order to analize kinematic features of the observed action such as its grip, direction and velocity, to predict grasping intentions for the programming of a congruent response by a human-machine interface. These models could in fact be implemented in robots, to facilitate daily activities allowing for gesture-based controls.

5. Supplementary information

Anatomical Area	*Left hemisphere*				*Right hemisphere*			
	z-scores	**Peak MNI coordinates**			**z-scores**	**Peak MNI coordinates**		
		x	y	z		x	y	z
FV_Grasp > FV_Ctrls								
Occipital Lobe								
hOc4la	inf	-50	-74	0	inf	48	-68	-6
Superior Occipital (SPOC)	inf	-24	-82	30	5.10	28	-78	32
FG4	inf	-42	-44	-22	inf	42	-44	-20
Frontal Lobe								
Precentral Gyrus (PMd)	Inf	-22	-12	58	4.63	28	-14	58
Precentral Gyrus (PMv)	Inf	-56	2	36				
Parietal Lobe								
Inferior Parietal	inf	-34	-40	-48	5.41	45	-60	-4
PFt (IPL)	inf	-46	-26	34				
7A (SPL)	inf	-18	-56	62				
7PC (SPL)					inf	24	-56	64
Area 2					inf	34	-42	56
hIP3 (IPS)					inf	32	-50	56
Other								
MCC	5.51	-12	-22	40				
Thalamus Visual	5.99	-16	-30	-2				
Cerebellar Lobule VIIIa					6.26	10	-72	-48
PLD_Grasp > PLD_Ctrls								
Occipital Lobe								
hOc4la	inf	-54	-74	0	inf	50	-70	0
Inferior Temporal					inf	46	-64	-6
Superior Occipital (SPOC)	inf	-24	-78	28	6.35	28	-72	30
FG4	7.05	-44	-44	-24	inf	42	-44	20
Frontal Lobe								
Precentral Gyrus (PMd)	6.80	-40	-4	60	5.40	38	-6	54
Precentral Gyrus (PMv)	inf	-58	2	36	6.46	56	10	28

Parietal Lobe								
Inferior Parietal	inf	-34	-42	50	inf	32	-40	52
PFt (IPL)	inf				6.51	52	-18	34
7A (SPL)	inf	-20	-58	56				
7PC (SPL)								
PSC 2	inf	-50	-24	36	inf	32	-40	52
PSC 3b					6.52	52	-18	34
Other								
MCC	5.18	-12	-22	40				
Thalamus Visual	5.99	-16	-30	-2				
Cerebellar Lobule VIIIa	5.98	-8	-74	-48	6.92	10	-74	-48

Supplementary table 1. Statistical values for univariate group analysis related to the contrasts between each experimental condition (FV_Grasp; PLD_Grasp) and their respective control conditions (FV_Static, FV_Box, FV_Scrambled (FV_Ctrls); PLD_Static, PLD_Box, PLD_Scrambled (PLD_Ctrls)). Left column reports the most probable anatomical regions derived from Anatomy Toolbox 2.1. Local maxima are given in MNI standard brain coordinates. Significant threshold is set at $P < 0.01$, FWE corrected at a voxel level.

Anatomical Area	*Left hemisphere*				*Right hemisphere*			
	z-scores	**Peak MNI coordinates**			**z-scores**	**Peak MNI coordinates**		
		x	y	z		x	y	z
DIRECTION								
Occipital Lobe								
hOc1 (V1)	inf	-6	-80	-10	inf	+12	-88	0
hOc2 (V2)	inf	-24	-82	30	inf	+8	-78	-6
hOc4v	inf	-34	-78	-18	inf	+30	-72	-10
hOc5 (hMT/V5)	6.08	-44	-76	+6	3.86	+44	-68	0
FG1	inf	-26	-74	-12				
Parietal Lobe								
PIP PO1	3.17	-16	-84	+34	3.51	+18	-84	36
VELOCITY								
Occipital Lobe								
hOc4la					inf	+48	-68	-2
hOc5 (hMT/V5)	inf	-44	-74	-2				
Parietal Lobe								
7A (SPL)	inf	-36	-46	+58	inf	+30	-56	+56
7PC (SPL)					inf	+36	-48	+60
hIP2 (IPS)					inf	+40	-40	54
hIP3 (IPS)	2.62	-34	-50	+52	inf	+34	-54	+54
PSC 2					inf	+38	-36	+48

Supplementary table 2. Statistical values for GLM group analysis related to the F contrasts for *DIRECTION* and *VELOCITY*. Left column reports the most probable anatomical regions derived from Anatomy Toolbox 3.0. Local maxima are given in MNI standard brain coordinates. Significant threshold is set at $p = 0.01$, FWE corrected at a cluster level.

L1 MKL Direction model weights				
ROI Label		**ROI weight (%)**	**ROI size (vox)**	**Expected Ranking**
	Right PO1 PIP	18.84	182	23.69
Left hMT/V5		18.28	87	23.31
Left PO1 PIP		14.88	223	22.00
	Right hMT/V5	9.78	88	20.75
Left hIP3 MIP		8.46	441	20.00
	Right hIP3 MIP	4.02	478	16.81
	Right PMv	3.86	479	17.19
	Right PMd1	3.71	691	16.81
	Right SPL 7PC	2.83	343	14.50
	Right SPL 7A	2.71	413	14.69
Left PMd2		2.55	329	13.56
	Right PMd2	2.33	322	13.06
	Right hIP1 VIP	2.10	340	12.94
	Right IPL PFt	1.69	416	11.31
	Right hIP2 AIP	1.11	226	9.69
Left hIP1 VIP		0.96	437	8.44
Left SPL 7A		0.84	624	7.56
Left PMv		0.40	540	1.25
Left IPL PF		0.28	245	0.75
Left PMd1		0.14	528	0.56
	Right IPL PF	0.12	492	0.50
Left IPL PFt		0.10	438	0.44
Left hIP2 AIP		0.02	300	0.19
Left SPL 7PC		0	160	0

Supplementary table 3. L1 MKL Direction model weights computation.

L1 MKL Velocity model weights				
ROI Label		**ROI weight (%)**	**ROI size (vox)**	**Expected Ranking**
	Right hMT/V5	13.12	88	23.62
Left PMv		11.55	540	23.06
Left SPL 7A		8.76	624	20.94
Left SPL 7PC		7.68	160	19.56
Left hMT/V5		7.56	87	19.38
Left hIP2 AIP		7.34	300	19.38
	Right hIP1 VIP	6.78	340	17.88
	Right PMd1	6.42	691	17.44
	Right PMv	5.41	479	16.12
Left IPL PFt		4.81	438	14.75
Left PMd1		4.04	528	13.56
Left PMd2		3.60	329	12.81
	Right PMd2	3.55	322	12.88
	Right SPL 7PC	2.54	343	11.06
	Right IPL PFt	2.43	416	10.38
	Right hIP2 AIP	2.02	226	9.50
	Right IPL PF	0.68	492	3.94
	Right hIP3 MIP	0.46	478	3.88
Left hIP1 VIP		0.42	437	3.25
Left IPL PF		0.21	245	0.75
Left PO1 PIP		0.19	223	1.81
Left hIP3 MIP		0.16	441	0.75
	Right PO1 PIP	0.12	182	0.38
	Right SPL 7A	0.12	413	0.31

Supplementary table 4. L1 MKL Velocity model weights computation.

References

Abdelgabar, A. R., Suttrup, J., Broersen, R., Bhandari, R., Picard, S., Keysers, C., De Zeeuw, C. I., & Gazzola, V. (2019). Action perception recruits the cerebellum and is impaired in patients with spinocerebellar ataxia. *Brain*, *142*(12), 3791-3805. https://doi.org/10.1093/brain/awz337

Amoruso, L., Finisguerra, A., & Urgesi, C. (2016). Tracking the Time Course of Top-Down Contextual Effects on Motor Responses during Action Comprehension. *J Neurosci*, *36*(46), 11590-11600. https://doi.org/10.1523/JNEUROSCI.4340-15.2016

Arcaro, M. J., Pinsk, M. A., Li, X., & Kastner, S. (2011). Visuotopic organization of macaque posterior parietal cortex: a functional magnetic resonance imaging study. *J Neurosci*, *31*(6), 2064-2078. https://doi.org/10.1523/JNEUROSCI.3334-10.2011

Battelli, L., Cavanagh, P., & Thornton, I. M. (2003). Perception of biological motion in parietal patients. *Neuropsychologia*, *41*(13), 1808-1816.

Beauchamp, M. S., Lee, K. E., Haxby, J. V., & Martin, A. (2003). FMRI responses to video and point-light displays of moving humans and manipulable objects. *J Cogn Neurosci*, *15*(7), 991-1001. https://doi.org/10.1162/089892903770007380

Beckers, G., & Zeki, S. (1995). The consequences of inactivating areas V1 and V5 on visual motion perception. *Brain*, *118 (Pt 1)*, 49-60. https://doi.org/10.1093/brain/118.1.49

Belmalih, A., Borra, E., Contini, M., Gerbella, M., Rozzi, S., & Luppino, G. (2009). Multimodal architectonic subdivision of the rostral part (area F5) of the macaque ventral premotor cortex. *J Comp Neurol*, *512*(2), 183-217. https://doi.org/10.1002/cne.21892

Biagi, L., Cioni, G., Fogassi, L., Guzzetta, A., & Tosetti, M. (2010). Anterior intraparietal cortex codes complexity of observed hand movements. *Brain Res Bull*, *81*(4-5), 434-440. https://doi.org/10.1016/j.brainresbull.2009.12.002

Binkofski, F., Buccino, G., Posse, S., Seitz, R. J., Rizzolatti, G., & Freund, H. (1999). A fronto-parietal circuit for object manipulation in man: evidence from an fMRI-study. *Eur J Neurosci*, *11*(9), 3276-3286. https://doi.org/10.1046/j.1460-9568.1999.00753.x

Blake, R., & Shiffrar, M. (2007). Perception of human motion. *Annu Rev Psychol*, *58*, 47-73. https://doi.org/10.1146/annurev.psych.57.102904.190152

Bonda, E., Petrides, M., Ostry, D., & Evans, A. (1996). Specific involvement of human parietal systems and the amygdala in the perception of biological motion. *J Neurosci*, *16*(11), 3737-3744. https://www.ncbi.nlm.nih.gov/pubmed/8642416

Borra, E., Belmalih, A., Calzavara, R., Gerbella, M., Murata, A., Rozzi, S., & Luppino, G. (2008). Cortical connections of the macaque anterior intraparietal (AIP) area. *Cereb Cortex*, *18*(5), 1094-1111. https://doi.org/10.1093/cercor/bhm146

Borra, E., Gerbella, M., Rozzi, S., & Luppino, G. (2011). Anatomical evidence for the involvement of the macaque ventrolateral prefrontal area 12r in controlling goal-directed actions. *J Neurosci*, *31*(34), 12351-12363. https://doi.org/10.1523/JNEUROSCI.1745-11.2011

Boussaoud, D., Ungerleider, L. G., & Desimone, R. (1990). Pathways for motion analysis: cortical connections of the medial superior temporal and fundus of the superior temporal visual areas in the macaque. *Journal of Comparative Neurology*, *296*(3), 462-495.

Buccino, G. (2014). Action observation treatment: a novel tool in neurorehabilitation. *Philos Trans R Soc Lond B Biol Sci*, *369*(1644), 20130185. https://doi.org/10.1098/rstb.2013.0185

Buccino, G., Binkofski, F., Fink, G. R., Fadiga, L., Fogassi, L., Gallese, V., Seitz, R. J., Zilles, K., Rizzolatti, G., & Freund, H. J. (2001). Action observation activates premotor and parietal areas in a somatotopic manner: an fMRI study. *European journal of neuroscience*, *13*(2), 400-404.

Buccino, G., Lui, F., Canessa, N., Patteri, I., Lagravinese, G., Benuzzi, F., Porro, C. A., & Rizzolatti, G. (2004a). Neural circuits involved in the recognition of actions performed by nonconspecifics: An fMRI study. *Journal of cognitive neuroscience*, *16*(1), 114-126.

Buccino, G., Vogt, S., Ritzl, A., Fink, G. R., Zilles, K., Freund, H.-J., & Rizzolatti, G. (2004b). Neural circuits underlying imitation learning of hand actions: an event-related fMRI study. *Neuron*, *42*(2), 323-334.

Calvo-Merino, B., Glaser, D. E., Grezes, J., Passingham, R. E., & Haggard, P. (2005). Action observation and acquired motor skills: an FMRI study with expert dancers. *Cereb Cortex*, *15*(8), 1243-1249. https://doi.org/10.1093/cercor/bhi007

Calvo-Merino, B., Grezes, J., Glaser, D. E., Passingham, R. E., & Haggard, P. (2006). Seeing or doing? Influence of visual and motor familiarity in action observation. *Curr Biol*, *16*(19), 1905-1910. https://doi.org/10.1016/j.cub.2006.07.065

Cardin, V., Sherrington, R., Hemsworth, L., & Smith, A. T. (2012). Human V6: functional characterisation and localisation. *PLoS One*, *7*(10), e47685. https://doi.org/10.1371/journal.pone.0047685

Carey, D. P., Perrett, D. I., & Oram, M. W. (1997). Recognizing, understanding and reproducing action. *Handbook of neuropsychology*, *11*, 111-130.

Casile, A., Dayan, E., Caggiano, V., Hendler, T., Flash, T., & Giese, M. A. (2010). Neuronal encoding of human kinematic invariants during action observation. *Cereb Cortex*, *20*(7), 1647-1655. https://doi.org/10.1093/cercor/bhp229

Caspers, S., Zilles, K., Laird, A. R., & Eickhoff, S. B. (2010). ALE meta-analysis of action observation and imitation in the human brain. *Neuroimage*, *50*(3), 1148-1167. https://doi.org/10.1016/j.neuroimage.2009.12.112

Cattaneo, L., Fabbri-Destro, M., Boria, S., Pieraccini, C., Monti, A., Cossu, G., & Rizzolatti, G. (2007). Impairment of actions chains in autism and its possible role in intention understanding. *Proc Natl Acad Sci U S A*, *104*(45), 17825-17830. https://doi.org/10.1073/pnas.0706273104

Cavina-Pratesi, C., Monaco, S., Fattori, P., Galletti, C., McAdam, T. D., Quinlan, D. J., Goodale, M. A., & Culham, J. C. (2010). Functional magnetic resonance imaging reveals the neural

substrates of arm transport and grip formation in reach-to-grasp actions in humans. *J Neurosci*, *30*(31), 10306-10323. https://doi.org/10.1523/JNEUROSCI.2023-10.2010

Chang, D. H. F., Ban, H., Ikegaya, Y., Fujita, I., & Troje, N. F. (2018). Cortical and subcortical responses to biological motion. *Neuroimage*, *174*, 87-96. https://doi.org/10.1016/j.neuroimage.2018.03.013

Chouchourelou, A., Matsuka, T., Harber, K., & Shiffrar, M. (2006). The visual analysis of emotional actions. *Soc Neurosci*, *1*(1), 63-74. https://doi.org/10.1080/17470910600630599

Cochin, S., Barthelemy, C., Roux, S., & Martineau, J. (1999). Observation and execution of movement: similarities demonstrated by quantified electroencephalography. *Eur J Neurosci*, *11*(5), 1839-1842. https://doi.org/10.1046/j.1460-9568.1999.00598.x

Colby, C. L., Duhamel, J. R., & Goldberg, M. E. (1993). Ventral intraparietal area of the macaque: anatomic location and visual response properties. *J Neurophysiol*, *69*(3), 902-914. https://doi.org/10.1152/jn.1993.69.3.902

Davare, M., Kraskov, A., Rothwell, J. C., & Lemon, R. N. (2011). Interactions between areas of the cortical grasping network. *Curr Opin Neurobiol*, *21*(4), 565-570. https://doi.org/10.1016/j.conb.2011.05.021

Davare, M., Zenon, A., Pourtois, G., Desmurget, M., & Olivier, E. (2012). Role of the Medial Part of the Intraparietal Sulcus in Implementing Movement Direction. *Cerebral cortex*, *22*(6), 1382-1394. https://doi.org/10.1093/cercor/bhr210

De Renzi, E. (1982). Disorders of space exploration and cognition. *JOHN WILEY & SONS, INC., 605 THIRD AVE., NEW YORK, NY 10158. 1982.*

Di Dio, C., Di Cesare, G., Higuchi, S., Roberts, N., Vogt, S., & Rizzolatti, G. (2013). The neural correlates of velocity processing during the observation of a biological effector in the parietal and premotor cortex. *Neuroimage*, *64*, 425-436. https://doi.org/10.1016/j.neuroimage.2012.09.026

Di Pellegrino, G., Fadiga, L., Fogassi, L., Gallese, V., & Rizzolatti, G. (1992). Understanding motor events: a neurophysiological study. *Experimental brain research*, *91*(1), 176-180. https://doi.org/Doi 10.1007/Bf00230027

Dittrich, W. H., Troscianko, T., Lea, S. E., & Morgan, D. (1996). Perception of emotion from dynamic point-light displays represented in dance. *Perception*, *25*(6), 727-738.

Eickhoff, S. B., Stephan, K. E., Mohlberg, H., Grefkes, C., Fink, G. R., Amunts, K., & Zilles, K. (2005). A new SPM toolbox for combining probabilistic cytoarchitectonic maps and functional imaging data. *Neuroimage*, *25*(4), 1325-1335. https://doi.org/10.1016/j.neuroimage.2004.12.034

Errante, A., & Fogassi, L. (2019a). Parieto-frontal mechanisms underlying observation of complex hand-object manipulation. *Sci Rep*, *9*(1), 348. https://doi.org/10.1038/s41598-018-36640-5

Errante, A., Di Cesare, G., Pinardi, C., Fasano, F., Sghedoni, S., Costi, S., Ferrari, A., & Fogassi, L. (2019b). Mirror neuron system activation in children with unilateral cerebral palsy during observation of actions performed by a pathological model. *Neurorehabilitation and neural repair*, *33*(6), 419-431.

Errante, A., & Fogassi, L. (2020). Activation of cerebellum and basal ganglia during the observation and execution of manipulative actions. *Sci Rep*, *10*(1), 12008. https://doi.org/10.1038/s41598-020-68928-w

Errante, A., Ziccarelli, S.,, Mingolla, G. P., & Fogassi, L. (2021a). Decoding grip type and action goal during the observation of reaching-grasping actions: A multivariate fMRI study. *Neuroimage*, *243*, 118511. https://doi.org/10.1016/j.neuroimage.2021.118511

Errante, A., Ziccarelli, S.,, Mingolla, G., & Fogassi. (2021b). Grasping and Manipulation: Neural Bases and Anatomical Circuitry in Humans. *Neuroscience*, *458*, 203-212. https://doi.org/10.1016/j.neuroscience.2021.01.028

Fadiga, L., Fogassi, L., Pavesi, G., & Rizzolatti, G. (1995). Motor facilitation during action observation: a magnetic stimulation study. *J Neurophysiol*, *73*(6), 2608-2611. https://doi.org/10.1152/jn.1995.73.6.2608

Fan, L., Li, H., Zhuo, J., Zhang, Y., Wang, J., Chen, L., Yang, Z., Chu, C., Xie, S., Laird, A. R., Fox, P. T., Eickhoff, S. B., Yu, C., & Jiang, T. (2016). The Human Brainnetome Atlas: A New Brain Atlas Based on Connectional Architecture. *Cereb Cortex*, *26*(8), 3508-3526. https://doi.org/10.1093/cercor/bhw157

Federici, A., Parma, V., Vicovaro, M., Radassao, L., Casartelli, L., & Ronconi, L. (2020). Anomalous Perception of Biological Motion in Autism: A Conceptual Review and Meta-Analysis. *Sci Rep*, *10*(1), 4576. https://doi.org/10.1038/s41598-020-61252-3

Felleman, D. J., & Van Essen, D. C. (1991). Distributed hierarchical processing in the primate cerebral cortex. *Cereb Cortex*, *1*(1), 1-47. https://doi.org/10.1093/cercor/1.1.1-a

Filimon, F., Nelson, J. D., Hagler, D. J., & Sereno, M. I. (2007). Human cortical representations for reaching: mirror neurons for execution, observation, and imagery. *Neuroimage*, *37*(4), 1315-1328. https://doi.org/10.1016/j.neuroimage.2007.06.008

Fogassi, L., Ferrari, P. F., Gesierich, B., Rozzi, S., Chersi, F., & Rizzolatti, G. (2005). Parietal lobe: From action organization to intention understanding. *Science*, *308*(5722), 662-667. https://doi.org/10.1126/science.1106138

Fogassi, L., Gallese, V., Buccino, G., Craighero, L., Fadiga, L., & Rizzolatti, G. (2001). Cortical mechanism for the visual guidance of hand grasping movements in the monkey: A reversible inactivation study. *Brain*, *124*(Pt 3), 571-586. https://doi.org/10.1093/brain/124.3.571

Fox, R., & McDaniel, C. (1982). The perception of biological motion by human infants. *Science*, *218*(4571), 486-487.

Franceschini, M., Ceravolo, M. G., Agosti, M., Cavallini, P., Bonassi, S., Dall'Armi, V., Massucci, M., Schifini, F., & Sale, P. (2012). Clinical relevance of action observation in upper-limb stroke rehabilitation: a possible role in recovery of functional dexterity. A randomized clinical

trial. *Neurorehabil Neural Repair*, *26*(5), 456-462. https://doi.org/10.1177/1545968311427406

Friston, K. J., Glaser, D. E., Henson, R. N., Kiebel, S., Phillips, C., & Ashburner, J. (2002). Classical and Bayesian inference in neuroimaging: applications. *Neuroimage*, *16*(2), 484-512. https://doi.org/10.1006/nimg.2002.1091

Friston, K. J., Holmes, A. P., Price, C. J., Buchel, C., & Worsley, K. J. (1999). Multisubject fMRI studies and conjunction analyses. *Neuroimage*, *10*(4), 385-396. https://doi.org/10.1006/nimg.1999.0484

Gaglianese, A., Fracasso, A., Fernandes, F. G., Harvey, B., Dumoulin, S. O., & Petridou, N. (2023). Mechanisms of speed encoding in the human middle temporal cortex measured by 7T fMRI. *Hum Brain Mapp*, *44*(5), 2050-2061. https://doi.org/10.1002/hbm.26193

Gallese, V., Fadiga, L., Fogassi, L., & Rizzolatti, G. (1996). Action recognition in the premotor cortex. *Brain*, *119 (Pt 2)*, 593-609. https://doi.org/10.1093/brain/119.2.593

Gallese, V., Murata, A., Kaseda, M., Niki, N., & Sakata, H. (1994). Deficit of hand preshaping after muscimol injection in monkey parietal cortex. *Neuroreport*, *5*(12), 1525-1529. https://doi.org/10.1097/00001756-199407000-00029

Gallivan, J. P., Cavina-Pratesi, C., & Culham, J. C. (2009). Is that within reach? fMRI reveals that the human superior parieto-occipital cortex encodes objects reachable by the hand. *J Neurosci*, *29*(14), 4381-4391. https://doi.org/10.1523/JNEUROSCI.0377-09.2009

Gatti, R., Rocca, M. A., Fumagalli, S., Cattrysse, E., Kerckhofs, E., Falini, A., & Filippi, M. (2017). The effect of action observation/execution on mirror neuron system recruitment: an fMRI study in healthy individuals. *Brain Imaging and Behavior*, *11*, 565-576.

Gazzola, V., & Keysers, C. (2009). The observation and execution of actions share motor and somatosensory voxels in all tested subjects: single-subject analyses of unsmoothed fMRI data. *Cereb Cortex*, *19*(6), 1239-1255. https://doi.org/10.1093/cercor/bhn181

Gazzola, V., Rizzolatti, G., Wicker, B., & Keysers, C. (2007). The anthropomorphic brain: the mirror neuron system responds to human and robotic actions. *Neuroimage*, *35*(4), 1674-1684.

Gerbella, M., Belmalih, A., Borra, E., Rozzi, S., & Luppino, G. (2011). Cortical connections of the anterior (F5a) subdivision of the macaque ventral premotor area F5. *Brain Struct Funct*, *216*(1), 43-65. https://doi.org/10.1007/s00429-010-0293-6

Gerbella, M., Borra, E., Tonelli, S., Rozzi, S., & Luppino, G. (2013). Connectional heterogeneity of the ventral part of the macaque area 46. *Cereb Cortex*, *23*(4), 967-987. https://doi.org/10.1093/cercor/bhs096

Grafton, S. T., Arbib, M. A., Fadiga, L., & Rizzolatti, G. (1996). Localization of grasp representations in humans by positron emission tomography: 2. Observation compared with imagination. *Experimental brain research*, *112*, 103-111.

Grafton, S. T., & Hamilton, A. F. (2007). Evidence for a distributed hierarchy of action representation in the brain. *Hum Mov Sci*, *26*(4), 590-616. https://doi.org/10.1016/j.humov.2007.05.009

Gregoriou, G. G., Borra, E., Matelli, M., & Luppino, G. (2006). Architectonic organization of the inferior parietal convexity of the macaque monkey. *J Comp Neurol*, *496*(3), 422-451. https://doi.org/10.1002/cne.20933

Grèzes, J., Armony, J. L., Rowe, J., & Passingham, R. E. (2003). Activations related to "mirror" and "canonical" neurones in the human brain: an fMRI study. *Neuroimage*, *18*(4), 928-937. https://doi.org/10.1016/s1053-8119(03)00042-9

Grezes, J., Costes, N., & Decety, J. (1999). The effects of learning and intention on the neural network involved in the perception of meaningless actions. *Brain*, *122*(10), 1875-1887.

Grezes, J., Fonlupt, P., Bertenthal, B., Delon-Martin, C., Segebarth, C., & Decety, J. (2001). Does perception of biological motion rely on specific brain regions? *Neuroimage*, *13*(5), 775-785. https://doi.org/10.1006/nimg.2000.0740

Grosbras, M. H., Beaton, S., & Eickhoff, S. B. (2012). Brain regions involved in human movement perception: a quantitative voxel-based meta-analysis. *Hum Brain Mapp*, *33*(2), 431-454. https://doi.org/10.1002/hbm.21222

Grossman, E., Donnelly, M., Price, R., Pickens, D., Morgan, V., Neighbor, G., & Blake, R. (2000). Brain areas involved in perception of biological motion. *J Cogn Neurosci*, *12*(5), 711-720. https://doi.org/10.1162/089892900562417

Grossman, E. D., Battelli, L., & Pascual-Leone, A. (2005). Repetitive TMS over posterior STS disrupts perception of biological motion. *Vision Res*, *45*(22), 2847-2853. https://doi.org/10.1016/j.visres.2005.05.027

Grossman, E. D., & Blake, R. (2002). Brain Areas Active during Visual Perception of Biological Motion. *Neuron*, *35*(6), 1167-1175. https://doi.org/10.1016/s0896-6273(02)00897-8

Hamilton, A. F., & Grafton, S. T. (2006). Goal representation in human anterior intraparietal sulcus. *J Neurosci*, *26*(4), 1133-1137. https://doi.org/10.1523/JNEUROSCI.4551-05.2006

Hamilton, A. F., & Grafton, S. T. (2008). Action outcomes are represented in human inferior frontoparietal cortex. *Cereb Cortex*, *18*(5), 1160-1168. https://doi.org/10.1093/cercor/bhm150

Hardwick, R. M., Caspers, S., Eickhoff, S. B., & Swinnen, S. P. (2018). Neural correlates of action: Comparing meta-analyses of imagery, observation, and execution. *Neurosci Biobehav Rev*, *94*, 31-44. https://doi.org/10.1016/j.neubiorev.2018.08.003

Herman, L. M., Morrel-Samuels, P., & Pack, A. A. (1990). Bottlenosed dolphin and human recognition of veridical and degraded video displays of an artificial gestural language. *J Exp Psychol Gen*, *119*(2), 215-230. https://doi.org/10.1037//0096-3445.119.2.215

Hickok, G., & Small, S. L. (2015). *Neurobiology of language*. Academic press.

Hiris, E. (2007). Detection of biological and nonbiological motion. *J Vis*, *7*(12), 4 1-16. https://doi.org/10.1167/7.12.4

Iacoboni, M., Koski, L. M., Brass, M., Bekkering, H., Woods, R. P., Dubeau, M.-C., Mazziotta, J. C., & Rizzolatti, G. (2001). Reafferent copies of imitated actions in the right superior temporal cortex. *Proceedings of the national academy of sciences*, *98*(24), 13995-13999.

Iacoboni, M., Molnar-Szakacs, I., Gallese, V., Buccino, G., Mazziotta, J. C., & Rizzolatti, G. (2005). Grasping the intentions of others with one's own mirror neuron system. *PLoS Biol*, *3*(3), e79. https://doi.org/10.1371/journal.pbio.0030079

Iacoboni, M., Woods, R. P., Brass, M., Bekkering, H., Mazziotta, J. C., & Rizzolatti, G. (1999). Cortical mechanisms of human imitation. *Science*, *286*(5449), 2526-2528.

Insafutdinov, E., Andriluka, M., Pishchulin, L., Tang, S., Levinkov, E., Andres, B., & Schiele, B. (2017). Arttrack: Articulated multi-person tracking in the wild. Proceedings of the IEEE conference on computer vision and pattern recognition,

Jastorff, J., & Orban, G. A. (2009). Human functional magnetic resonance imaging reveals separation and integration of shape and motion cues in biological motion processing. *J Neurosci*, *29*(22), 7315-7329. https://doi.org/10.1523/jneurosci.4870-08.2009

Jastorff, J., Popivanov, I. D., Vogels, R., Vanduffel, W., & Orban, G. A. (2012). Integration of shape and motion cues in biological motion processing in the monkey STS. *Neuroimage*, *60*(2), 911-921. https://doi.org/10.1016/j.neuroimage.2011.12.087

Jeannerod, M., Arbib, M. A., Rizzolatti, G., & Sakata, H. (1995). Grasping objects: the cortical mechanisms of visuomotor transformation. *Trends Neurosci*, *18*(7), 314-320. https://www.ncbi.nlm.nih.gov/pubmed/7571012

Jellema, T., Baker, C., Oram, M., & Perrett, D. (2002). Cell populations in the banks of the superior temporal sulcus of the macaque monkey and imitation.(Eds: Meltzoff AN, Prinz W). The Imitative Mind: Development, Evolution, and Brain Bases. In: Cambridge: Cambridge University Press.

Jellema, T., Baker, C., Wicker, B., & Perrett, D. (2000). Neural representation for the perception of the intentionality of actions. *Brain and cognition*, *44*(2), 280-302.

Jellema, T., Maassen, G., & Perrett, D. I. (2004). Single cell integration of animate form, motion and location in the superior temporal cortex of the macaque monkey. *Cerebral cortex*, *14*(7), 781-790.

Jellema, T., & Perrett, D. I. (2002). Coding of visible and hidden actions. *Common mechanisms in perception and action, attention and performance. London: Academic*, 356-380.

Jellema, T., & Perrett, D. I. (2006). Neural representations of perceived bodily actions using a categorical frame of reference. *Neuropsychologia*, *44*(9), 1535-1546.

Johansson, G. (1973). Visual perception of biological motion and a model for its analysis. *Perception & Psychophysics*, *14*(2), 201-211. https://doi.org/10.3758/BF03212378

Kamitani, Y., & Tong, F. (2006). Decoding seen and attended motion directions from activity in the human visual cortex. *Current biology*, *16*(11), 1096-1102. https://doi.org/10.1016/j.cub.2006.04.003

Kandel, E., Schwartz, J., Jessell, T., Siegelbaum, S., & Hudspeth, A. J. (2012). *Principles of neural science* (Fifth edition. ed.). McGraw-Hill Publishing. https://ebookcentral.proquest.com/lib/brunelu/detail.action?docID=4959346

Kandel, E. R., Jessell, T. M., Kandel, E. R., Koester, J. D., Mack, S. H., Siegelbaum, S. A., & Vlebooks. (2021). *Principles of Neural Science* (6th edition. ed.). McGraw-Hill Education LLC.

Kemmerer, D. (2021). What modulates the Mirror Neuron System during action observation?: Multiple factors involving the action, the actor, the observer, the relationship between actor and observer, and the context. *Prog Neurobiol*, *205*, 102128. https://doi.org/10.1016/j.pneurobio.2021.102128

Kohler, E., Keysers, C., Umiltà, M. A., Fogassi, L., Gallese, V., & Rizzolatti, G. (2002). Hearing sounds, understanding actions: action representation in mirror neurons. *Science*, *297*(5582), 846-848. https://doi.org/10.1126/science.1070311

Koski, L., Wohlschläger, A., Bekkering, H., Woods, R. P., Dubeau, M.-C., Mazziotta, J. C., & Iacoboni, M. (2002). Modulation of motor and premotor activity during imitation of target-directed actions. *Cerebral cortex*, *12*(8), 847-855.

Koul, A., Cavallo, A., Cauda, F., Costa, T., Diano, M., Pontil, M., & Becchio, C. (2018). Action Observation Areas Represent Intentions From Subtle Kinematic Features. *Cereb Cortex*, *28*(7), 2647-2654. https://doi.org/10.1093/cercor/bhy098

Kozlowski, L. T., & Cutting, J. E. (1977). Recognizing the sex of a walker from a dynamic point-light display. *Perception & Psychophysics*, *21*(6), 575-580. https://doi.org/10.3758/BF03198740

Lacquaniti, F., Terzuolo, C., & Viviani, P. (1983). The law relating the kinematic and figural aspects of drawing movements. *Acta Psychol (Amst)*, *54*(1-3), 115-130. https://doi.org/10.1016/0001-6918(83)90027-6

Lanzilotto, M., Ferroni, C. G., Livi, A., Gerbella, M., Maranesi, M., Borra, E., Passarelli, L., Gamberini, M., Fogassi, L., Bonini, L., & Orban, G. A. (2019). Anterior Intraparietal Area: A Hub in the Observed Manipulative Action Network. *Cereb Cortex*, *29*(4), 1816-1833. https://doi.org/10.1093/cercor/bhz011

Lanzilotto, M., Livi, A., Maranesi, M., Gerbella, M., Barz, F., Ruther, P., Fogassi, L., Rizzolatti, G., & Bonini, L. (2016). Extending the Cortical Grasping Network: Pre-supplementary Motor Neuron Activity During Vision and Grasping of Objects. *Cereb Cortex*, *26*(12), 4435-4449. https://doi.org/10.1093/cercor/bhw315

Lapenta, O. M., Xavier, A. P., Correa, S. C., & Boggio, P. S. (2017). Human biological and nonbiological point-light movements: Creation and validation of the dataset. *Behav Res Methods*, *49*(6), 2083-2092. https://doi.org/10.3758/s13428-016-0843-9

Lestou, V., Pollick, F. E., & Kourtzi, Z. (2008). Neural substrates for action understanding at different description levels in the human brain. *J Cogn Neurosci*, *20*(2), 324-341. https://doi.org/10.1162/jocn.2008.20021

Lewis, J. W., & Van Essen, D. C. (2000). Mapping of architectonic subdivisions in the macaque monkey, with emphasis on parieto-occipital cortex. *J Comp Neurol*, *428*(1), 79-111. https://doi.org/10.1002/1096-9861(20001204)428:1<79::aid-cne7>3.0.co;2-q

Lingnau, A., Ashida, H., Wall, M. B., & Smith, A. T. (2009). Speed encoding in human visual cortex revealed by fMRI adaptation. *J Vis*, *9*(13), 3 1-14. https://doi.org/10.1167/9.13.3

Luppino, G., Matelli, M., Camarda, R. M., Gallese, V., & Rizzolatti, G. (1991). Multiple representations of body movements in mesial area 6 and the adjacent cingulate cortex: an intracortical microstimulation study in the macaque monkey. *J Comp Neurol*, *311*(4), 463-482. https://doi.org/10.1002/cne.903110403

Luppino, G., Murata, A., Govoni, P., & Matelli, M. (1999). Largely segregated parietofrontal connections linking rostral intraparietal cortex (areas AIP and VIP) and the ventral premotor cortex (areas F5 and F4). *Exp Brain Res*, *128*(1-2), 181-187. https://doi.org/10.1007/s002210050833

Maeda, K., Ishida, H., Nakajima, K., Inase, M., & Murata, A. (2015). Functional properties of parietal hand manipulation-related neurons and mirror neurons responding to vision of own hand action. *J Cogn Neurosci*, *27*(3), 560-572. https://doi.org/10.1162/jocn_a_00742

Majdandzic, J., Bekkering, H., van Schie, H. T., & Toni, I. (2009). Movement-specific repetition suppression in ventral and dorsal premotor cortex during action observation. *Cereb Cortex*, *19*(11), 2736-2745. https://doi.org/10.1093/cercor/bhp049

Maldjian, J. A., Laurienti, P. J., Kraft, R. A., & Burdette, J. H. (2003). An automated method for neuroanatomic and cytoarchitectonic atlas-based interrogation of fMRI data sets. *Neuroimage*, *19*(3), 1233-1239. https://doi.org/10.1016/s1053-8119(03)00169-1

Matelli, M., Luppino, G., & Rizzolatti, G. (1985). Patterns of cytochrome oxidase activity in the frontal agranular cortex of the macaque monkey. *Behav Brain Res*, *18*(2), 125-136. https://doi.org/10.1016/0166-4328(85)90068-3

Matelli, M., Luppino, G., & Rizzolatti, G. (1991). Architecture of superior and mesial area 6 and the adjacent cingulate cortex in the macaque monkey. *J Comp Neurol*, *311*(4), 445-462. https://doi.org/10.1002/cne.903110402

Matthews, N., Luber, B., Qian, N., & Lisanby, S. H. (2001). Transcranial magnetic stimulation differentially affects speed and direction judgments. *Exp Brain Res*, *140*(4), 397-406. https://doi.org/10.1007/s002210100837

Mayka, M. A., Corcos, D. M., Leurgans, S. E., & Vaillancourt, D. E. (2006). Three-dimensional locations and boundaries of motor and premotor cortices as defined by functional brain imaging: a meta-analysis. *Neuroimage*, *31*(4), 1453-1474. https://doi.org/10.1016/j.neuroimage.2006.02.004

McKeefry, D. J., Burton, M. P., Vakrou, C., Barrett, B. T., & Morland, A. B. (2008). Induced deficits in speed perception by transcranial magnetic stimulation of human cortical areas V5/MT+ and V3A. *J Neurosci*, *28*(27), 6848-6857. https://doi.org/10.1523/JNEUROSCI.1287-08.2008

McLeod, P., Dittrich, W., Driver, J., Perrett, D., & Zihl, J. (1996). Preserved and impaired detection of structure from motion by a "motion-blind" patient. *Visual Cognition*, *3*(4), 363-391. https://doi.org/10.1080/135062896395634

Molenberghs, P., Cunnington, R., & Mattingley, J. B. (2012). Brain regions with mirror properties: a meta-analysis of 125 human fMRI studies. *Neurosci Biobehav Rev*, *36*(1), 341-349. https://doi.org/10.1016/j.neubiorev.2011.07.004

Murata, A., Fadiga, L., Fogassi, L., Gallese, V., Raos, V., & Rizzolatti, G. (1997). Object representation in the ventral premotor cortex (area F5) of the monkey. *J Neurophysiol*, *78*(4), 2226-2230. https://doi.org/10.1152/jn.1997.78.4.2226

Murata, A., Gallese, V., Luppino, G., Kaseda, M., & Sakata, H. (2000). Selectivity for the shape, size, and orientation of objects for grasping in neurons of monkey parietal area AIP. *J Neurophysiol*, *83*(5), 2580-2601. https://doi.org/10.1152/jn.2000.83.5.2580

Muthukumaraswamy, S. D., Johnson, B. W., & McNair, N. A. (2004). Mu rhythm modulation during observation of an object-directed grasp. *Brain Res Cogn Brain Res*, *19*(2), 195-201. https://doi.org/10.1016/j.cogbrainres.2003.12.001

Nath, T., Mathis, A., Chen, A. C., Patel, A., Bethge, M., & Mathis, M. W. (2019). Using DeepLabCut for 3D markerless pose estimation across species and behaviors. *Nat Protoc*, *14*(7), 2152-2176. https://doi.org/10.1038/s41596-019-0176-0

Nelissen, K., Borra, E., Gerbella, M., Rozzi, S., Luppino, G., Vanduffel, W., Rizzolatti, G., & Orban, G. A. (2011). Action observation circuits in the macaque monkey cortex. *J Neurosci*, *31*(10), 3743-3756. https://doi.org/10.1523/JNEUROSCI.4803-10.2011

Nelissen, K., Fiave, P. A., & Vanduffel, W. (2017). Decoding Grasping Movements from the Parieto-Frontal Reaching Circuit in the Nonhuman Primate. *Cerebral cortex*, *28*(4), 1245-1259. https://doi.org/10.1093/cercor/bhx037

Oldfield, R. C. (1971). The assessment and analysis of handedness: the Edinburgh inventory. *Neuropsychologia*, *9*(1), 97-113. https://doi.org/10.1016/0028-3932(71)90067-4

Oram, M., & Perrett, D. (1994). Responses of anterior superior temporal polysensory (STPa) neurons to "biological motion" stimuli. *Journal of cognitive neuroscience*, *6*(2), 99-116.

Oram, M., & Perrett, D. (1996). Integration of form and motion in the anterior superior temporal polysensory area (STPa) of the macaque monkey. *Journal of neurophysiology*, *76*(1), 109-129.

Pandya, D. N., & Seltzer, B. (1982). Intrinsic connections and architectonics of posterior parietal cortex in the rhesus monkey. *J Comp Neurol*, *204*(2), 196-210. https://doi.org/10.1002/cne.902040208

Papadourakis, V., & Raos, V. (2019). Neurons in the Macaque Dorsal Premotor Cortex Respond to Execution and Observation of Actions. *Cereb Cortex*, *29*(10), 4223-4237. https://doi.org/10.1093/cercor/bhy304

Pavlova, M., Krageloh-Mann, I., Sokolov, A., & Birbaumer, N. (2001). Recognition of point-light biological motion displays by young children. *Perception*, *30*(8), 925-933. https://doi.org/10.1068/p3157

Pavlova, M. A. (2012). Biological motion processing as a hallmark of social cognition. *Cereb Cortex*, *22*(5), 981-995. https://doi.org/10.1093/cercor/bhr156

Peelen, M. V., Wiggett, A. J., & Downing, P. E. (2006). Patterns of fMRI activity dissociate overlapping functional brain areas that respond to biological motion. *Neuron*, *49*(6), 815-822. https://doi.org/10.1016/j.neuron.2006.02.004

Peeters, R., Simone, L., Nelissen, K., Fabbri-Destro, M., Vanduffel, W., Rizzolatti, G., & Orban, G. A. (2009). The representation of tool use in humans and monkeys: common and uniquely human features. *J Neurosci*, *29*(37), 11523-11539. https://doi.org/10.1523/JNEUROSCI.2040-09.2009

Pelosin, E., Avanzino, L., Bove, M., Stramesi, P., Nieuwboer, A., & Abbruzzese, G. (2010). Action observation improves freezing of gait in patients with Parkinson's disease. *Neurorehabil Neural Repair*, *24*(8), 746-752. https://doi.org/10.1177/1545968310368685

Pelphrey, K. A., Morris, J. P., Michelich, C. R., Allison, T., & McCarthy, G. (2005). Functional anatomy of biological motion perception in posterior temporal cortex: an FMRI study of eye, mouth and hand movements. *Cereb Cortex*, *15*(12), 1866-1876. https://doi.org/10.1093/cercor/bhi064

Peng, Y., Lee, H., Shu, T., & Lu, H. (2021). Exploring biological motion perception in two-stream convolutional neural networks. *Vision Res*, *178*, 28-40. https://doi.org/10.1016/j.visres.2020.09.005

Perrett, D. I., Harries, M. H., Bevan, R., Thomas, S., Benson, P. J., Mistlin, A. J., Chitty, A. J., Hietanen, J. K., & Ortega, J. E. (1989). Frameworks of analysis for the neural representation of animate objects and actions. *J Exp Biol*, *146*, 87-113. https://doi.org/10.1242/jeb.146.1.87

Perrett, D. I., Smith, P., Potter, D. D., Mistlin, A. J., Head, A., Milner, A. D., & Jeeves, M. A. (1985). Visual cells in the temporal cortex sensitive to face view and gaze direction. *Proceedings of the Royal society of London. Series B. Biological sciences*, *223*(1232), 293-317.

Peuskens, H., Vanrie, J., Verfaillie, K., & Orban, G. A. (2005). Specificity of regions processing biological motion. *Eur J Neurosci*, *21*(10), 2864-2875. https://doi.org/10.1111/j.1460-9568.2005.04106.x

Pitzalis, S., Fattori, P., & Galletti, C. (2015). The human cortical areas V6 and V6A. *Vis Neurosci*, *32*, E007. https://doi.org/10.1017/S0952523815000048

Pitzalis, S., Sereno, M. I., Committeri, G., Fattori, P., Galati, G., Patria, F., & Galletti, C. (2010). Human v6: the medial motion area. *Cereb Cortex*, *20*(2), 411-424. https://doi.org/10.1093/cercor/bhp112

Puce, A., & Perrett, D. (2003). Electrophysiology and brain imaging of biological motion. *Philosophical Transactions of the Royal Society of London. Series B: Biological Sciences*, *358*(1431), 435-445.

Quadrelli, E., Roberti, E., Turati, C., & Craighero, L. (2019). Observation of the point-light animation of a grasping hand activates sensorimotor cortex in nine-month-old infants. *Cortex*, *119*, 373-385. https://doi.org/10.1016/j.cortex.2019.07.006

Regolin, L., Tommasi, L., & Vallortigara, G. (2000). Visual perception of biological motion in newly hatched chicks as revealed by an imprinting procedure. *Animal Cognition*, *3*, 53-60.

Rizzolatti, G., Cattaneo, L., Fabbri-Destro, M., & Rozzi, S. (2014). Cortical mechanisms underlying the organization of goal-directed actions and mirror neuron-based action understanding. *Physiol Rev*, *94*(2), 655-706. https://doi.org/10.1152/physrev.00009.2013

Rizzolatti, G., Fadiga, L., Gallese, V., & Fogassi, L. (1996). Premotor cortex and the recognition of motor actions. *Cognitive brain research*, *3*(2), 131-141.

Rizzolatti, G., & Gentilucci, M. (1988). Motor and visual-motor functions of the premotor cortex. *Neurobiology of neocortex*, *42*, 269-284.

Rizzolatti, G., & Luppino, G. (2001). The cortical motor system. *Neuron*, *31*(6), 889-901.

Rozzi, S., Ferrari, P. F., Bonini, L., Rizzolatti, G., & Fogassi, L. (2008). Functional organization of inferior parietal lobule convexity in the macaque monkey: electrophysiological characterization of motor, sensory and mirror responses and their correlation with cytoarchitectonic areas. *Eur J Neurosci*, *28*(8), 1569-1588. https://doi.org/10.1111/j.1460-9568.2008.06395.x

Sack, A. T., Kohler, A., Linden, D. E. J., Goebel, R., & Muckli, L. (2006). The temporal characteristics of motion processing in hMT/V5+: Combining fMRI and neuronavigated TMS. *Neuroimage*, *29*(4), 1326-1335. https://doi.org/10.1016/j.neuroimage.2005.08.027

Sakata, H., Taira, M., Kusunoki, M., Murata, A., Tanaka, Y., & Tsutsui, K. (1998). Neural coding of 3D features of objects for hand action in the parietal cortex of the monkey. *Philos Trans R Soc Lond B Biol Sci*, *353*(1373), 1363-1373. https://doi.org/10.1098/rstb.1998.0290

Sakata, H., Taira, M., Murata, A., & Mine, S. (1995). Neural mechanisms of visual guidance of hand action in the parietal cortex of the monkey. *Cereb Cortex*, *5*(5), 429-438. https://doi.org/10.1093/cercor/5.5.429

Saygin, A. P. (2007). Superior temporal and premotor brain areas necessary for biological motion perception. *Brain*, *130*(9), 2452-2461. https://doi.org/10.1093/brain/awm162

Saygin, A. P., Wilson, S. M., Hagler, D. J., Jr., Bates, E., & Sereno, M. I. (2004). Point-light biological motion perception activates human premotor cortex. *J Neurosci*, *24*(27), 6181-6188. https://doi.org/10.1523/JNEUROSCI.0504-04.2004

Schrouff, J., Monteiro, J. M., Portugal, L., Rosa, M. J., Phillips, C., & Mourao-Miranda, J. (2018). Embedding Anatomical or Functional Knowledge in Whole-Brain Multiple Kernel Learning Models. *Neuroinformatics*, *16*(1), 117-143. https://doi.org/10.1007/s12021-017-9347-8

Schrouff, J., Mourao-Miranda, J., Phillips, C., & Parvizi, J. (2016). Decoding intracranial EEG data with multiple kernel learning method. *J Neurosci Methods*, *261*, 19-28. https://doi.org/10.1016/j.jneumeth.2015.11.028

Schrouff, J., Rosa, M. J., Rondina, J. M., Marquand, A. F., Chu, C., Ashburner, J., Phillips, C., Richiardi, J., & Mourao-Miranda, J. (2013). PRoNTo: pattern recognition for neuroimaging toolbox. *Neuroinformatics*, *11*(3), 319-337. https://doi.org/10.1007/s12021-013-9178-1

Senna, I., Bolognini, N., & Maravita, A. (2014). Grasping with the foot: goal and motor expertise in action observation. *Hum Brain Mapp*, *35*(4), 1750-1760. https://doi.org/10.1002/hbm.22289

Servos, P., Osu, R., Santi, A., & Kawato, M. (2002). The neural substrates of biological motion perception: an fMRI study. *Cereb Cortex*, *12*(7), 772-782. https://doi.org/10.1093/cercor/12.7.772

Sgandurra, G., Ferrari, A., Cossu, G., Guzzetta, A., Fogassi, L., & Cioni, G. (2013). Randomized trial of observation and execution of upper extremity actions versus action alone in children with unilateral cerebral palsy. *Neurorehabil Neural Repair*, *27*(9), 808-815. https://doi.org/10.1177/1545968313497101

Shim, J., Carlton, L. G., & Kim, J. (2004). Estimation of lifted weight and produced effort through perception of point-light display. *Perception*, *33*(3), 277-291. https://doi.org/10.1068/p3434

Simion, F., Regolin, L., & Bulf, H. (2008). A predisposition for biological motion in the newborn baby. *Proc Natl Acad Sci U S A*, *105*(2), 809-813. https://doi.org/10.1073/pnas.0707021105

Taira, M., Mine, S., Georgopoulos, A. P., Murata, A., & Sakata, H. (1990). Parietal cortex neurons of the monkey related to the visual guidance of hand movement. *Exp Brain Res*, *83*(1), 29-36. https://doi.org/10.1007/BF00232190

Tanisaro, P., Lehman, C., Sütfeld, L., Pipa, G., & Heidemann, G. (2017). Classifying bio-inspired model of point-light human motion using echo state networks. International Conference on Artificial Neural Networks,

Thiebaut de Schotten, M., Dell'Acqua, F., Valabregue, R., & Catani, M. (2012). Monkey to human comparative anatomy of the frontal lobe association tracts. *Cortex*, *48*(1), 82-96. https://doi.org/10.1016/j.cortex.2011.10.001

Thornton, I. M. (2006). Biological Motion: Point-Light Walkers and Beyond. In *Human body perception from the inside out: Advances in visual cognition.* (pp. 271-303). Oxford University Press.

Tkach, D., Reimer, J., & Hatsopoulos, N. G. (2007). Congruent activity during action and action observation in motor cortex. *J Neurosci*, *27*(48), 13241-13250. https://doi.org/10.1523/JNEUROSCI.2895-07.2007

Toshev, A., & Szegedy, C. (2014). Deeppose: Human pose estimation via deep neural networks. Proceedings of the IEEE conference on computer vision and pattern recognition,

Tremblay, C., Robert, M., Pascual-Leone, A., Lepore, F., Nguyen, D. K., Carmant, L., Bouthillier, A., & Theoret, H. (2004). Action observation and execution: intracranial recordings in a human subject. *Neurology*, *63*(5), 937-938. https://doi.org/10.1212/01.wnl.0000137111.16767.c6

Ulloa, E. R., & Pineda, J. A. (2007). Recognition of point-light biological motion: mu rhythms and mirror neuron activity. *Behav Brain Res*, *183*(2), 188-194. https://doi.org/10.1016/j.bbr.2007.06.007

Umiltà, M. A., Escola, L., Intskirveli, I., Grammont, F., Rochat, M., Caruana, F., Jezzini, A., Gallese, V., & Rizzolatti, G. (2008). When pliers become fingers in the monkey motor system. *Proc Natl Acad Sci U S A*, *105*(6), 2209-2213. https://doi.org/10.1073/pnas.0705985105

Umiltà, M. A., Kohler, E., Gallese, V., Fogassi, L., Fadiga, L., Keysers, C., & Rizzolatti, G. (2001). I know what you are doing: A neurophysiological study. *Neuron*, *31*(1), 155-165.

Vaina, L. M., & Gross, C. G. (2004). Perceptual deficits in patients with impaired recognition of biological motion after temporal lobe lesions. *Proc Natl Acad Sci U S A*, *101*(48), 16947-16951. https://doi.org/10.1073/pnas.0407668101

Vaina, L. M., Lemay, M., Bienfang, D. C., Choi, A. Y., & Nakayama, K. (1990). Intact "biological motion" and "structure from motion" perception in a patient with impaired motion mechanisms: A case study. *Visual neuroscience*, *5*(4), 353-369.

Vaina, L. M., Solomon, J., Chowdhury, S., Sinha, P., & Belliveau, J. W. (2001). Functional neuroanatomy of biological motion perception in humans. *Proc Natl Acad Sci U S A*, *98*(20), 11656-11661. https://doi.org/10.1073/pnas.191374198

Vallortigara, G., & Regolin, L. (2006). Gravity bias in the interpretation of biological motion by inexperienced chicks. *Curr Biol*, *16*(8), R279-280. https://doi.org/10.1016/j.cub.2006.03.052

Vallortigara, G., Regolin, L., & Marconato, F. (2005). Visually inexperienced chicks exhibit spontaneous preference for biological motion patterns. *PLoS Biol*, *3*(7), e208. https://doi.org/10.1371/journal.pbio.0030208

van Kemenade, B. M., Muggleton, N., Walsh, V., & Saygin, A. P. (2012). Effects of TMS over premotor and superior temporal cortices on biological motion perception. *J Cogn Neurosci*, *24*(4), 896-904. https://doi.org/10.1162/jocn_a_00194

Verzelloni, J., Errante, A., Beccani, L., Filippi, M., Bressi, B., Cavuto, S., Ziccarelli, S., Bozzetti, F., Costi, S., Pineschi, E., Fogassi, L., & Ferrari, A. (2021). Can a pathological model improve the abilities of the paretic hand in hemiplegic children? The PAM-AOT study protocol of a randomised controlled trial. *Bmj Open*, *11*(12). https://doi.org/ARTN e053910

10.1136/bmjopen-2021-053910

Weiner, K. S., & Zilles, K. (2016). The anatomical and functional specialization of the fusiform gyrus. *Neuropsychologia*, *83*, 48-62. https://doi.org/10.1016/j.neuropsychologia.2015.06.033

Wilke, M., & Lidzba, K. (2007). LI-tool: a new toolbox to assess lateralization in functional MR-data. *J Neurosci Methods*, *163*(1), 128-136. https://doi.org/10.1016/j.jneumeth.2007.01.026

Yoshida, K., Saito, N., Iriki, A., & Isoda, M. (2011). Representation of others' action by neurons in monkey medial frontal cortex. *Curr Biol*, *21*(3), 249-253. https://doi.org/10.1016/j.cub.2011.01.004

Zeki, S., Watson, J. D., Lueck, C. J., Friston, K. J., Kennard, C., & Frackowiak, R. S. (1991). A direct demonstration of functional specialization in human visual cortex. *J Neurosci*, *11*(3), 641-649. https://doi.org/10.1523/JNEUROSCI.11-03-00641.1991

Zhang, F., Bazarevsky, V., Vakunov, A., Tkachenka, A., Sung, G., Chang, C.-L., & Grundmann, M. (2020). Mediapipe hands: On-device real-time hand tracking. *arXiv preprint arXiv:2006.10214*.

Ziccarelli, S., Errante, A., & Fogassi, L. (2022). Decoding point-light displays and fully visible hand grasping actions within the action observation network. *Hum Brain Mapp*, *43*(14), 4293-4309. https://doi.org/10.1002/hbm.25954